JAERI-Conf
98-002

PROCEEDINGS OF THE MEETING ON TUNNELING REACTION AND LOW TEMPERATURE CHEMISTRY, 97 OCTOBER —TUNNELING REACTION AND QUANTUM MEDIUM— OCTOBER 13-14, 1997, JAERI, TOKAI, JAPAN

February 1998

(Eds.) Tetsuo MIYAZAKI,* Yasuyuki ARATONO,
Tsuneki ICHIKAWA* and Masaru SHIOTANI**

日本原子力研究所
Japan Atomic Energy Research Institute

本レポートは，日本原子力研究所が不定期に公刊している研究報告書です。
入手の問合わせは，日本原子力研究所研究情報部研究情報課（〒319-1195　茨城県那珂郡東海村）あて，お申し越しください。なお，このほかに財団法人原子力弘済会資料センター〒319-1195　茨城県那珂郡東海村日本原子力研究所内）で複写による実費領布をおこなっております。

This report is issued irregularly.
Inquiries about availability of the reports should be addressed to Research Information Division, Department of Intellectual Resources, Japan Atomic Energy Research Institure, Tokai-mura, Naka-gun, Ibaraki-ken 319-1195, Japan.

編集兼発行　日本原子力研究所
印　　刷　㈱原子力資料サービス

The Meeting on Tunneling Reaction and Low Temperature Chemistry, 97 October －Tunneling Reaction and Quantum Medium－

October 13-14, 1997

Japan Atomic Energy Research Institute
Tokai, Japan

Sponsored and Organized
by
Advanced Science Research Center,
Japan Atomic Energy Research Institute,
and
Japanese Society of Radiation Chemistry

Supported
by
Chemical Society of Japan

This is a blank page.

JAERI－Conf 98－002

Proceedings of the Meeting on Tunneling Reaction and Low Temperature Chemistry, 97 October －Tunneling Reaction and Quantum Medium－ October 13-14, 1997, JAERI, Tokai, Japan

(Eds.) Tetsuo MIYAZAKI※, Yasuyuki ARATONO, Tsuneki ICHIKAWA* and Masaru SHIOTANI**

Advanced Science Research Center
(Tokai Site)
Japan Atomic Energy Research Institute
Tokai-mura, Naka-gun, Ibaraki-ken

(Received January 6, 1998)

Present report is the proceedings of the 3rd Meeting on Tunneling Reaction and Low Temperature Chemistry held in Oct. 13 and 14, 1997. The main subject of the meeting is "Tunneling Reaction and Quantum Medium". The 1st meeting on "Tunneling Reaction and Low Temperature Chemistry, -Tunneling Reaction and Cryotechnique" was held in July 21 and August 1, 1995. (JAERI Conf 95-020). In the 2nd meeting held in August 22 and 23, 1996, "The Tunneling Reaction and Biology" was placed on the subject. (JAERI-Conf 96-015)

In the present meeting, the physical and chemical phenomena in the liquid helium such as quantum nucleation, spectroscopy of atoms and molecules, and tunneling abstraction reaction of tritium atom were discussed as the main topics as well as the tunneling reactions in the solid hydrogen and organic compounds.

Through the meetings held in 1995, 1996, and 1997, the tunneling phenomena proceeding at various temperatures (room temperature to mK) in the wide fields of chemistry, biology, and physics were discussed intensively and the importance of the tunneling phenomena in the science has been getting clear.

The number of the participants was 40 and 14 invited lectures were presented The editors believe that the present proceedings will contribute to understanding of the tunneling reaction in the quantum media.

Keywords: Tunneling Reaction, Quantum Medium, Low Temperature Chemistry, Liquid Helium, Solid Hydrogen, Organic Compound

※ Invited Researcher : Nagoya University
* Hokkaido University
** Hiroshima University

トンネル反応および低温化学についての研究会報告集（III）
第３回低温化学セミナー「トンネル反応と量子媒体」
１９９７年１０月１３日―１０月１４日、東海研究所、東海村

日本原子力研究所先端基礎研究センター
（編）宮崎 哲郎※・荒殿 保幸・市川 恒樹*・塩谷　優**

（１９９８年1月6日受理）

本報告集は１９９７年１０月１３日―１０月１４日の２日間にわたって開催した第３回低温化学セミナーの講演のプロシーディングスである。今回の主題は「トンネル反応と量子媒体」である。本セミナーでは、１９９５年に第１回低温化学セミナー「トンネル反応と極低温技術」（JAERI-Conf 95-020）を、１９９６年に第２回低温化学セミナー「トンネル反応と生物効果」（JAERI-Conf 96-015）を開催してきた。

今回は、固体水素の関係するトンネル現象に加えて、より量子性の強い液体ヘリウムを初めて取り上げ、物理・化学分野におけるトンネル現象の媒体としての液体ヘリウムの特異性を主題として議論した。従って、内容的にもｍＫ領域での量子核形成等の純粋なトンネル物理現象のみならず液体ヘリウム中でのバブル原子の分光やトリチウムの化学反応等、物理と化学との境界領域を開拓する研究等の発表が行われた。

今回を含め、３回の低温化学セミナーにおいて、分野的には化学、生物、物理、温度領域もｍＫから室温と非常に幅広い領域でのトンネル現象をカバーしたことになり、トンネル現象の奥行きの深さが次第に明らかになってきた。

研究会の参加者は約４０名で、固体水素や、液体ヘリウム等の量子媒体を対象に研究を進めている化学・物理分野の研究者がそれぞれの立場から、１４件の研究発表を行った。

本報告集が、量子媒体中でのトンネル現象の研究の発展にいささかでも寄与できれば幸いである。

日本原子力研究所（東海駐在）：〒319-1195 茨城県那珂郡東海村白方白根 2-4
※客員研究員：名古屋大学
*北海道大学
**広島大学

Contents

目　次

1. Decay of H_2^- anions in solid parahydrogen by quantum tunneling : observations of electron bubbles

T. Kumada,[1] N. Kitagawa,[2] T. Takayanagi,[1] Y. Aratono,[1] and T. Miyazaki[1,2]
[1] Advanced Science Research Center, Japan Atomic Energy Research Institute, Tokai-mura, Naka-gun, Ibaraki 319-11, Japan
[2] Department of Applied Chemistry, School of Engineering, Nagoya University, Furo-cho, Chikusa-ku, Nagoya 464-01, Japan

Decay mechanism of H_2^- anions produced by γ-ray or X-ray radiolysis of solid para-H_2 (p-H_2) has been studied using high-resolution ESR spectroscopy in the temperature range between 2.7-6.6 K. The results can be summarized as follows; First, the decay rate constant of the H_2^- anion is not proportional to initial yields of reactive species such as H radical and cation but proportional to concentrations of HD and D_2 impurities in p-H_2. Second, ESR spectra assigned as electron bubbles were observed in solid p-H_2 containing large amount of HD or D_2 (11 mol %), while they were not observed in pure solid p-H_2. Third, the decay rate constant of the H_2^- anion increases with the decrease in temperature between 2.7-5 K, while it decreases with the decrease between 5-6.6 K. Fourth, the decay of the H_2^- anion is suppressed by addition of ortho-H_2 (o-H_2) impurity. The first and second results suggest that the H_2^- anion reacts with the HD or D_2 molecule to produce the electron bubble. The third and fourth results are interpreted in terms of two-phonon scattering quantum diffusion and thermally activated diffusion below and above 5 K, respectively.

I. INTRODUCTION

The interest in isolating charged species in solid hydrogen has persisted since Souers and co-workers reported new infrared absorption peaks induced by the Stark effect, which suggest the existence of positive and negative charged species produced by β-ray radiolysis of T atoms, in solid D_2, HT, DT, and T_2 mixtures in 1980.[1,2] Brooks and co-workers have thus extended these researches using proton-beam bombardment instead of the β-rays of the T atoms and found several absorption peaks, which suggest the existence of electron bubbles, small polaron holes, interference effects, and ion clustering.[3] In 1990's, Oka and his co-workers reported that resolutions of infrared absorption and Raman spectra of solid hydrogen were drastically improved using p-H_2 matrices and found new infrared absorption and Raman peaks induced by the Condon effect, which also suggest the existence of positive ions, in γ-rays irradiated solid p-H_2, while the previous results such as the near infrared transition ascribed to electron bubbles and some of the Stark shifted lines were not reproduced.[4,5]

In these researches, the existence of the positive and negative charges has been suggested by observing spectra of surrounding H_2 molecules; however, the spectra of charged species themselves have not been observed. On the other hand, Miyazaki and his co-workers have reported that solid p-H_2 is useful as a matrix for high-resolution ESR spectroscopy and have found new quartet ESR spectra assigned as H_2^- anions in γ-rays

irradiated solid p-H_2. This is the first observation of ionic species themselves in solid hydrogen.[6,7] Although the H_2^- anion is unstable in gas phase,[8] it is presumably stabilized by surrounding crystal fields of solid.[9]

An interesting phenomenon was reported on the decay behaviors of the H_2^- anions. ESR intensity of the H_2^- anions at 2.2 K decays faster than at 4.2 K.[10] This result may be interpreted by quantum tunneling diffusion of the reactant, because generally the decay rate should decrease with the decrease in temperature in classical theory. In this paper, we extend our previous research and report two interesting results which elucidate the detailed decay mechanism of the H_2^- anions: transformation of the H_2^- anion into an electron bubble and an anomalous temperature dependence of the decay rate constant, which is related to quantum and classical diffusions.

II. EXPERIMENTAL PROCEDURE

A p-H_2 sample was synthesized from normal hydrogen at 14 K using a catalyst of powdered iron(III) hydroxide (FeO(OH)). Purity of the p-H_2 molecules was about 97 mol %. Thus, it should be noted that the (pure) p-H_2 sample in this paper originally contains natural abundance of HD (0.03 mol %) and o-H_2 about 3 mol %. In some cases, HD, D_2, or o-H_2 molecules were added to the pure p-H_2 sample. This p-H_2 gas was contained in a quartz cell and solidified by cooling to 4.2 K. The radicals, generated by white X-ray (60 kV, 45 mA, 2.5 h) or γ-ray (Co-60, 0.3 kGy) radiolysis at 4.2 K, were measured by the JEOL JES-TE200 ESR spectrometer. In order to reduce the amounts of color centers in X-rays irradiated quartz, the sample was irradiated above an ESR cavity and then pushed down to a center of the cavity for ESR measurements. Temperatures of the sample were exactly controlled by heating injected cold helium gas above 4.2 K or by cooling the helium gas by pumping below 4.2 K. Stability of the temperatures was ±0.05 K for each storage time.

III. RESULTS

Fig. 1 shows the ESR spectrum of the H_2^- anions in γ-rays irradiated solid p-H_2 at 4.2 K. The B1, B3, and B4 peaks are of ortho-H_2^- (o-H_2^-) (I=1) and B2 is of para-H_2^-(p-H_2^-) (I=0). the g-value (g) and hyperfine field (A) of the spectra were observed to be 2.0023 and 203 G, respectively.[7,9] The splitting between B1 and B2 is derived from 2nd-order hyperfine interaction. The detailed discussions on the assignment of the H_2^- anion were described in previous papers.[7,10,11]

A. Effects of HD and D_2 impurities

Effects of HD and D_2 impurities on the decay behaviors of the H_2^- anions were examined. Fig. 2 shows the decay behaviors of the H_2^- anions in γ-rays irradiated solid p-H_2 mixtures at 4.2 K. Relative ESR intensity of the H_2^- anion in p-H_2-HD(0.072 mol %) mixture decays faster than that in pure p-H_2. Moreover, amount of the H_2^- anion in p-H_2-D_2(0.10 mol %) mixture decays much faster than that in the p-H_2-HD mixture,

although the concentration of the D_2 molecule is comparable to that of the HD molecule.[10] On the contrary, the decay of the H_2^- anion is suppressed by addition of o-H_2 impurities. The decay rate constant (D) of the H_2^- anion was determined by assuming the following first-order decay mechanism:

$$I(t) = I_0 \exp(-D\,t), \tag{1}$$

where $I(t)$ and I_0 indicate relative ESR intensities of the H_2^- anions at times of $t = t$ and $t = 0$, respectively. Fig. 3 shows the decay rate constant of the H_2^- anions as a function of the concentration of HD and/or D_2 impurities. It has been found that the decay rate constant was proportional to the concentration of HD (solid line). The dashed lines fitted to the open and closed squares did not pass through the origin, probably because the open and closed squares were plotted as a function of total concentration of D_2 and natural abundance of HD (0.03 mol %). It is interesting to note that the effect of the D_2 impurity on the decay rate constant is much significant than that of the HD impurity.

Fig. 4 shows ESR spectra of γ-rays irradiated solid p-H_2-D_2 (11 mol %), p-H_2-HD (11 mol %), and pure p-H_2 at 4.2 K with low microwave power of 5 nW. Very sharp singlet peaks with g-value very close to 2.0023 was observed in the p-H_2-D_2 and p-H_2- HD mixtures (Fig. 1(a)(b)), while it was not observed in the pure p-H_2 sample (Fig. 1(c)). In addition, the ESR intensity of the singlet peak in the p-H_2-D_2 mixture was observed to be larger than that in the p-H_2-HD mixture. Fig. 5 shows microwave power saturation behavior of the singlet peak shown in Fig. 4(a) at 4.2 K. The ESR intensity of the singlet peak was found to be very easy to saturate compared to that of the H_2^- anions.

B. Temperature dependence for decay rate constant of H_2^-

Fig. 6 shows the decay behavior of the H_2^- anion in X-rays irradiated solid p-H_2 at 2.9, 4.5, and 6.6 K. It is seen that the relative intensity of the H_2^- anions decays exponentially for three temperatures. The intensity of the H_2^- anion at 2.9 or 6.6 K decay about five times faster than that at 4.5 K, respectively. Fig. 7 shows the decay rate constant of the H_2^- anion as a function of temperature between 2.7-6.6 K. The decay rate constant drastically increases with the decrease in temperature below 5 K, it decreases with the decrease above 5 K, showing a minimum at around 5 K.

IV. DISCUSSION

A. Decay mechanism of H_2^-

1. Reaction of H_2^- with H atom or cation

Table 1 shows initial yields of the H_2^- anions and H atoms and the decay rate constants of the H_2^- anions at 4.5 K in solid p-H_2 irradiated by X-rays for 17 and 150 minutes. In spite of the large difference in their irradiation times, both the decay rate constants are the same within their experimental errors, while the initial yields of the H_2^-

anions and H atoms increase almost linearly with the increase in the irradiation time. Accompanied by anionic species such as H_2^-, cationic species must be produced by the X(γ)-ray radiolysis as follows:

$$H_2 \wwvy H_2^+ + e^-.$$

Therefore, the initial yields of cations also must increase with the increase in the irradiation time. Note that, although the existence of cationic species in γ-rays irradiated solid p-H_2 were reported, they have not been assigned.[5] If the H_2^- anion reacts with the H atom via the electron transfer reaction, $H_2^- + H \rightarrow H_2 + H^-$, or neutralize with the cation, the decay rate constant of the H_2^- anion must be proportional to the initial yield of the H atom or cation. However, as discussed above, the decay rate constant does not depend on the initial yields of the H atom nor cations, suggesting that the decay process of the H_2^- anion is due to neither the reaction with the H atoms nor that with the cations.[10]

2. Transformation of H_2^- into electron bubble by HD (or D_2)

As shown in Fig. 3, the decay rate constant is proportional to the concentrations of the HD (solid lines) molecules, which are much higher than those of the H_2^- anions (~10^{-11} mol %). Therefore, the decay of the H_2^- anion obeys pseudo-first-order decay kinetics as follows:

$$\frac{d[H_2^-]}{dt} = -k_2[HD][H_2^-],$$

where $k_2 = D$ / [HD]. The solid lines fitted to the open and closed circles in Fig. 3 approximately pass through the origin, suggesting that amount of the H_2^- anions even in pure p-H_2 decay by the reaction with HD at natural abundance (0.03 mol %), which is much higher than concentration of the H radicals and cations (< 10^{-4} mol %). One possible decay mechanism of the H_2^- anion is the electron transfer reaction from the H_2^- anion to the HD (or D_2) impurity: $H_2^- + HD$ (or D_2) $\rightarrow H_2 + HD^-$ (or D_2^-). However, these reactions are endothermic process, because zero-point vibrational energy of the H_2 molecule (0.27 eV) is larger than that of the HD (0.23 eV) and D_2 (0.19 eV) molecules and the H_2^-, HD^-, and D_2^- anions.[10] In fact, ESR spectra of HD^- and D_2^- could not be observed.

New ESR spectra of very sharp singlet peak, shown in Fig. 4, was observed in γ-rays irradiated solid p-H_2-D_2 (11 mol %) and p-H_2-HD (11 mol %) mixtures at 4.2 K. This singlet peak is probably ascribed to electron bubbles.[1,3] The reasons are as follows: First, the linewidth of the singlet peak is very small (< 0.5 G) and the *g*-value is very close to that of free electron (g_e = 2.0023). Second, as shown in Fig. 5, the ESR intensity of the signal is easy to saturate. Third, the ESR intensity of the singlet peak decays in the solid with a half life of few hours at 4.2 K (not shown), indicating that the species is reactive.

This finding of the singlet peak is the first observation of electron bubbles themselves in solid hydrogen, although the existence of the electron bubble has been suggested by the observation of charge induced spectra of surrounding H_2 molecules.[1,3]

Although the ESR spectra of the electron bubbles were observed in the p-H_2-HD (11 mol %) and p-H_2-D_2 (11 mol %) mixtures, they were not observed at all in pure p-H_2 (c.f. Fig. 4(c)). On the contrary, while the ESR spectra of the H_2^- anions were observed in pure p-H_2, they were not observed in the p-H_2-HD and p-H_2-D_2 mixtures. These compensating properties and the fact that the decay rate constant of the H_2^- anion is proportional to concentrations of HD and D_2 suggest that the H_2^- anion reacts with the HD or D_2 molecule to produce the electron bubble. The ESR intensity of the electron bubbles in the p-H_2-D_2 (11 mol %) mixture is much larger than that in the p-H_2-HD (11 mol %) mixture. This indicates that D_2 molecule is more effective to produce electron bubbles than HD. This trend is consistent with the result that the D_2 molecule is more effective to accelerate the decay rate constant of the H_2^- anions than HD. These impurities may disturb homogeniety of the solid p-H_2. This may produce distortions, cracks, and defects in the solid, where these excess electrons are easily trapped. Further experimental studies would be required to elucidate the detailed mechanism.

B. Quantum diffusion on decay of H_2^-

1. Quantum diffusion

Fig. 7 shows that the decay rate constant of the H_2^- anions significantly increases with the decrease in temperature below 5 K, while it decreases with the decrease above 5 K. The similar temperature dependence has also been reported in other systems: diffusion rates of muonium in ionic and N_2 crystals,[12,13] ^{3}He in solid ^{4}He,[14] and HD in solid p-H_2.[15] The diffusion rates of these light impurities are explained by competition between two-phonon scattering quantum tunneling diffusion (QD) and thermally activated diffusion (TD). Since QD is significantly disturbed by phonons and vacancies, the rate of QD becomes slower with the increase in temperature, while the rate of TD becomes faster with the increase in temperature. Therefore, the temperature dependence of these diffusion rate constant show a minimum at T^*.[16] It is probable that QD plays a role on the decay of the H_2^- anion, because of the small mass and low activation barrier for the diffusion in this system. When the decay of the H_2^- anion is due to QD below 5 K and the TD above 5 K, the decay rate constant in Fig. 7 can be fitted by the following equation:[16]

$$D = D_1 (\Theta_D / T)^{\alpha} + D_2 \exp(-E_a / kT). \qquad (2)$$

over the temperature range 3-6.6 K with parameters $D_1 = 9.7\times10^{-12}$ s^{-1}, $\alpha = 4.9$, $D_2 = 250$ s^{-1}, $E_a / k = 92$ K. E_a represents the thermal activation energy for the diffusion. A Debye temperature Θ_D of 100 K was assumed.[17] The first and the second terms represent the decay rate constants correspond to QD and TD, respectively. It is interesting to note that the value of E_a / k is comparable to the activation energies for the recombination of H atoms in solid normal H_2 (107 ± 10 K),[18] the tunneling reaction: D + DH → D_2 + H in

solid HD (95 K),[19] and vacancy formation (91 ± 8, 91 ± 10,[15] 112 K[20]) and vacancy migration (105 ± 4, 104 ± 5,[15] 85 K[20]) in solid p-H_2. Although the value of α is expected to be 9 on the basis of the theory of ideal QD,[16] the observed value of 4.9 would be acceptable compared to other cases; For example, α = 3 was obtained for QD of muonium in solid KCl and NaCl below 80 K.[12]

If the decay of the H_2^- anion is mainly due to QD below 5 K, it must decrease with the increase in concentration of localized impurities, because not only the phonons and vacancies but also the localized impurities disturb QD of particles in the solid. Fig. 2 shows that the decay rate constant of the H_2^- anion decreases with the increase in concentration of o-H_2, which is localized in solid p-H_2.[21] The result also supports the QD model on the decay of the H_2^- anion below 5 K. It is noted that the initial yields and the decay rate constants of the p-H_2^- and o-H_2^- were observed to be independent of the concentration of the o-H_2 molecules within errors (not shown), showing that the reaction: p-H_2^- + o-H_2 → p-H_2 + o-H_2^- does not occur in the solid, although the reaction is exothermic.

2. Mobile species on the decay mechanism of H_2^-

At low temperatures below 5 K, the H_2^- anion decays via the reaction with HD to produce electron bubble. Then, we encounter a question, which of the H_2^- anions and the HD molecules mainly migrate in the solid p-H_2. Sullivan et al. reported that the HD molecules migrate in the solid p-H_2 by QD below 9 K.[15] On the other hand, the charge of the H_2^- anion strongly attracts surrounding molecules with a long-range interaction ($\propto r^{-4}$), resulting in the drastic increase of the effective mass. Therefore, QD of the H_2^- anion is expected to be strongly hindered. QD of charged particle such as μ^+ was reported in metal matrices; however, an electric shield of surrounding free electron in the metals plays an important role on the tunneling.[22,23] Thus, the decay of the H_2^- anion in solid p-H_2 is probably due to the rate of QD of HD molecule to the anions below 5 K. However, the possibility of QD of the H_2^- anions cannot be completely rejected. For example, diffusion mechanisms of the H_2^- anions with repetitions of reactions with surrounding p-H_2 molecules:

$$\text{p-}H_2^- + \text{p-}H_2 \rightarrow \text{p-}H_2 + \text{p-}H_2^-, \quad (3)$$

$$\text{o-}H_2^- + \text{p-}H_2 \rightarrow \text{p-}H_2 + \text{o-}H_2^-. \quad (4)$$

should also occur. Because of light mass of excess electron in the H_2^- anion, which transfer from one H_2 to nearby H_2, and good symmetry between the reactant and the product, the reactions (3) and (4) may occur by quantum tunneling. Since the information on the H_2^- anions in solid hydrogen is yet insufficient at present, we cannot discuss this possibility further.

At high temperatures above 5 K, HD molecules, H radicals, and ionic species were reported to migrate in solid H_2 with nearly same activation energies,[15,24,25] indicating that many kinds of species migrate simultaneously by thermally activated processes. Therefore, main mobile species on the decay mechanism of the H_2^- cannot be specified.

V. CONCLUSION

Decay mechanism of the H_2^- anion in solid parahydrogen was studied using high-resolution ESR spectroscopy. As concentrations of HD or D_2 molecule increased, the H_2^- anions gradually disappear in the solid p-H_2, while electron bubbles appear, suggesting that the H_2^- anion react with HD (or D_2) to produce the electron bubble. The decay rate constant of the H_2^- anion increase with the decrease in temperature below 5 K, while it decrease with the decrease above 5 K. In addition, the decay rate constant decrease with the increase in concentration of o-H_2 molecule at 4.2 K. These results suggest that the decay of the H_2^- anion is due to two-phonon scattering quantum diffusion of HD below 5 K and thermally activated diffusion above 5 K.

ACKNOWLEDGMENT

We would like to acknowledge helpful discussion with Professor M. Uwaha of Nagoya University. We also thank Dr. S. Ohira of Japan Atomic Energy Research Institute, and Mr. H. Inagaki of Nagoya University for their help in these experiments. This work was supported in part by Grant-in-Aid for Scientific Research from the Japanese Ministry of Education, Science, and Culture.

References

1 P. C. Souers, E. M. Fearon, P. E. Roberts, R. J. Tsugawa, J. D. Poll, and J. L. Hunt, Phys. Lett. A **77**, 277 (1980); P. C. Souers, E. M. Fearon, R. L. Stark, R. T. Tsugawa, J. D. Poll, and J. L. Hunt, Can. J. Phys. **59**, 1408 (1981).
2 P. C. Souers, *Hydrogen Properties for Fusion Energy* (University of California Press, Berkeley, 1986).
3 R. L. Brooks, S. K. Bose, J. L. Hunt, Jack R. MacDonald, and J. D. Poll, Phys. Rev. B **32**, 2478 (1985); R. L. Brooks, J. L. Hunt, Jack R. MacDonald, J. D. Poll, and J. C. Waddington, Can. J. Phys. **63**, 937 (1985).
4 T. Oka, Rev. Mod. Phys. **45**, 1141 (1992).
5 T. Momose, K. E. Kerr, D. P. Weliky, C. M. Gabrys, R. M. Dickson, and T. Oka, J. Chem. Phys. **100**, 7840 (1994).
6 T. Miyazaki, K. Yamamoto, and Y. Aratono, Chem, Phys, Lett. **232**, 229 (1995).
7 T. Kumada, H. Inagaki, T. Nagasawa, Y. Aratono, and T. Miyazaki, Chem. Phys. Lett. **251**, 219 (1996).
8 E. F. DeRose, E. A. Gislason, N. H. Sabelli, and K. M. Sluis, J. Chem. Phys. **88**, 4878 (1988).
9 T. Ichikawa, H. Tachikawa, J. Kumagai, T. Kumada, and T. Miyazaki, J. Phys. Chem. in press.
10 T. Kumada, T. Inagaki, N. Kitagawa, Y. Aratono, and T. Miyazaki, J. Phys. Chem. **101**, 1198 (1997).
11 M. C. R. Symons, Chem, Phys, Lett. **247**, 607 (1995).
12 R. F. Kiefl, R. Kadono, J. H. Brewer, G. M. Luke, H. K. Yen, Phys. Rev. Lett. **62**, 792 (1989); R. Kadono, R. F. Kiefl, E. J. Ansaldo, J. H. Brewer, M. Celio, S. R.

Kreitzmann, and G. M. Luke, Phys. Rev. Lett. **64**, 665 (1990); R. Kadono, Hyp. Int. **64,** 615 (1990).
13 V. Storchak, J. H. Brewer, W. N. Hardy, S. R. Kreitzman, and G. D. Morris, Phys. Rev. Lett. **72**, 3056 (1994); V. G. Storchak, J. H. Brewer, and G. D. Morris, Hyp. Int. **85**, 31 (1994).
14 V. N. Grigoriev, B. N. Esel'son, V. A. Mikheev, V. A. Slusarev, M. S. Strzhemechny, and Yu. E. Shul'mann, J. Low. Temp. Phys. **13,** 65 (1973); A. F. Andreev, Sov. Phys. Usp. **19**, 137 (1976).
15 M. Rall, D. Zhou, Erika G. Kisvarsanyi, and N. S. Sullivan, Phys. Rev. B **45**, 2800 (1992); D. Zhou, C. M. Edwards, and N. S. Sullivan, Phys. Rev. Lett. **62**, 1528 (1989).
16 Y. Kagan, M. I. Klinger, J. Phys. C **7**, 2791 (1974); Yu. M. Kagan and N. V. Prokof'ev, in *Quantum Tunneling in Condensed Media*, (North-Holland, Amsterdam, 1992).
17 M. L. Klein and J. A. Venables, *Rare Gas Solid* (Academic Press, London, 1976).
18 A. Ya. Katunin, I. I. Lukashevich, S. T. Orozmamatov, V. V. Sklyarevskii, V. V. Suraev, V. V. Filippov, and V. A. Shevtov, Piz'ma Zh. Eksp. Theo. Fiz. **34**, No. 6, 375 (1981) [JETP Lett. **34**, No. 6, 357, (1982)]
19 T. Kumada, K. Komaguchi, Y. Aratono, and T. Miyazaki, Chem. Phys. Lett. **261**, 463, (1996).
20 C. Ebner and C. C. Sung, Phys. Rev. A **5**, 2625 (1972).
21 J. M. Delrieu and N. S. Sullivan, Phys. Rev. B **23**, 3197 (1981).
22 R. Kadono, J. Imazato, T. Matsuzaki, K. Nishiyama, K. Nagamine, T. Yamazaki, D. Richter, and J. M. Welter, Phys. Rev. B **39**, 23 (1989); G. M. Luke, J. H. Brewer, S. R. Kreitzman, D. R. Noakes, M. Celio, R. Kadono, and E. J. Ansoldo, Phys. Rev. B **43**, 3284 (1991).
23 S. Fujii and Y. Uemura, Solid State Commun, **26**, 761 (1978); S. Fujii, J. Phys. Soc. Jpn. **46**, 1833 (1979).
24 A. A. Levchenko and L. P. Mezhov-Deglin, Zh. Eksp. Teor. Fiz. **98**, 349 (1990) [Sov. Phys. JETP **71**, 196 (1990)].
25 J. R. Gaines, P. A. Fedders, G. W. Collins, J. D. Sater, and P. C. Souers, Phys. Rev. B **52**, 7243 (1995).

Figure Legend.

Fig. 1 ESR spectrum of H_2^- anions in γ-rays-irradiated solid p-H_2 at 4.2 K. B1, B3, and B4 are of o-H_2^- and B2 is of p-H_2^- anions. The peak depicted by A has not been identified. Peaks depicted by Mn are those of manganese as an ESR marker. Stick diagram scaled below is of the H_2^- anions with I = 0, 1, g = 2.0023, and A = 203 G.

Fig. 2 Relative amount of H_2^- anions as a functions of storage time in γ-rays-irradiated solid p-H_2 samples at 4.2 K. Open circles correspond to solid p-H_2. Triangles, and reciprocal triangles correspond to the p-H_2 samples containing 2.99 and 6.01 mol % of additional o-H_2, respectively. Squares and diamonds correspond to the p-H_2 samples containing additional HD of 0.072 mol % and D_2 of 0.10 mol %, respectively. All the initial yields were normalized to 10.

Fig. 3 Decay rate constant of H_2^- anion in γ-rays irradiated solid p-H_2 containing additional HD or D_2 impurities. Open and closed circles, fitted by solid lines, indicate the decay rate constants of p-H_2^- and o-H_2^- as a function of concentration of HD molecule in p-H_2, respectively. Open and closed squares, fitted by dashed lines, indicate the decay rate constants of p-H_2^- and o-H_2^- as a function of total concentration of D_2 molecule and natural abundance of HD (0.03 mol %).

Fig. 4 ESR spectrum of γ-rays-irradiated solid hydrogen mixtures at 4.2 K with low microwave power of 5 nW. (a) p-H_2- D_2(10 %), (b) p-H_2-HD(10 %), and (c) p-H_2. g-value of the singlet peak is very close to 2.0023. The broad peak in these spectra are due to color centers of irradiated quartz cell.

Fig. 5 Microwave power saturation behavior of the singlet peak in Fig. 4(a) at 4.2 K. Closed squares in the inset indicate microwave power saturation behavior of H_2^- anions in solid p-H_2 at 4.2 K.

Fig. 6 Relative amount of H_2^- anions in X-rays irradiated solid p-H_2 at 2.9, 4.5, and 6.6 K as a function of storage time. The vertical scale has been made logarithmic. All the initial yields were normalized to 1000.

Fig. 7 Decay rate constants of H_2^- anions in X-rays-irradiated solid p-H_2 in the temperature range between 2.7-6.6 K. The horizontal and vertical scales have been made logarithmic. Error-bars indicate standard deviations. Accuracy of the temperature is ±0.2 K. Solid curve is obtained by fitting to the function: $D(T) = D_1 (\Theta_D / T)^{\alpha} + D_2 \exp(-E_a / kT)$ with parameters, $D_1 = 9.7\times10^{-12}$ s^{-1}, Θ_D = 100 K, α = 4.9 , D_2 = 250 s^{-1}, and E_a / k = 92 K.

Table I: Decay rate constant of H_2^- anions and initial yields of H_2^- anions and H atoms in X-rays irradiated p-H_2 at 4.5 K.

Irradiation time (min)	17	150
Initial yields of H_2^- (arb. unit)	0.43	3.5
Initial yields of H (arb. unit)	2.5×10^3	2.3×10^4
Decay rate constant of H_2^- (sec^{-1})	$(6\pm3)\times10^{-5}$	$(3.8\pm.2)\times10^{-5}$

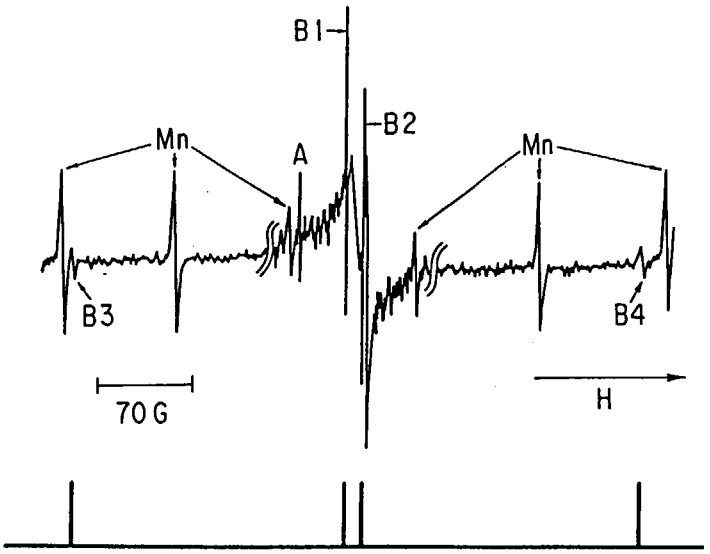

Fig. 1

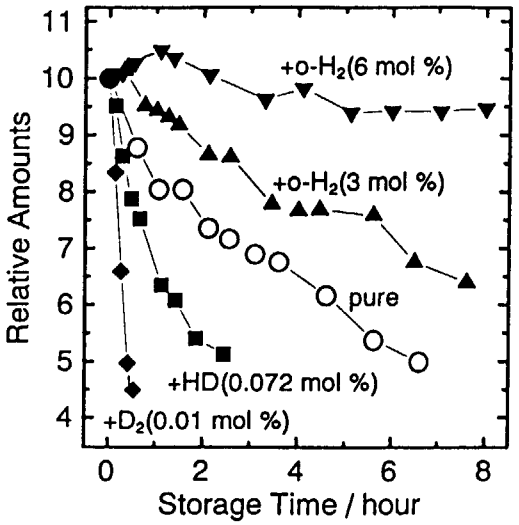

Fig. 2

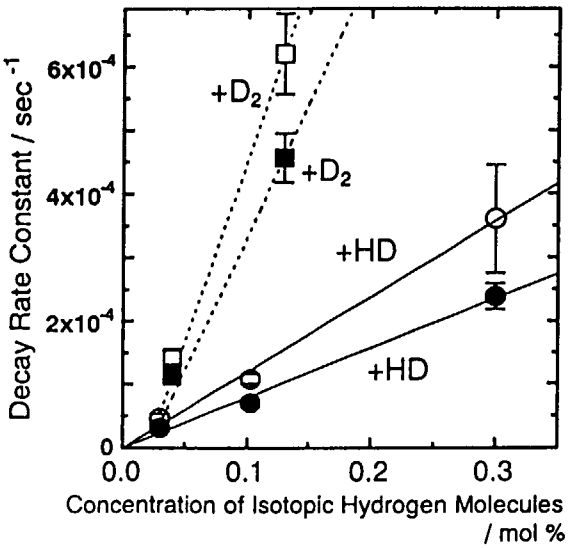

Fig. 3

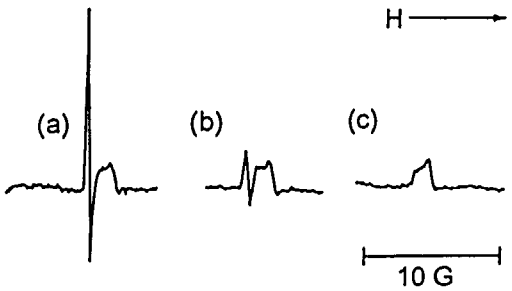

Fig. 4

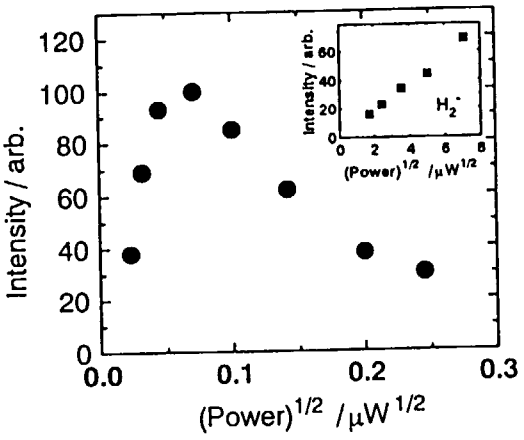

Fig. 5

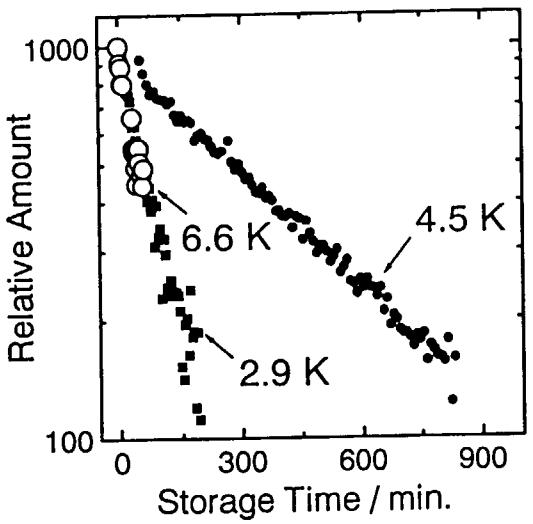

Fig. 6

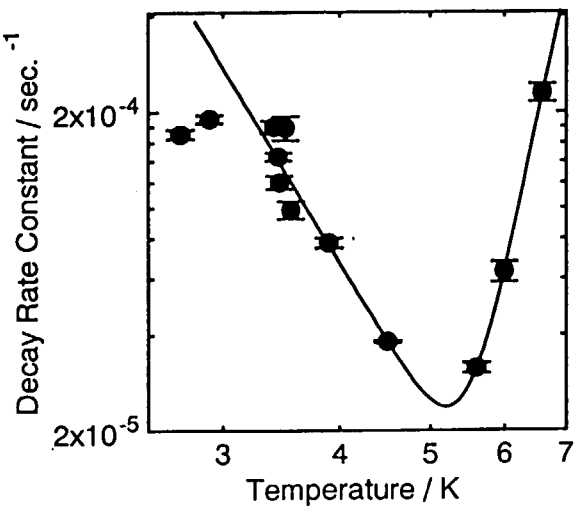

Fig. 7

2. Mechanism of H_2^- Formation in Solid Hydrogen

Tsuneki Ichikawa,[a] Hiroto Tachikawa,[a] Jun Kumagai[b],
Takayuki Kumada[b] and Tetsuo Miyazaki[b,c]

[a] Division of Molecular Chemistry, Graduate School of Engineering, Hokkaido University, Sapporo, 060 Japan

[b] Advanced Science Research Center, Japan Atomic Energy Research Institute, Tokai-mura, Ibaraki, 319-11 Japan

[c] Department of Applied Chemistry, School of Engineering, Nagoya University, Nagoya, 464-01 Japan

Abstract

The singlet and the triplet ESR lines with the common g-factor of 2.0023 and the hyperfine coupling constant of 20.3 mT observed after γ-irradiation of crystalline para hydrogen at 4.2 K agreed with the expected ESR spectra of the radical anions of the para and the ortho hydrogen molecules, respectively. A novel model has been proposed for explaining the formation and stabilization of H_2^- in crystalline H_2. The model assumes H_2^- to be located at the center of a cavity which has previously been occupied by a trapped electron. The excess electron of H_2^- is forced to be attached on one H_2 in the cavity due to strong repulsive interactions between the excess electron and H_2 molecules surrounding the cavity. A quantum-mechanical calculation shows that an electron trapped in the vacancy of crystalline H_2 automatically converts to H_2^- by drawing one of the surrounding H_2 molecules into the center of the vacancy.

Introduction

The radical anion of hydrogen molecule, H_2^-, is expected to be the simplest molecular anion. However, because of its instability, the molecular property of the anion has not been extensively studied. H_2^- may have two electrons in a bonding $1\sigma_g$ orbital and one electron in an antibonding $1\sigma_u$ orbital, so that it is expected to be stable. However because of strong repulsive interactions among electrons, H_2 is highly electro-repulsive and H_2^- in the gas phase releases its excess electron within 10^{-14} s.[1,2]

Recently Miyazaki et al. proved the presence of stable ortho and para H_2^- in a γ-irradiated solid para H_2 crystal[3,4]. They succeeded in detecting the singlet ESR line of ortho H_2^- with the g factor of ca. 2.003 and the quartet ESR lines of para H_2^- with the hyperfine coupling constant of 20.3 mT, which is in good agreement with that predicted by Symons.[5] The observed hyperfine coupling constant is smaller than a half of that of H (50.8 mT), which shows the expansion of 1s orbitals due to the excess charge of H_2^-.

Although the observed ESR hyperfine structure strongly suggests the formation of H_2^-, there are two evidences which do not support the presence of H_2^-. One is the discrepancy between the observed and the theoretical g–factors. The observed hyperfine coupling suggests that the unpaired electron of H_2^- is in a $1\sigma_u$ orbital composed of 1s–like atomic orbitals. The positive shift of the g–factor from that of the free electron (2.0023) indicates that the excited spin state inducing the positive shift is generated by the excitation of one electron from $1\sigma_g$ to $1\sigma_u$. However, since the σ states have no angular momentum, no spin-orbit coupling is expected by the excitation. The g–factor of H_2^- should therefore be very close to 2.0023. Recently Bruna et al. made an ab initio calculation on the ESR g-factors of free H_2^-, and found a large discrepancy between the calculated and the observed g factors.[6]

The other difficulty is the stability of H_2^-. H_2^- embedded in crystalline H_2 as a substitutional–type impurity may give its excess electron to one of nearby H_2 molecules very quickly. The hopping rate of the excess electron and therefore the decay rate of H_2^- is expected to be very fast even the electron is occasionally trapped on a H_2 molecule. The lifetime of H_2^- in neat para-hydrogen at 4.2 K is, however as long as 10 hrs.[7]

In this paper, we would like to report that the observed g–factor is not 2.003 but 2.0023, and to propose that the observed singlet and triplet lines are due to H_2^- which is stabilized at the center of a cavity in crystalline H_2 due to very strong repulsive

interactions between the excess electron of H_2^- and H_2 molecules surrounding the cavity.

Determination of ESR g-factor

The ESR g-factor of H_2^- in γ-irradiated para-hydrogen at 4.2 K was determined with a X-band ESR spectrometer equipped with a calibrated Gauss meter and a microwave frequency meter. The obtained g-factor was 2.0023, which accorded well with the expected g-factor of H_2^-. The error in the previous measurement was found to arise mainly from the inaccuracy of the magnetic field.

Model and calculation

Figure 1 shows our model on the formation and stabilization of H_2^- in crystalline H_2. Crystalline H_2 generally contains many vacancies. Vacancies or cavities with enough potential depth and radius can trap free electrons to generate trapped electrons. The zero-point energy of trapped electrons, E_t is derived from [8]

$$\sqrt{V_0 - E_t} = -\sqrt{U_p(r_c) + E_t}\,\cot\left[\sqrt{\frac{2m\{U_p(r_c) + E_t\}}{\hbar^2}}\,r_c\right] \qquad (1)$$

where V_0 is the minimum energy of free electrons in a medium, r_c is the radius of a vacancy or cavity and is 0.218 nm for crystalline H_2, and $U_p(r_c)$ is the polarization potential arising from dipole interactions between the electron and the medium, and is

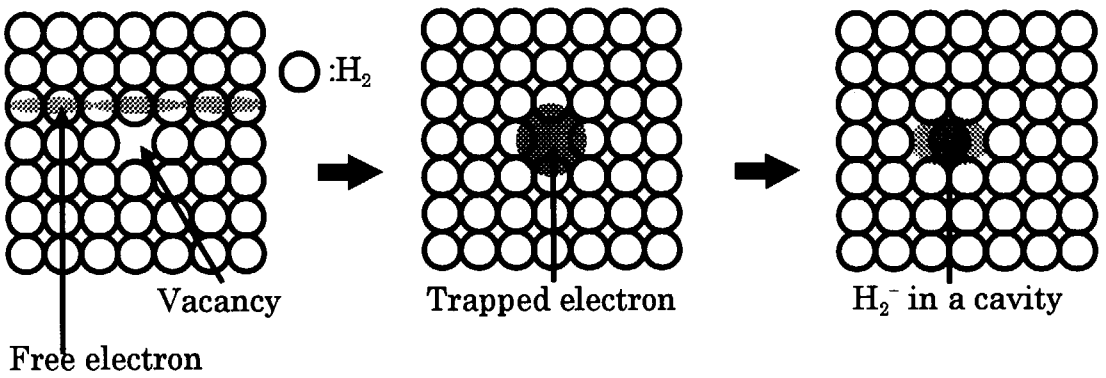

Fig. 1. Schematic representation of the process of H_2^- formation in crystalline H_2. A free electron generated by ionizing radiations is first trapped in a vacancy. The trapped electron then pick up one of the adjacent H_2 molecule to convert to H_2^-.

approximately given by

$$U_p(r_c) = \frac{e^2(D_{op}-1)}{2D_{op}r_c} \qquad (2)$$

Here D_{op} is the optical dielectric constant of the medium and is 1.34 for crystalline H_2. The value of V_0 for liquid H_2 has been estimated by a photoelectron emission study to be larger than 2 eV.[9] Assuming V_0=2 eV for crystalline H_2, the zero-point energy of a localized electron in a vacancy of crystalline H_2 is estimated to be 1.82 eV. Conversion of free electrons into trapped electrons, e_t^- , is therefore a spontaneous exothermic reaction.

The observed anionic specimen is, however, not e_t^- but H_2^-. H_2^- can be generated from e_t^- by transferring a H_2 molecule from the wall of the vacancy to the center of the resultant cavity. Although H_2^- in vacuum automatically dissociates into H_2 and a free electron, H_2^- in crystalline H_2 can be stabilized in the cavity due to very strong repulsive interaction between the excess electron of the anion and surrounding H_2 molecules. The heat of H_2^- formation, E_f, from e_t^- is defined as the difference of total energies between the $H_2 + e_t^-$ state and the trapped H_2^- state ,$H_{2,t}^-$, as

$$E_f = E_{H2,t^-} - (E_{H2} + 1.82eV) \qquad (3)$$

The total energy of $H_{2,t}^-$ depends on the potential curve. Assuming H_2^- to be trapped in a spherical cavity with a volume corresponding to two H_2 molecules, the potential energy for $H_{2,t}^-$ is estimated by a first-order perturbation method, as

$$\begin{aligned} U_{H2,t^-}(R) &= U_{H2^-}(R) - \int_0^{r_c} \psi(R,r)U_p(r_c)\psi(R,r)d^3r + \int_0^{r_c} \psi(R,r)V_0\psi(R,r)d^3r \\ &= U_{H2^-}(R) - [U_p(r_c)+V_0]\rho(R,r_c) + V_0 \end{aligned} \qquad (4)$$

Here R is the bond length of H_2^-, r_c = 0.275 nm is the radius of the cavity, $U_{H2^-}(R)$ is the potential energy of H_2^- in vacuum, $\psi(R,r)$ is the wave function of the excess electron of H_2^-, and $\rho(R,r_c)$ is the density of the negative charge of H_2^- in the cavity.

The energies and the wave functions of H_2^- have been calculated quantum-mechanically by using several types of basis sets.[10-17] One of the fundamental difficulties for the calculation is that the result strongly depends on the basis set. Since H_2 has negative electron affinity, the most stable state for H_2^- is obviously a ground-state neutral H_2 molecule with a ground-state free electron. For preventing the

dissociation of H_2^- into H_2 and a free electron, it is necessary to eliminate a free electron-type basis set and to use only an atomic orbital-type basis set. This very artificial confinement of electrons around two protons inevitably causes strong dependence of the calculated result on the basis set. The purpose of the present study is, however, not to calculate the correct energy of H_2^- but to know whether H_2^- is possible to be trapped in crystalline H_2. Selection of a basis set is not so critical for this purpose as long as a wave function obtained satisfies the criterion of excess electron localization on a H_2 molecule. Fig. 2 shows the potential curves of H_2 and H_2^- as calculated with the double substituted coupled cluster (CCD) method with 6-311++G(3d,3p) basis set.[18] The Fermi contact term and the value of $\rho(R,r_e)$ are shown in Fig. 3 for representing the characteristics of the wave function of the excess electron of H_2^-. The Fermi term increases with R and approaches a plateau value of about a half of that of the H atom, which implies that H_2^- becomes H^- + H at $R=\infty$. As shown in Fig. 2, H_2^- is more stable than the H_2 + free electron state at $R=\infty$, because the H atom has an electron affinity of 0.754 eV.[19] The H^- + H state, however, has the highest potential energy. With decreasing R the H^- + H state gradually converts to the H_2 + free electron state, accompanying the expansion of the orbital of the excess electron. Although the most stable state of H_2^- is H_2 + free electron, the calculated potential energy of the most stable H_2^- is higher than that of H_2 + free electron. This is simply because the wave function of a free electron is not included in the ab initio calculation of H_2^-.

Fig. 4 compares the potential curves for $H_{2,t}^-$ and $H_2 + e_t^-$. The potential curve for $H_{2,t}^-$ was obtained by substituting the value of $\rho(R,r_e)$ in Fig. 3 into Eq. (4). The potential curve for the $H_2 + e_t^-$ state was obtained simply by adding 1.82 eV to the potential energy of H_2. It is evident from the figure that $H_{2,t}^-$ is potentially more stable than $H_2 + e_t^-$. Since the curvature of the potential energies near the equilibrium bond length is similar for H_2 and $H_{2,t}^-$, it is reasonable to assume that the zero-point vibrational and probably the rotational energies of H_2^- in the cavity are approximately the same as those of H_2. The heat of $H_{2,t}^-$ formation is then positive and the conversion of e_t^- to $H_{2,t}^-$ becomes a spontaneous exothermic process.

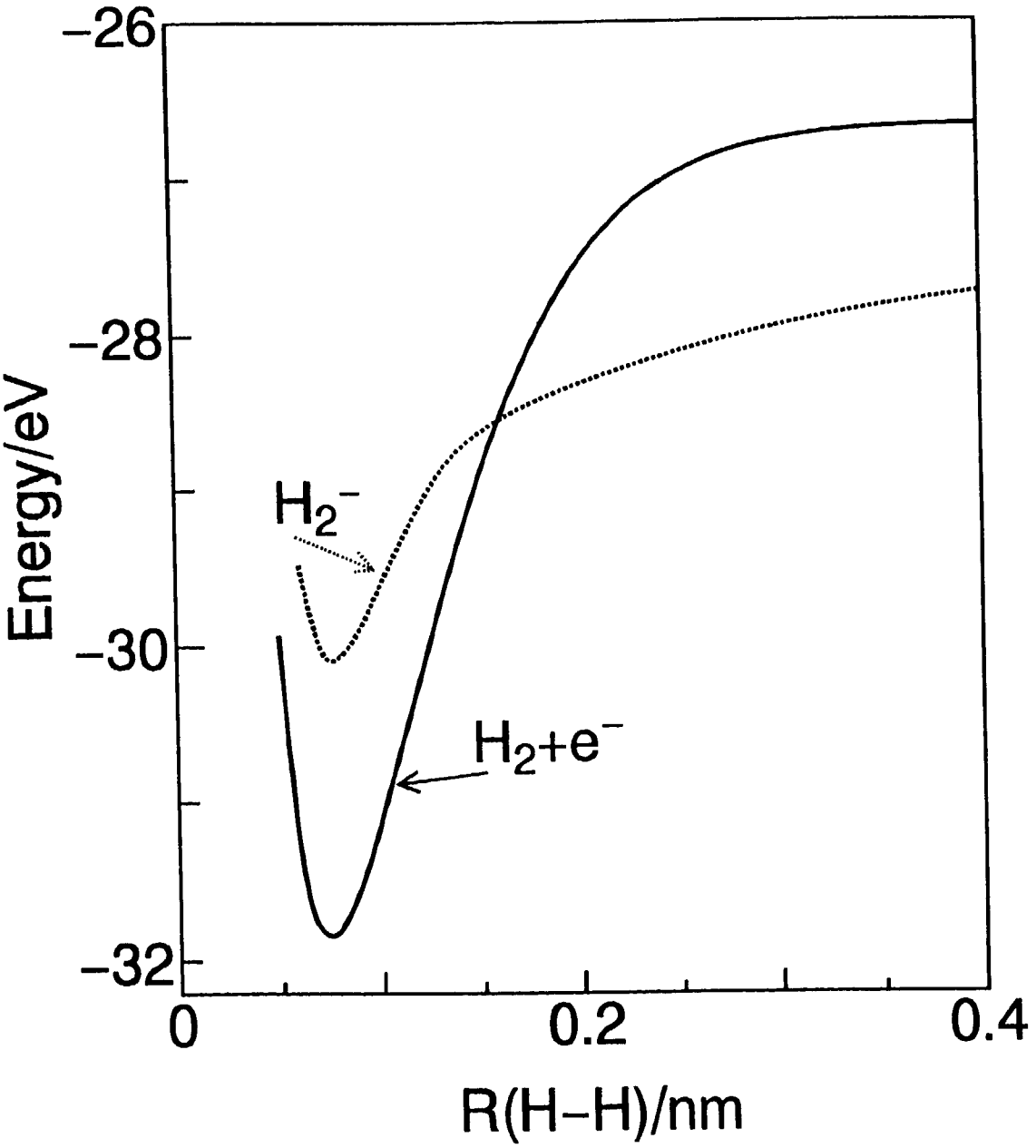

Fig. 2. Potential curves for free H_2^- and free H_2 + free electron with zero kinetic energy.

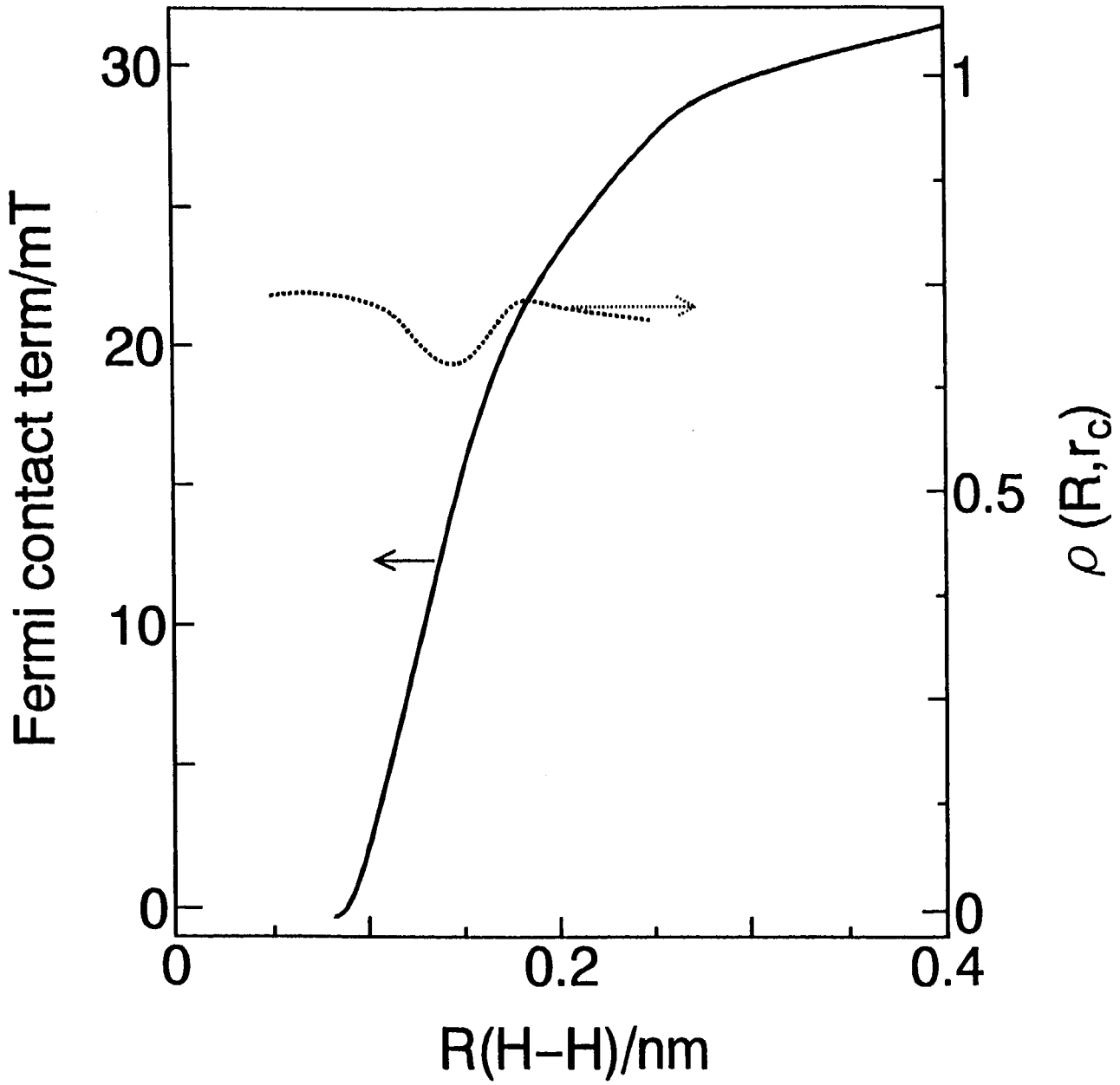

Fig. 3. Fermi contact term and the density of the excess electron of free H_2^-, $\rho(R,r_c)$, within the radius of r_c=0.275 nm, .

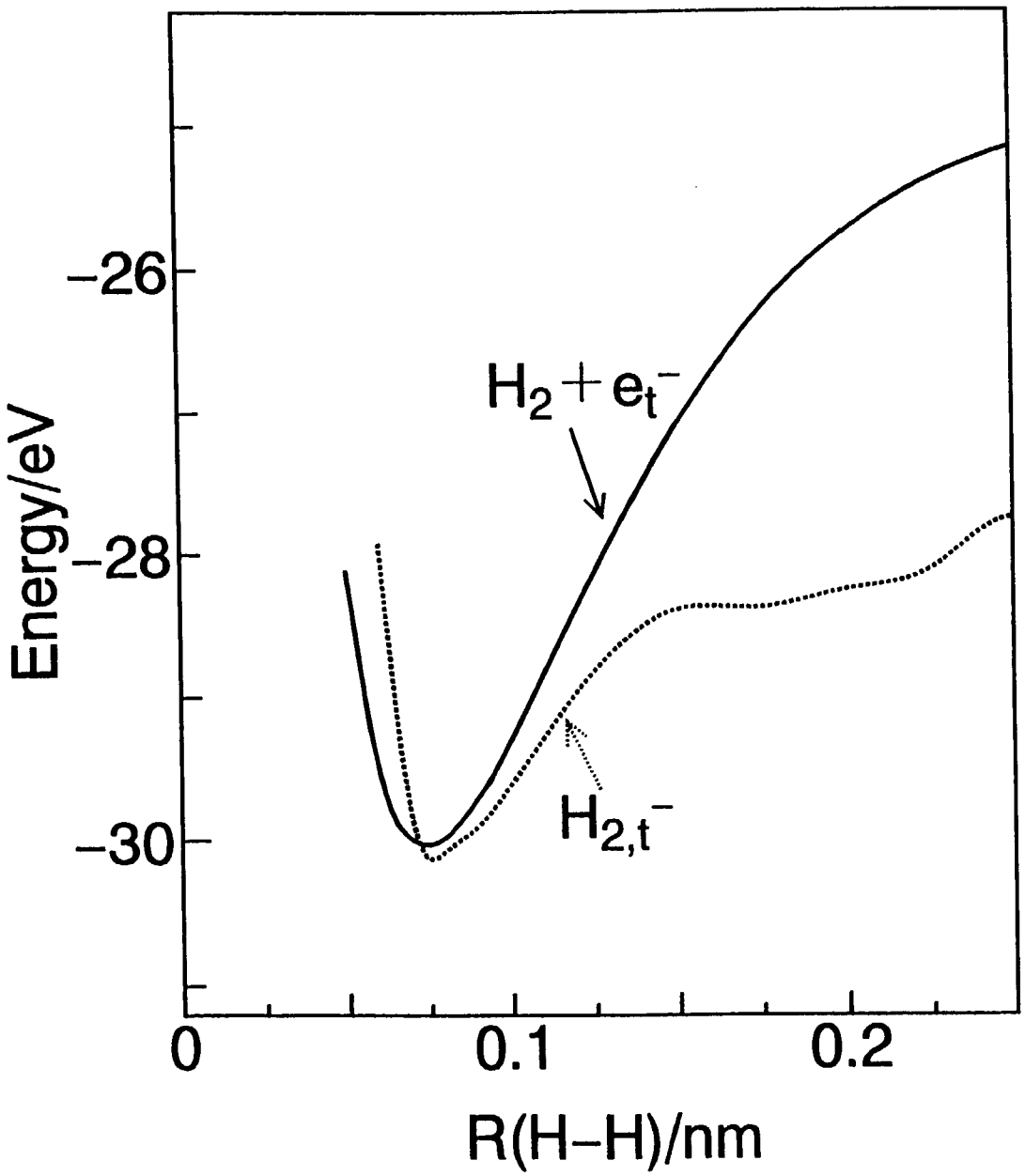

Fig. 4. Comparison of the potential curves of $H_2 + e_t^-$ (trapped electron) in a vacancy with the radius of 0.218 nm and H_{2t}^- (trapped H_2^-) in a cavity with the radius of 0.275 nm.

Discussion

The simple quantum-mechanical calculation shows that H_2^- is generated and trapped in crystalline H_2 by the exothermic reaction of the trapped electron and H_2. The actual heat of H_{2t}^- formation is probably much higher than the calculated one, since the wave function used is not accurate enough for expressing the observed H_{2t}^- state. The observed Fermi contact term for H_{2t}^- is 20.3 mT, which indicates that the excess electron is mainly in the 1s orbitals of two H atoms. However the orbital used for the calculation of H_{2t}^- at the optimum configuration is not s-type, since the calculated Fermi term at the optimum configuration is zero. The heat of H_{2t}^- formation can be increased by using a variation method instead of the perturbation one. However, the calculation becomes more complex.

Our model also answer the question why the excess electron of H_2^- does not migrate freely in crystalline H_2. The excess electron can migrate freely if it is located in the homogeneous (defect free) region of crystalline H_2. However, since H_2^- is stabilized in a cavity, migration of the excess electron needs the migration of the cavity.

Radiation-chemical reactions taking place by γ-irradiation of crystalline H_2 are,

$$H_2 + \gamma \rightarrow H_2^+ + e^-, \quad H_2^+ + H_2 \rightarrow H_3^+ + H,$$
$$e^- + H_3^+ \rightarrow H_2 + H, \quad e^- + \otimes \rightarrow e_t^-,$$
$$e_t^- + H_2 \rightarrow H_{2t}^-.$$

where ⊗ denotes a vacancy. The stability of thus generated H_{2t}^- depends on the rigidity of a cavity trapping H_2^-. H_{2t}^- may dissociates into H_2 and e_t^- if the medium is soft enough for allowing the expansion of the cavity, since the stability of e_t^- increases with increasing cavity radius.

References

(1) Buchelkinov, N.S. *Usp. Fiz. Nauk*, **1958**, 65, 351.

(2) Schulz, G.L. *Rev. Mod. Phys.* **1973**, 45, 423.

(3) Miyazaki, T. ; Yamamoto, K. ; Aratono, Y. *Chem. Phys. Lett.* **1995**, 232, 229.

(4) Kumada, T. ;Inagaki, H.; Nagasawa, T.; Aratono, Y.; Miyazaki, T. *Chem. Phys. Lett.* **1996**, 251, 219.

(5) Symons, M.C.R. *Chem. Phys. Lett.* **1995**, 247, 607.

(6) Bruna, P.J.; Lushington, G.H.; Grein, F. *Chem. Phys. Lett.* **1996**, 258, 427.

(7) Kumada, T.; Inagaki, H.; Kitagawa, N.; Komaguchi, K.; Aratono, Y.; Miyazaki, T. *J. Phys. Chem.* **1997**, 101, 1198.

(8) Ichikawa, T.; Yoshida, H. *J. Chem. Phys.* **1980**, 73 , 1540.

(9) Halpern, B.; Lekner, J.; Rice, S.A. *Phys. Rev.* **1967**, 156, 351.

(10) Van der Hart, J.A; Mulder J. *Chem. Phys. Lett.* **1979**, 61, 111.

(11) McCurdy, C.W. *Phys. Rev.* **1982**, A25, 2529.

(12) Senekowich, J.; Rosmus, P.; Domcke, W.; Werner, H.J. *Chem Phys. Lett.* **1984**, 11, 211.

(13) Sabelli, N.H.; Gislason, E.A. *J. Chem. Phys.* **1984**, 81, 4002.

(14) Derose, E.; Gislason, E.AQ.; Sabelli, N.H. *J. Chem. Phys.* **1985**, 82, 4577.

(15) Roach, A.C.; Kuntz, P.J. *J. Chem. Phys.* **1986**, 84, 822.

(16) Derose, E.F.; Gislason, E.A.; Sabelli, N.H.; Sluis K.M. *J. Chem. Phys.* **1988**, 88, 4878.

(17) Shalabi, A.S. *Mol. Phys.* **1995**, 85, 1033.

(18) Ab-initio MO calculation program, Gaussian 92, Revision F.3, M. J. Frisch, G. W. Trucks, M. Head-Gordon, P. M. W. Gill, M. W. Wong, J. B. Foresman, B. G. Johnson, H. B. Schlegel, M. A. Robb, E. S. Replogle, R. Gomperts, J. L. Andres, K. Raghavachari, J. S. Binkley, C. Gonzalez, R. L. Martin, D. J. Fox, D. J. Defrees, J. Baker, J. J. P. Stewart, and J. A. Pople, Gaussian, Inc., Pittsburgh PA, **1992**.

(19) Peckeris, C.L. *Phys. Rev.* **1962**, 126, 1470.

3. Infrared Spectroscopic Study on a Tunneling Chemical Reaction in Solid Parahydrogen

Takamasa Momose
Division of Chemistry, Graduate School of Science, Kyoto University, Kyoto 606-01, JAPAN

Solid parahydrogen is found to be a useful matrix for matrix isolation spectroscopy because it allows both high-resolution rotation-vibration spectroscopy in favorable cases [1-6] and kinetic study of photolysis of embedded molecules [7-9]. In a series of our work on alkyl iodides in parahydrogen matrix [7-9] we have shown that the iodide is easily photolyzed as in the gas phase which is in contrast to conventional rare gas matrices. The feasibility of *in situ* photolysis in parahydrogen matrix is attributed to the fact that the solid parahydrogen is a quantum solid having 1) a large lattice constant, 2) a large amplitude of zero-point lattice vibration, and 3) a large thermal conductivity.

Here we report that CD_3 radical derived from the photolysis of CD_3I in solid parahydrogen is subjected to the reaction $CD_3 + H_2 \rightarrow CD_3H + H$ at 5K [10]. Since the thermal activation for the reaction at 5 K is prohibitive with an activation energy of 10.9 Kcal/mol ($\cong$3700cm^{-1}) [11], the occurrence of the reaction is ascribed exclusively to quantum tunneling.

Figure 1 shows the infrared absorption spectrum of a parahydrogen crystal doped with CD_3I before UV irradiation (a), after 3 hours UV irradiation (b), and after a subsequent standing for about two days at 5K(c). Traces a, b, and c show the spectral regions of CD_3I, CD_3 and CD_3H, respectively. It is clearly seen that the peaks of CD_3 radical produced by the UV photolysis diminish after the standing with the appearance of the absorption of CD_3H. The decrease of the absorption of CD_3 radical and the increase of the absorption of CD_3H are synchronous as plotted in Figure 2. The ordinate in Figure 2 is the logarithms of the absorption intensity I. The t=0 in Figure 2 corresponds to the time when the UV irradiation light is tuned off. Due to the noise and the uncertainty of the background absorption the accuracy of the intensity measurement is estimated roughly as ±5%. From the plots the first-order reaction rate constant of $CD_3 + H_2 \rightarrow CD_3H + H$ is determined to be $(3.2\pm0.2)\times10^{-6}$ s^{-1}. The rate determined here is the rate constant of the pure tunneling process.

It is noted that the binding energy of hydrogen molecules in the crystal is only 2.9 cm^{-1} resulting in the large amplitude of the zero point vibration as large as 18% of the lattice constant. The

tunneling process is induced by the overlap of the wavefunction of hydrogen molecule due to this large amplitude of the zero point vibration.

The present work is partially supported by the Grant-in-Aid for Scientific Research of the Ministry of Education, Science, Culture and Sports in Japan.

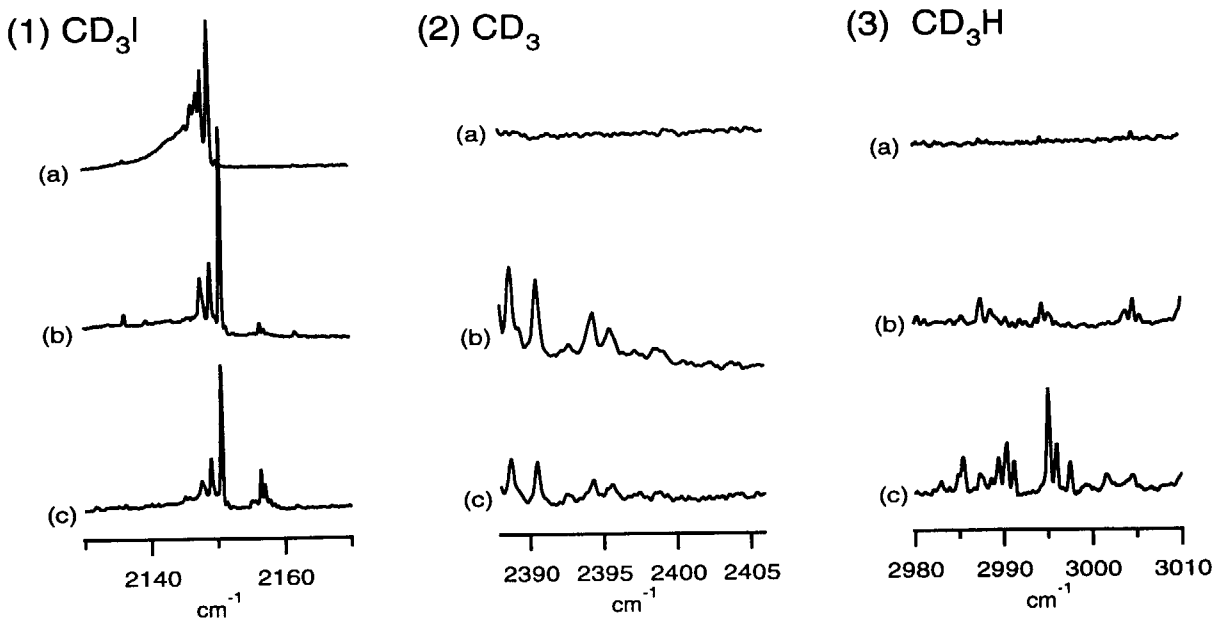

Figure 1. Infrared absorption spectra of (1) CD_3I, (2) CD_3, and (3) CD_3H. In each figure traces (a), (b), and (c) corerspond to the spectrum before UV irradiation, after UV irradiation, and after standing 36 hours, respctively.

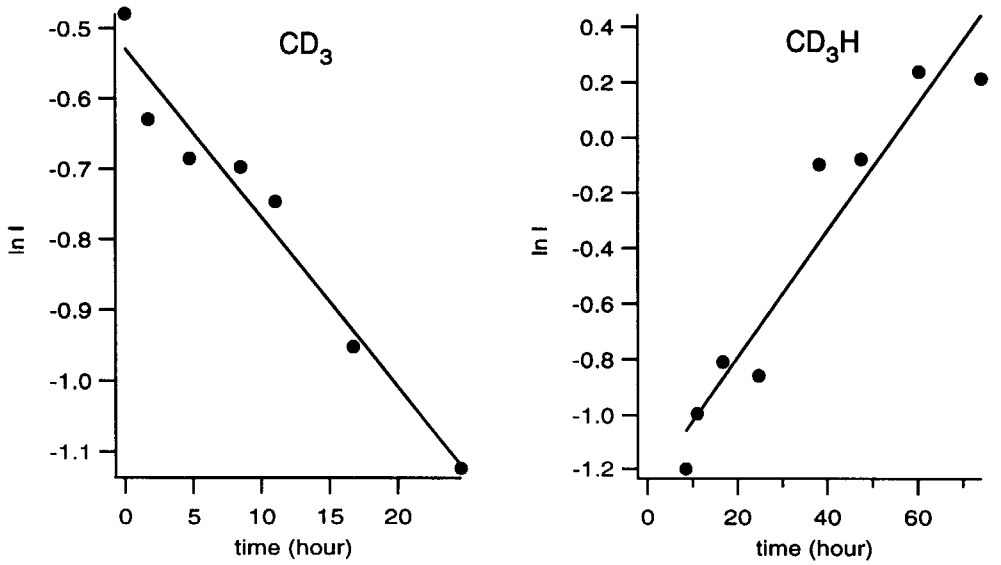

Figure 2. Decay of CD_3 (left) and appearance of CD_3H (reight).

References

1. D. P. Weliky, K. E. Kerr, T. J. Byers, Y. Zhang, T. Momose, and T. Oka, *J. Chem. Phys.* **105** , 4461 (1996).

2. M. Miki, T. Wakabayashi, T. Momose, and T. Shida, *J. Phys. Chem.* **100**, 12135 (1996).

3. T. Momose, M. Miki, T. Wakabayashi, T. Shida, M.-C. Chan, S. S. Lee, and T. Oka, *J. Chem. Phys.* **107**, Nov. 15 (1997).

4. T. Momose, *J. Chem. Phys.* **107**, Nov. 15 (1997).

5. T. Momose, H. Katsuki, H. Hoshina, N. Sogoshi, T. Wakabayashi, and T. Shida, *J. Chem. Phys.* **107**, Nov. 15 (1997).

6. T. Momose and T. Shida, Bull. Chem. Soc. Jpn. (Jan. 1998)

7. T. Momose, M. Miki, M. Uchida, T. Shimizu, I. Yoshizawa, and T. Shida, *J. Chem. Phys.* **103**,

1400 (1995).

8. T. Momose, M. Uchida, N. Sogoshi, M. Miki, S. Masuda, and T. Shida, *Chem. Phys. Lett.* **246**, 583 (1995).

9. N. Sogoshi, T. Wakabayashi, T. Momose, and T. Shida, *J. Phys. Chem.* **101A**, 522 (1997).

10. T. Momose, H. Hoshina, Katsuki, N. Sogoshi, T. Wakabayashi, and T. Shida, *to be submitted.*

11. E. Kraka, J. Gauss, and D. Cremer, *J. Chem. Phys.* **99**, 5306 (1993).

4. Structures and Properties of Dense Hydrogen

Hitose Nagara[1,2], Kazutaka Nagao[1], and Hiroshi Miyagi[1,2]
[1] *Division of Materials Physics, Department of Physical Science, Graduate School of Engineering Science, Osaka University, Toyonaka, Osaka 560, JAPAN*
[2] *CREST, Japan Science and Technology Corporation (JST)*
(October 13, 1997)

(Abstract)

Detecting the metallic transition in the compressed hydrogen has long been one of the central interest. Recent experiments on the molecular hydrogen have revealed rich phases at megabar pressures and substantial increase in the electrical conductivity in liquid phase at megabar pressures. At low temperatures, however, the metallic behavior has not been detected up to around 2.5 Mbar. Centered on our recent study on the structures in the atomic phase and that on the Raman and infrared active vibrational modes in the molecular phase, recent experimental and theoretical studies have been reviewed briefly.

I. INTRODUCTION

For a long time the metallic hydrogen has been attracting astro-physicists. In these days, however, the experiments on hydrogens up to several megabars have been done in our laboratories. Wigner and Huntington [1] were the first to state, in their pioneering theoretical work, that the molecular hydrogen go over to the metallic state under pressure. Many articles followed to predict theoretically the transition pressure and the properties of the metallic hydrogen or to detect the metallic hydrogen experimentally.

A hydrogen atom consists of a nucleus and one electron. So, as a standard textbook [2] on the solid state theory predicts, when hydrogen atoms form a crystal in which each primitive cell contains one hydrogen atom, the crystal is a metal very much like an alkaline metal. From the point of view of the band theory, the electronic band in such a crystal is half-filled where each of the lower half of the electronic states is occupied by two electrons with up and down spin states. In the partially filled band, the electrons can move around by infinitesimally small amount of excitation energy, i.e. metallic. In the solid molecular hydrogen, on the other hand, where the crystal consists of the molecule which have two electrons, the electronic bands are formed from completely filled lower bands and empty upper bands separated by a band gap. In such bands, the electron needs the excitation energy larger than the energy gap to move around the crystal.

Under very high pressures, however, the solid hydrogen can become metallic. This is because the electronic bands become broad and the band gap becomes small under the pressure, and at very high pressure the band gap disappear and some electrons in the lower bands transfer to the empty bands, leaving partially filled bands.

In most of earlier studies, they thought that the metallization might occur by the molecular dissociation i.e. a transformation into an atomic crystal like an alkaline crystal, and studied the lattices of the hydrogen atoms. Many theoretical studies were done based on the many body perturbational expansion [3–6]. The results are exact at high density limits. However, the perturbational treatments become difficult owing to slow convergence at lower densities or the singularities contained in the expansion for some kind of structures. After Barbee III *et al.* [7]'s first principles LDA calculation supporting the anisotropic structures [3] predicted by the many body perturbational expansion and the prediction of the hcp structure in the molecular phase [7], many first principles band theoretical studies on the structures and properties in the molecular phase have followed. The band theory can treat the molecular phase and the atomic one on the same foot, so it is preferable to discuss the transitions between those two phases [8,9].

Meanwhile, the intensive experimental studies have been performed by the use of diamond-anvil cell techniques up to megabar pressures [10]. Rich phases in the molecular phase has been reported by the optical measurements such as the Raman and infrared spectroscopy, though the structures are not yet determined [10,11]. Very recently, the X-ray diffraction experiments have confirmed the hcp lattice of the molecular centers up to $\sim$ 120 GPa (1 Mbar = 100 GPa) at room temperature [12]. And the low-lying rotational and librational modes together with the high-lying vibron and the phonon modes have become clearer by the infrared (IR) and Raman measurements [13–15]. However, the evidences for the metallic transition in the solid hydrogen has not been confirmed up to around 220 GPa [14,15]. It is probable that the molecules persists over 200 GPa judging from the persistence of the vibron peak there [10].

In the liquid phase also, a substantial increase in the electric conductivity in the liquid hydrogen has been reported by the shock compression experiments [16].

We give, in this article, results of our recent theoretical studies on the structures in the atomic phase with review of the former theoretical studies.(Sec. II) In the next sec-

tion, we present results of our recent theoretical studies on the Raman and infrared active modes in the molecular phase with some recent experiments on the molecular solid hydrogen.(Sec. III) In the final section, we briefly introduce recent experiments on the liquid hydrogen by the shock compression.

II. ATOMIC SOLID PHASE

So far any evidences of the molecular dissociation has been observed experimentally. And the most of the studies on the atomic phase at low temperature are theoretical. The crystal structures in the atomic phases as well as the molecular ones are essential to the prediction of the pressures for the molecular dissociation at low temperatures.

While the earlier studies were based on the many body perturbational expansion [3–6]. many recent theoretical studies have been done mainly by the band theoretical approach [7,9,17] based on the local density approximation(LDA). And the quantum Monte Carlo(QMC) calculations [18] also have been carried out.

However, owing to vanishingly small energy differences among structures together with the possible large effects of the zero point motion of the atoms, predicting the stable structures has been a difficult task.

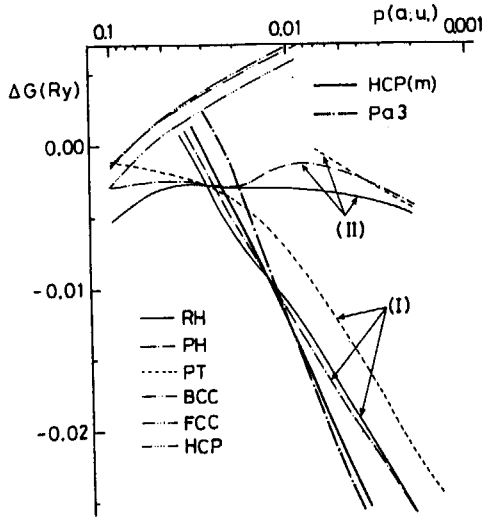

FIG. 1. Free energy diferencies relative to SC in the atomic phase with Pa3 and m-hcp structures in the molecular phase.(1 a.u.= 14.7 TPa.)

We compare in Fig.1 the free enery among structures in the atomic phase. At pressures of celestial interests, the dominant contribution to the structural energy is from the Madelung energy, which prefers the densely packed structures, for which the bcc structure is lowest. As the pressure decreases the electronic energy begins to play a significant role which leads the structure to less densely packed ones, and the possibilities of the anisotropic structures was first pointed out based on the structural expansion [3,4].

According to our LDA calculation [8] in the atomic phase, the bcc structure becomes stable beyond 4 TPa and the hexagonal-close-packed(hcp) in the region 2 TPa $\sim$ 4 TPa. These pressure regions are high compared with other results [7,18], which is due to the presence of the region of "planar" structures [8]. In the early studies, based on the many body perturbational expansion, Brovman *et al.* [3] predicted the "filamentary" structure in the atomic phase, and Barbee *et al.* [7] supported its stability and showed the possibility of high temperature superconductivity [19].

However, Natoli, Martin, and Ceperley [18] later performed the QMC and LDA calculations for atomic phases of compressed hydrogen at zero temperature, and reported no region of the anisotropic structures and the diamond structure to be stable in the atomic phase. We also performed the detailed study of the total energy for the structures of compressed hydrogen using band theoretical calculation based on the LDA, with special concern for the structures in the tetragonal diamond family.

The β-Sn, the cubic diamond, and the Cs-IV structure belong to the tetragonal diamond family. They transform into each other by the stretch or compression along the c-axis of the rectangular unit cell. The Madelung energy of the diamond is located at the local maximum. So the diamond structure must become unstable at higher densities.

From our total energy calculation we obtained low energy structures. In Fig.2 we compare the Gibbs free-energy at T = 0 (enthalpy) with those studied earlier [9,8] and those in the molecular phase to be explained in the next section. The β-Sn structure is the lowest at pressures lower than 360 GPa and the Cs-IV structure becomes the lowest in the region 360 GPa $< P <$ 1700 GPa. There are no stable region for the γ-nitrogen structure. At 1700 GPa, the Cs-IV structure transforms into another "planar", rh(II), structure [8].

Our results do not include the zero point energy of the proton motion. But there are some reasons [20] that the present Cs-IV structure ($c/a \sim 3.0$) might not become higher owing to the high zero-point motion energy, as Straus and Ashcroft [21] showed for the anisotropic structures.

There are no stable region of pressure for the anisotropic structures for which possibilities of high temperature superconductivity has been predicted [19].

III. MOLECULAR SOLID PHASE

After the possibility of the metallization by the band overlap in the molecular phase has been reported by an experiment, many theoretical calculations have been done for the structures in the molecular phase. The experimental results showed no evidences of apparent phase change from hcp structure of molecular center up tp 150

GPa at which vibron drop of about 100 cm^{-1} has been observed as an indication of the phase transition.

We studied again varieties of supposed structures and calculated the LDA total energies and compared with the free energy (enthalpy) [9]. The results are shown above in Fig.2. The results show that the structures with hcp lattice of the molecular centers have low energies. The lowest energy structure is $Pca2_1$ in which the molecules are canted from the c-axis. The $Pca2_1$ structure allows some more optimization of the structure with respect to, for example, c/a and the displacements of the molecular center within the $Pca2_1$ symmetry. The later calculations supported our results for the structures with hcp lattice of the molecular centers.

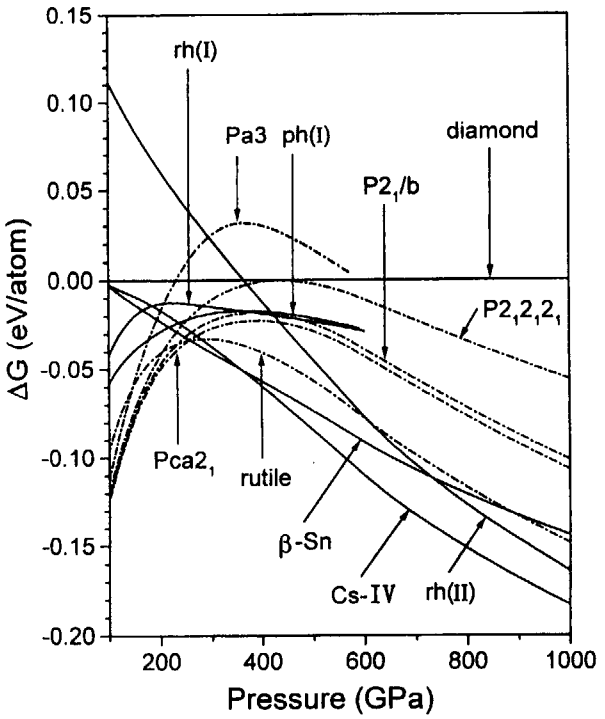

FIG. 2. Free energy differencies, $\delta G = G - G_{diamond}$ per atom. The solid lines represent the curves for the atomic phase and the dot-broken lines for the molecular phase.

In the experimental side, the vibron, libron, and some phonon modes have been studied in the molecular phase for pure para(p)-hydrogen, pure ortho(o)-deuterium, and ortho-para(o-p)-mixed systems at megabar pressures [10,14,15,22–24]. For hydrogen (deuterium) para designates the even (odd) J and ortho the odd (even) J species.

Carnegie group [10] performed the experiments mainly on mixed systems and reported three phases in the solid hydrogen under pressure and degignated by phases I, II, and III while Harvard group [22] performed the experiments with special concern with the para- ortho- concentration. They also reported three phases and for para-hydrogen they called them low pressure symmetric phase, broken symmetry phase(BSP), and Hydrogen-A(H-A) [D-A for ortho-Deuterium].

While experimental data on the Raman and infrared active vibrational modes which restrict the possible structures in the molecular phase at megabar pressures have accumulated, we have rather small number of theoretical studies on the frequencies of vibrational modes at megabar pressures [22,25–28]. We performed the theoretical studies of the vibrational modes to understand the behavior of experimentally obtained vibrational modes and to help determine the structures in the molecular phase at megabar pressures.

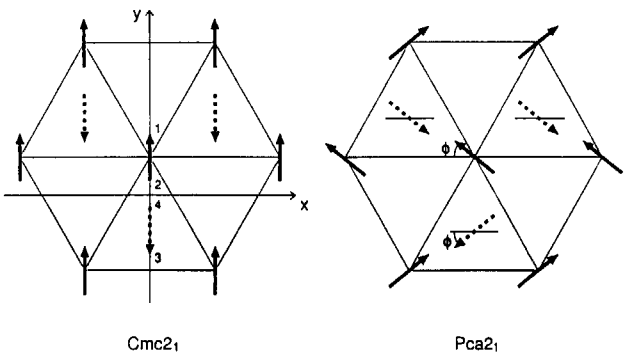

FIG. 3. The structures studied for the vibrational modes

We diagonalized the dynamical matrices obtained by frozen-phonon method and the Hellman-Feynman theorem [29] for some modes specified by the group theory.

Since the lattice of the solid hydrogen has not been determined experimentally at megabar pressures and at low temperatures, we studied the structures with hcp lattice of the centers of the molecules, assuming some candidate molecular orientations in the lattice.

We first study intensively the $Cmc2_1$ structure [22] which is shown in Fig.3 with the $Pca2_1$ structure studied in the present paper. This structure was first studied by Kaxiras, Broughton, and Hemley [30] to be of lowest energy in the structures they had studied. Later this structure, which corresponds to the special case of the $Pca2_1$ structure with the azimuthal angle, $\phi = 90°$, is shown to have slightly higher energy than the $Pca2_1$ [9,31].

In Fig.4 we show, for H_2 of the $Cmc2_1$ structure, the pressure dependencies of the frequencies for some modes. The pressures on the abscissa are obtained from the equation of state from our total energy calculation [9], which is $\sim$ 200 GPa at r_s=1.4, $\sim$ 120 GPa at r_s=1.5, and $\sim$ 70 GPa at r_s=1.6. One of the remarkable points of the results is the B_2 phonon-like mode, which lies in the frequency region of 1400 $\sim$ 1900cm^{-1}. This mode is IR

as well as Raman active and corresponds to the motion of the molecular centers along the z-axis. An IR active mode has been observed experimentally for pure p-H_2 in this frequency region in the phase III, although the peak has not been detected in the phase II [14]. At room temperature where the system is a o-p mixed crystal, an IR peak has been observed also in this frequency region at pressures 30 $\sim$ 180 GPa [23].

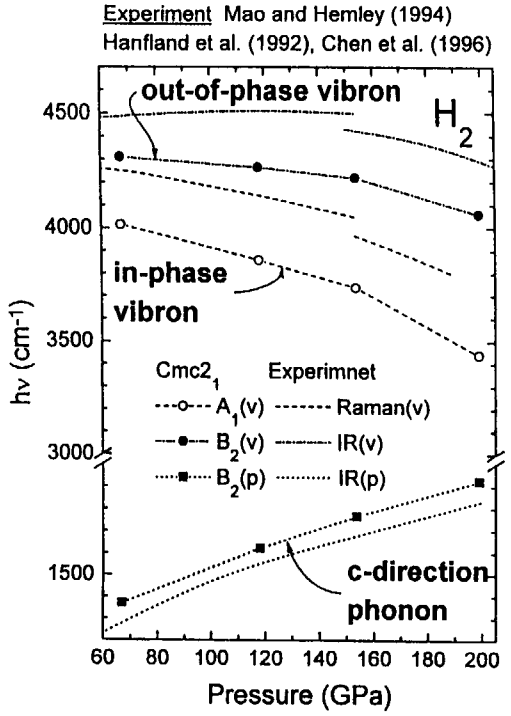

FIG. 4. The pressure dependencies of the vibrational modes for the $Cmc2_1$

Another point is that the B_2 vibron, which corresponds to the out-of-phase stretching mode of the two molecules in the unit cell, has higher frequency than the A_1 vibron corresponding to the in-phase stretching mode, with the frequency difference $\sim 480cm^{-1}$ at 150 GPa. This difference is in good agreement with that experimentally observed value, $\sim 430cm^{-1}$, between the IR vibron and the Raman one, at the same pressure. The calculated B_2 and A_1 vibron frequencies themselves are about 5 % lower than the experimental ones [10,22], which may be attributed to the LDA. We note here that the frequency difference comes from the molecular interaction in the system containing the molecules of the same bond length, which is in contrast to a result of the first-principles molecular dynamics (MD) where the longer and shorter molecules exist in the system [27].

The other modes remain in the low frequency region of $\leq$ 1000 cm^{-1} up to the pressure $\sim$ 200 GPa, though one of the B_2 modes grows to $1300cm^{-1}$ at $\sim$ 200 GPa, which is the librational motion in the y-z plane.

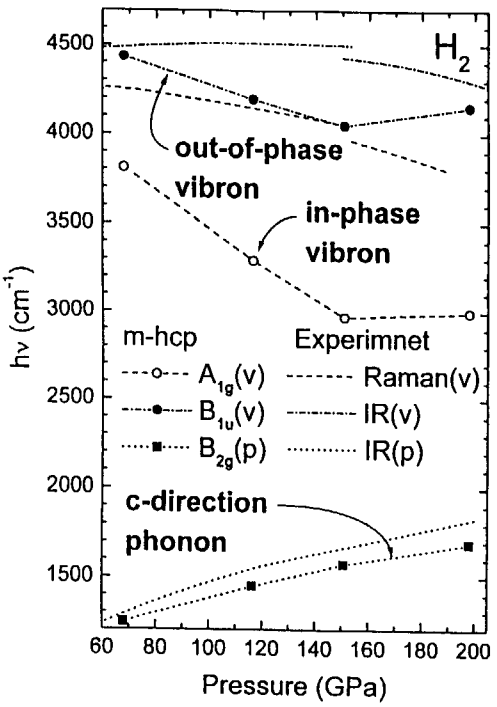

FIG. 5. The pressure dependencies of the vibrational modes for the m-hcp

To study further the properties of the above mid-lying B_2 phonon-like mode, we performed the similar calculation for the m-hcp ($P6_3/mmc$) structure by setting the polar angle $\theta = 0°$ in the $Cmc2_1$ structure. The pressure dependencies of the frequencies are shown in Fig.5. The B_2 phonon-like mode shows the similar pressure dependence with that of the B_2 phonon-like modes in the $Cmc2_1$, with lower frequency (by $200cm^{-1}$ at 200 GPa) than that in the $Cmc2_1$. This result shows that the mid-lying B_2 phonon-like mode is rather insensitive to the orientation of the molecule and is a characteristic of the solid molecular hydrogen in the hcp lattice at high pressures. However the behavior of the pressure dependencies of the frequencies of the vibronic modes in the m-hcp deviates appreciably from the experimental ones for both vibrons.

We studied further the $Pca2_1$ structure shown in Fig.3. The pressure dependencies are shown in Fig.6. In this structure also, the mid-lying phonon mode shows good agreement with the experiments. As observed in the $Cmc2_1$ structure, the frequency difference between the two vibronic modes also is in good agreement with experiments at $\sim$ 70 GPa but is smaller by $\sim$ 100 cm^{-1} at 150 GPa.

Our results suggest that the lattice of the centers of molecules is hcp and the molecules are canted from the

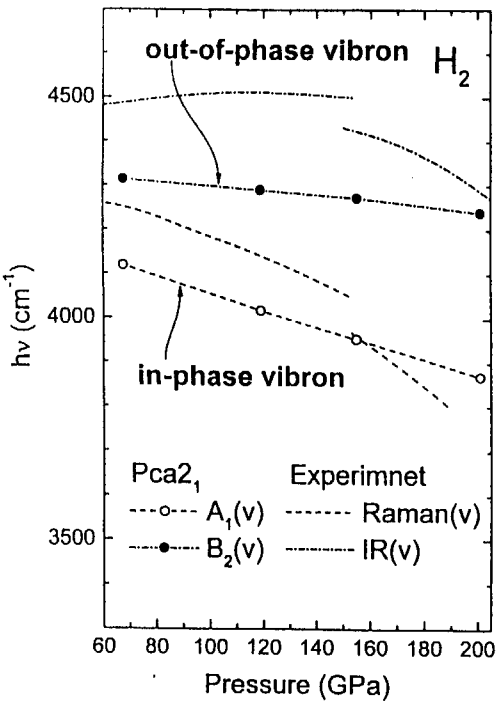

FIG. 6. The pressure dependencies of the vibrational modes for the $Pca2_1$

c-axis in the solid molecular hydrogen at megabar pressures.

Above $\sim$ 150 GPa, where the vibron drop has been observed, it has been suggested that more overall optimization is needed because the experiments show the evidences of the increase of anisotropic force on the molecular site. The intensive studies are under way using the recent first principles MD technique [28].

IV. LIQUID MOLECULAR PHASE

The recent shock experiments revealed decrease in the resistivity about four orders of magnitude [16] (Fig.7). The temperature estimated in the experiments is around 2000K-4000K. The melting temperature reaches to room temperature at several GPa. The molecules at above temperature are thought to be in the liquid states. The resisitivity reduced to a value typical of liquid metals. This results are thought to change the former estimated values especially in the field of the plasma physics and astrophysics.

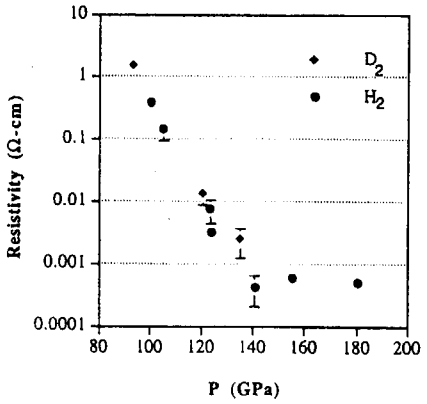

FIG. 7. The decrease in the electrical resistivity for fluid hydrogen.

[1] E. Wigner and H. B. Huntington, J. Chem. Phys. **3**, 764 (1935).

[2] See for example, J. M. Ziman, *Principles of the theory of solids* Cambridge (1972).

[3] E. G. Brovman, Yu. Kagan, and A. Kholas, Sov. Phys. JETP **34**, 1300 (1972). This is the first extensive studies of the structures in the atomic phase.

[4] For the many body perturbational expantion, see for example, T. Nakamura, H. Nagara, and H. Miyagi, Prog. Theor. Phys. **63**, 368 (1980), and references therein.

[5] H. Nagara, H. Miyagi, and T. Nakamura, Prog. Theor. Phys. **64**, 731 (1980).

[6] For the perturbational expantional expansion based on the density functional theory, see H. Miyagi, T. Hatano, and H. Nagara, J. Phys. Soc. Japan, **57**, 2751 (1988).

[7] T. W. Barbee III *et al.*, Phys. Rev. Lett. **62**, 1150 (1989).

[8] H. Nagara, J. Phys. Soc. Jpn. **58**, 3861 (1989).

[9] H. Nagara and T. Nakamura, Phys. Rev. Lett. **68**, 2468 (1992).

[10] H. K. Mao and R. J. Hemley, Rev. Mod. Phys. **66**, 671 (1994) and references therein.

[11] A. F. Goncharov *et al.*, Phys. Rev. Lett. **75**, 2514 (1995).

[12] P. Loubeyre *et al.*, Nature, **383**, 702 (1996).

[13] I. I. Mazin *et al.*, Phys. Rev. Lett. **78**, 1066 (1997).

[14] N. H. Chen, E. Sterer, and I. F. Silvera, Phys. Rev. Lett. **76**, 1663 (1996).

[15] R. J. Hemley *et al.*, Phys. Rev. Lett. **76**, 1667 (1996).

[16] S. T. Weir, A. C. Mitchell, and W. J. Nellis, Phys. Rev. Lett. **76**, 1860 (1996).

[17] B. I. Min, H. J. F. Jansen, and A. J. Freeman, Phys. Rev. B**33**, 6383 (1986). 3

[18] V. Natoli, R. M. Martin, and D. M. Ceperley, Phys. Rev. Lett. **70**, 1952 (1993) and references therein.

[19] T. W. Barbee III and M. L. Cohen, Phys. Rev. B**43**, 5269 (1991).

[20] K. Nagao, H. Nagara and S. Matsubara, Phys. Rev. B**56**, 2295 (1997).

[21] D. M. Straus and N. W. Ashcroft, Phys. Rev. Lett. **38**, 415 (1977).
[22] L. Cui, N. H. Chen, and I. F. Silvera, Phys. Rev. B**51**, 14987 (1995). The structure $Pmc2_1$ in their Table I should be rather identified to be $Cmc2_1$; L. Cui *et al.*, Phys. Rev. Lett. **72**, 3048 (1994).
[23] M. Hanfland *et al.*, Phys. Rev. Lett. **69**, 1129 (1992).
[24] M. Hanfland, R. J. Hemley, and H. K. Mao, Phys. Rev. Lett. **70**, 3760 (1993).
[25] J. H. Eggert, H. K. Mao, and R. J. Hemley, Phys. Rev. Lett. **70**, 2301 (1993); M. I. M. Scheerboom and J. A. Schouten, Phys. Rev. B**53**, R14705 (1996).
[26] M. P. Surh, T. W. Barbee III, and C. Mailhiot, Phys. Rev. Lett. **70**, 4090 (1993)
[27] J. S. Tse and D. D. Klug, Nature **378**, 595(1995).
[28] J. Kohanoff *et al.*, Phys. Rev. Lett. **78**, 2783 (1997).
[29] See, for example, J. C. Slater, J. Chem. Phys. **57**, 2389 (1972).
[30] E. Kaxiras, J. Broughton, and R. J. Hemley, Phys. Rev. Lett. **67**, 1138 (1991).
[31] I. I. Mazin and R. E. Cohen, Phys. Rev. B**52**, R8597 (1995).

5. Tunneling Abstraction Reactions of Tritium Atoms with HD and with mixtures of H_2 and D_2 in Super-and Normalfluid ^{3}He-^{4}He media at 1.3K

Y. Aratono,[1] T. Matsumoto,[2] T. Takayanagi,[1] T. Kumada,[1] K. Komaguchi,[3] and T. Miyazaki[1,2]

1 Advanced Science Research Center, Japan Atomic Energy Research Institute, Tokai-mura, Ibaraki-ken 319-11, Japan

2 Department of Applied Chemistry, School of Engineering, Nagoya University, Furo-cho, Chikusa-ku, Nagoya 464-01, Japan

3 Faculty of Engineering, Hiroshima University, Higashi Hiroshima 739, Japan

The abstraction reactions, T + HD(DH) → HT(DT) + D(H) and T + H_2(D_2)→ HT(DT) + H(D) were studied experimentally in liquid ^{3}He-^{4}He media at 1.3 K and theoretically using the gas-phase reaction model. The experimental reaction system has two characteristics; one is that the tritium atom(T) is produced from one of the constituents, ^{3}He, through ^{3}He(n, p)T nuclear reaction and the other is that super- or normalfluid reaction medium can be chosen arbitrarily by changing the composition and temperature of the sample. The experimental isotope effect defined by {[HT]/[H_2]}/{[DT]/[D_2]} for the reactions T + H_2(D_2)→ HT(DT) + H(D) was found to be 158 in superfluid and 146 in normalfluid solutions, respectively. The large isotope effects observed were qualitatively explained via quantum mechanical tunneling on the basis of the theoretical calculations of thermal rate constants for these reactions. In the T + HD(DH) → HT(DT) + D(H) reactions, the experimental isotope effect was observed to be less than 19.8. From the considerations on both the reaction processes based on the experimental results and the theoretical calculations, it has been suggested that the quantum mechanical tunneling abstraction through van der Waals complex plays a predominant role for both the reactions.

Introduction

Liquid and solid helium are the most typical quantum media and show very significant quantum effects due to its small mass and very weak van der Waals interaction. Many peculiar phenomena of liquid helium arising from its quantum properties, such as superfluid, formation of snow ball, and electron bubble have been attracting many scientists. However, the studies have been focused mostly on the physical aspects such as spectroscopy of alkali atoms introduced by laser abrasion or ion implantation, motions of electrons, and cluster formation of helium with H_2.[1] The

observation of the chemical reactions in liquid helium medium has not been attempted previously.

The tunneling abstraction reactions by H and D in hydrogen molecules(H_2, HD, D_2, and their mixtures) have been investigated experimentally[2-6] in the solid state at very low temperature. However, no report has been published on the reaction in the liquid helium. One of the most difficult points in the study of the chemical reaction of hydrogen isotopes in the liquid helium is how to introduce reactive species in it and how to detect reaction products at very low concentration. In order to solve these difficulties, the nuclear activation method and radioactivity analysis of reaction products were successfully applied to the study of the reaction of T, which is one of the hydrogen isotopes, by choosing a mixture of 3He and 4He as a reaction medium. Helium-3(3He) has a very large activation cross section for thermal neutron(5.33 x 103 barns) to give T through 3He(n, p)T process. Since T is the radioactive nuclide emitting β-ray, even trace amount of tritiated products can be detected with high sensitivity. In addition, the mixture of 3He and 4He shows very interesting property, i.e., it takes super- or normalfluid state depending on the composition and temperature(Fig. 1). Therefore, the reaction medium can be chosen arbitrarily. In the present paper, by applying these characteristics, the abstraction reactions of T + HD(DH) → HT(DT) + D(H) and T + H_2(D_2) → HT(DT) + H (D) are experimentally investigated in the super- and normalfluid 3He - 4He mixtures from the viewpoint of how the chemical reaction of T proceeds in such a quantum liquid at ultralow temperature. Though there are some studies on the theoretical calculation of rate constants for the abstraction reactions of H or D with H_2, HD and D_2,[7-11] no report has been published on the rate constants of T with them. In the present work, theoretical calculation of the rate constants was carried out and the reaction mechanism is discussed both from the experimental results and from the theoretical prediction.

Experimental Section

Helium-3 was purchased from Isotec Inc. and isotopic enrichment was more than 99.9 atom %. Tritium content in the gas was below detection limit for the present T counting system. Deuterium gas(D_2) was also the product of Isotec Inc. and isotopic content of D was more than 99.96%. The purity of HD gas was 96 mol %. Main impurities in HD gas were H_2(2 mol %) and D_2(2 mol %). The purity of other gases was more than 99.999 %.

The mixture of 3He, 4He, and 1 mol % of the reactants, H_2, HD, D_2 or H_2 + D_2, was introduced into Pyrex glass reaction vessel(about 3.8×10^3 cm^3) with quartz-made irradiation tube(6 mm in inner diameter, 1 m in length) and cooled to 1.3 K. The atomic compositions of the liquefied solution were 3He : 4He = 0.670 : 0.330(normalfluid solution), and 3He : 4He = 0.282 :

0.718(superfluid solution).

Deuterization of OH group in the quartz-made irradiation tube was carried out by heating for 1 day at 1273 K under D_2 pressure of 4.4x104 Pa. The conversion of OH group to OD group was monitored by IR spectrometer.

Thermal neutron irradiation was performed at JRR-2(Japan Research Reactor No. 2) for about 50 hrs at 1.30±0.02K. Since the irradiation port was designed for neutron scattering experiment, γ-ray dose rate was very low and thus the secondary effect caused by γ-ray could be neglected. The thermal neutron flux measured by Au-foil activation method was 8.41x1010 m-2 sec-1. The irradiated sample was analyzed by radiogas chromatograph equipped with a gas-flow proportional counter. The reaction products, HT and DT, were separated at 77 K using γ-alumina column coated with Fe_2O_3. Typical gas chromatogram is shown in Fig. 2. A complete separation is seen for HT and DT. Total radioactivity was 1-2.5 x 10^4 counts for each experiment.

Results and Discussion

Product distribution and isotope effects for HT and DT formation

Table 1 shows the product distribution and isotope effects under the various experimental conditions. Though T is formed through the nuclear reaction with an initial kinetic energy of 192 keV, most of them are thermalized very efficiently before reaction by the successive collision with liquid helium due to close mass among T, ^{3}He, and ^{4}He and to very high concentration of ^{3}He and ^{4}He in the reaction medium. In addition, as the recoil range of T(14 μm) is very short compared with inner diameter of the quartz tube, almost all T is considered to react in the sample and thus the reaction with surface hydrogen can be neglected. This is supported by the experimental results in H_2 addition - deuterated quartz tube system, i.e., no DT was observed in spite of the deuterated quartz tube was used(first column in Table 1).

The effect of D_2 addition is very suggestive. In spite of no addition of H_2, 62.8±2.9 % of T is observed as HT. The most plausible source of H is considered to be impurity included in D_2 gas. If so, the result suggests a large isotope effect for HT and DT formation. In order to confirm the isotope effect definitely, a predetermined amount of H_2/D_2 was added in the system. A clear evidence of preferential formation of HT over DT was observed in this reaction system. From the yields of HT and DT shown in Table 1, the isotope effects, defined as $\{[HT]/[H_2]\}/\{[DT]/[D_2]\}$, were calculated to be 158 for superfluid and 146 for normalfluid solutions, which are also shown in the last column of Table 2 for comparison with higher temperature experiments.

Reaction mechanism

The possible pathways leading to the formation of HT and DT in $T + H_2 (D_2) \rightarrow HT(DT) + H(D)$ system can be considered as follows.

(1) formation of tritium

As T is formed through the nuclear reaction, it is initially in translationally excited(T*) state.

$$^3He + n \rightarrow T* + p \quad (1)$$

(2) thermalization of T*

T* loses its kinetic energy very efficiently by the successive collision with a large amount of 3He and 4He and is finally thermalized before subsequent reactions(reactions 3,4,7,and 8) occur. During thermalization, translationally and electronically excited state of He(He*) will be produced along the track of T.

$$T* + He \rightarrow He* + T \quad (2)$$

(3) formation of HT and DT

Two pathways are possible for the formation of HT and DT. One is the abstraction reaction of thermalized T with H_2 and D_2 (reactions 3 and 4) and the other one is the recombination of the thermalized T with H and D (reactions 7 and 8) which are formed by the energy transfer process from He* to H_2 and D_2(reactions 5 and 6).

$$T + H_2 \rightarrow HT + H \quad (3)$$

$$T + D_2 \rightarrow DT + H \quad (4)$$

$$He* + H_2 \rightarrow H + H + He \quad (5)$$

$$He* + D_2 \rightarrow D + D + He \quad (6)$$

$$T + H \rightarrow HT \quad (7)$$

$$T + D \rightarrow DT \quad (8)$$

First of all, we consider the processes (5) and (6). If the efficiency of the energy transfer from He* to H_2 and D_2 is different very much between (5) and (6), the subsequent recombination reactions (7) and (8) result in the preferential formation of HT or DT if the reactivity of (7) and (8) is identical. In order to evaluate the formation fraction of H against D, $[H]/([H]+[D])$, as a function of H_2 fraction, $[H_2]/([H_2]+[D_2])$, the amount of H and D was experimentally determined in γ-ray irradiated $Xe-H_2-D_2$(H_2+D_2=1 mol %) at 4.2 K and X-ray irradiated $Ar-H_2-D_2$(H_2+D_2=1 mol %) at 4.5 K by ESR spectroscopy. In these systems, Xe^* or Ar^* formed by γ- or X-ray absorption transfers their excited energy to H_2 and D_2 and decomposes them into H and D. Since these atoms cannot diffuse in the matrix at the experimental temperatures, the initial distribution of H and D is preserved in these systems.

The results are shown in Fig. 3. From the figure, it is clear that [H]/([H]+[D]) is approximately proportional to $[H_2]/([H_2]+[D_2])$. Therefore, the energy transfer efficiency from He^* is supposed to be nearly equal both for H_2 and D_2 and the preferential formation of HT over DT observed experimentally cannot be explained by the difference in the reactions (5) and (6) if the reactivities of (7) and (8) are identical.

In general, the isotope effect of recombination reaction between hydrogen isotopes is small. Even at ultralow temperature like the present case, the reactivity difference among hydrogen isotopes cannot be expected since the recombination is no-barrier radical-radical reaction, The recent experiment by Hyden et al. at ultralow temperature supports the above prediction.[12] They determined the gas phase recombination reaction rate constants $k_{H\cdot D}$ and $k_{D\cdot D}$ for $H + D + {}^4He \rightarrow HD + {}^4He$ and $D + D + {}^4He \rightarrow D_2 + {}^4He$ in the superfluid helium coated wall under zero magnetic field at around 1 K. They obtained $k_{H'D} / k_{D'D} = 1.03$. Thus, the preferential formation of HT over DT is not due to the difference in the recombination reactions (7) and (8).

In conclusion, the reactions (3) and (4) are supposed to be the most plausible processes to result in the very large isotope effects, $k_{(T+H2)}/k_{(T+D2)}$=158 for superfluid and 146 for normalfluid solutions, and the tunneling abstraction is considered to be the main reaction mechanism. The more detailed discussions on the reaction mechanism will be given in the later section together with the consideration of T + HD(DH) → HT(DT) + D(H) system by using the theoretical rate constants and the experimental results.

Comparison of isotope effects of the abstraction reactions of $T + H_2 \rightarrow HT + H$ and $T + D_2 \rightarrow DT + H$ at various temperatures

The isotope effects for $T + H_2(D_2) \rightarrow HT(DT) + H(D)$ above 77 K have been experimentally examined by some workers.[13-15] Table 2 summarizes the results including the present results. Though the isotope effects in the gas phase somewhat depend on the experimental conditions, the values lie below 2.7. On the other hand, the value of 7 obtained by some of the present authors at 77 K in highly moderated $Xe-H_2-D_2$ system is 2.5 times higher than those in the gas phase. This suggests the partial contribution of the tunneling in the abstraction reaction. The present results exceed by about two orders of magnitude over the gas phase values and are rather close to the isotope effects of the abstraction reactions of H and D in the solid H_2, D_2, and HD at around 4 K where the importance of the tunneling in the abstraction reaction was well established.[2-6]

Theoretical calculation of thermal rate constants for the $T + H_2$, D_2, and HD reactions

We employed gas-phase reaction rate theory to study isotope effect of rate constants at low

temperatures. As mentioned previously, the present experiment has been done in condensed phase, liquid He media. Although the use of the gas-phase reaction model is, of course, a crude approximation, there are important advantages for this. The first advantage is that highly accurate potential energy surface for the T reaction system is now available.[16] The second one is that computational methodology to calculate absolute values of the thermal rate constants has been well established. This means that we can obtain accurate thermal rate constants without any adjustable parameters if the potential energy surface is given.

The thermal rate constant, $k(T)$, for the bimolecular A + BC reaction is written as[17,18]

$$k(T) = \frac{1}{hQ_{\mathrm{int}}(T)Q_{trans}(T)} \sum_{J=0}^{\infty} (2J+1) \int_0^{\infty} N^J(E) e^{-E/k_B T} dE \qquad (9)$$

where J is the total angular momentum. $Q_{int}(T)$ and $Q_{trans}(T)$ are the internal partition function of BC and the relative translational partition function, respectively. h and k_B are Planck's constant and Boltzmann's constant, respectively. $N^J(E)$ is the cumulative reaction probability, which is the sum over all initial and final open channels, for total angular momentum J as a function of the energy, E.

The cumulative reaction probability, $N^J(E)$, can be calculated accurately using three-dimensional quantum scattering theory. We have employed a time-independent hypersphercal coulpled-channel method. The computaional code we used has been described in detail in Ref. 17. The scattering calculations were done only for $J = 0$ using the *ab initio* LSTH (Liu-Siegbahn-Truhlar-Horowitz)[16] potential energy surface. Figure 4 shows the $J = 0$ cumulative reaction probabilities for the T + H_2 and T + D_2 reactions as a function of energy which is measured from the ground ro-vibrational state of H_2 or D_2. As is expected, the cumulative reaction probability for T + H_2 is much larger than that for T + D_2 by a factor of 100 at low energies because the contribution of quantum mechanical tunneling for T + H_2 may be more significant.

In order to calculate accurate thermal rate constants below T < 100 K, we need to calculate $N^J(E)$ at very low energies. However, we could not obtain converged results at low energies where the cumulative reaction probabilty is less than 10^{-8} using our quantum scattering code. This is because the coordinate transfer from the hyperspherical coordinates to the Jacobi coordinates was not done in the asymptotic region; the reaction probability was calculated using simple averaging procedure.[17] In addition, we have to carry out the scattering calculations for $J > 0$ to obtain accurate thermal rate constants. Instead of these time-consuming calculations, we employed the reduced-dimensionality method[18,19] developed by Bowman to calculate the cumulative reaction probability at low energies. This method is essentially based on the two-dimensional collinear scattering model, where the rotational degree-of-freedom is treated as an adiabatic bending vibration during collision. Although fully state-to-sate information cannot be obtained from this method, Bowman shows that this approximate method gives reliable cumulative reaction probabilities for several chemical reactions such as D + H_2 for which accurate quantum scattering results are available. This indicates that the reduced dimensionality method also gives accurate thermal rate constants. The reduced dimensionality Schrödinger equation was numerically solved

using a standard R-matrix propagation on a natural collision coordinate system. Bending vibrational energies were calculated on all the two-dimensional grid points using a standard Harminic basis expansion method. The details of the computational procedure are described elsewhere.[9] The J-shifting approximation[18,19] was not employed in the reduced dimensionality calculations since it has been found that the rate constants at low temperatures are very sensitive to the choice of the rotational constant used in the approximation.

In Fig. 4 we compare the $J=0$ cumulative reaction probabilities for T + H_2 and D_2 calculated using the reduced-dimensionality theory with the accurate results. The agreement with accurate three-dimensional results is seen to be excellent. In addition, we could obtain converged cumulative reaction probability down to very low energies where the cumulative reaction probability is about 10^{-20}. Table 3 reports the calculated thermal rate constants in the temperature range 1.3-300 K for the T + H_2, D_2 and HD reactions. Figure 5 shows the Ahhrenius plot of the calculated thermal rate constants. Also plotted in Fig. 5 is the ratio of rate constants, $k_{(T+H_2)}/k_{(T+D_2)}$, because this value is important for the present experiment.

From Fig. 5 a significant curvature of the Ahhrenius plot is seen around 80 K for all the reactions. This result is consistent with the previous calculations[9,11] for other isotopic variants. The ratio of rate constants, $k_{(T+H_2)}/k_{(T+D_2)}$, is calculated to be larger than 10^6 below 50 K. This large isotope effect at low temperatures has also been reported in the comparison of the rate constants between D + H_2 and D + D_2.[9,11] It is interesting to note that the difference in the rate constants between the T + HD → HT + D and T + DH → TD + H is not so large for all the temperatures considered in this calculation. It may be expected that the rate constant for the former reaction would be larger than that for the latter reaction because quantum mechanical tunneling would be significant in light atom transfer. However, for these reactions, we found that this simple consideration cannot be applied from a reaction path analysis. For example, saddle point zero point energies of symmetric stretch and bending vibration for T + HD are found to be larger than those for T + DH. This indicates that the vibrational adiabatic barrier height for T + HD is larger than that for T + DH.

Consideration of reaction mechanism based on the experimental results and theoretical abstraction rate constants

Here, we discuss the reaction mechanisms of T + HD(DH) → HT(DT) +D(H) and T + H_2(D_2) → HT(DT) + H(D) (the reactions 3 and 4) based on the experimental results and theoretical abstraction rate constants shown in Table 3.

The experimental isotope effect for the abstraction reactions of T + HD→ HT + D and T + DH → DT + H was 19.8. In the present experimental system, H_2 and D_2 are included as the impurities. Therefore, HT and DT are produced not only by the reaction with HD but also by the

reactions with H_2 and D_2. The total processes leading to HT and DT formation can be written as,

$$T + HD \rightarrow HT + D \quad (10)$$

$$T + H_2 \rightarrow HT + H \quad (11)$$

$$T + DH \rightarrow DT + H \quad (12)$$

$$T + D_2 \rightarrow DT + D \quad (13)$$

The formation rate of HT and DT are expressed as,

$$d[HT]/dt = k_{10}[T][HD] + k_{11}[T][H_2] \quad (14)$$

and

$$d[DT]/dt = k_{12}[T][DH] + k_{13}[T][D_2], \quad (15)$$

where, k_{10}, k_{11}, k_{12}, and k_{13} are the rate constants of the reactions (10) – (13), respectively. Therefore, the isotope effect, [HT]/[DT], is written as,

$$[HT]/[DT] = \{ k_{10}[T][HD] + k_{11}[T][H_2]\}/\{k_{12}[T][DH] + k_{13}[T][D_2] \} \quad (16)$$

Since k_{13} is expected to be much lower than k_{12} (cf. Table 3) and the concentration of the impurity D_2 is much smaller than that of HD, $k_{13}[T][D_2]$ can be neglected in equation (16). However, $k_{11}[T][H_2]$ may be the same order of magnitude as $k_{10}[T][HD]$, since k_{11} is expected to be large in Table 3. Thus, a part of HT yields is formed by the reaction (11) in addition to the reaction (10). Therefore, the isotope effect(k_{10}/k_{12}) on the abstraction reactions (10) and (12) is probably much less than 19.8. The smaller isotope effect(ca. 0.4) is expected from the theoretical calculation in Table 3.

The large isotope effects of 158 and 146 on the reactions (3) and (4) is qualitatively explained by the large isotope effect of about 10^6(c.f. Fig. 5) calculated theoretically for the tunneling reactions (3) and (4). There exist, however, two questions on the tunneling reactions. First, why the experimental isotope effect is much smaller than the calculated values ? The second question is as follows: the experimental rate constant for the tunneling reaction $D + H_2 \rightarrow HD + H$ at 4K is 6×10^{-25} cm^3 $molecule^{-1}$ sec^{-1},[5] which is approximately similar to the theoretical rate constant(1.4×10^{-25} cm^3 $molecule^{-1}$ sec^{-1}) for the tunneling reaction $T + H_2 \rightarrow HT + H$ at 1.3 K. Then the frequency of the tunneling reaction T(D) + H_2 is about 1/60 sec^{-1}. Why does such a slow reaction take place in the liquid helium ?

The most plausible solution to the above questions might be given by taking the formation of a van der Waals complex prior to the abstraction reaction into consideration. Since the interaction of T and H_2 or D_2 has a long-range and attractive force and the experimental temperature is very low, the formation of a van der Waals complex $(T\cdots H_2)_{comp.}$ or $(T\cdots D_2)_{comp.}$ prior to the abstraction reaction is considered to be reasonable. Actually, the van der Waals complex of a hydrogen atom and a hydrogen molecule has been predicted theoretically[9, 20] and

observed experimentally very recently by the authors in tunneling reaction HD + D → H + D_2 in argon matrix at 20 K.[21] According to the ab initio calculation by Boothroyd et al.,[20] well depth of van der Waals interaction is reported to be 0.047 kcal mol^{-1}. The geometry at the minimum of the van der Waals Well is collinear and the distance between H and the center of mass of H_2 is to be 3.7A.. If we take the formation of this van der Waals complex into our kinetic model, the possible pathways leading to the formation of HT and DT may be expressed as follows,

$$T + H_2 + (He) \rightarrow (T\cdots H_2)_{comp.} - (reaction) \rightarrow HT + H \quad (17)$$

or the complex would dissociate by the collision with He,

$$(T\cdots H_2)_{comp.} + He - (dissociation) \rightarrow T + H_2 . \quad (18)$$

The similar reaction scheme will hold for $T + D_2$,

$$T + D_2 + (He) \rightarrow (T\cdots D_2)_{comp.} - (reaction) \rightarrow DT + H \quad (19)$$

$$\text{or} \quad (T\cdots D_2)_{comp.} + He - (dissociation) \rightarrow T + D_2 . \quad (20)$$

Although the branching ratio of the reaction to the dissociation has not been well known, it seems to be reasonable that the life time of $(T\cdots D_2)_{comp.}$ is longer than that of the complex $(T\cdots H_2)_{comp.}$ and thus the reaction (17) might prevail over the reaction (19) to lead to the preferential formation of HT.

As for the reaction rate, the question on the higher rate at 1.3K still remains. However, it seems that the interaction of T with H_2 or D_2 within the complex surrounded by liquid helium promotes the reaction. Further theoretical and experimental investigations are necessary for the quantitative understanding of the reaction mechanism.

Conclusion

The abstraction reactions, T + HD(DH) → HT(DT) +D(H) and T + $H_2(D_2)$ → HT(DT) + H(D) were studied at 1.3 K by introducing T directly through the nuclear reaction of $^3He(n, p)T$ in super− and normalfluid ^3He−^4He media. The rate constants of the above abstraction reactions were theoretically calculated using the gas−phase reaction model. Based on the experimental isotope effects and theoretical rate constants, the tunneling abstraction reaction through van der Waals complex has been proposed. This is the first experimental study on the chemical reactions in quantum liquid helium. The more detailed study using the superfluid helium as a new solvent for chemical reaction is now in progress.

Acknowledgements

The authors thank to Mr. Minagawa H. and Mr. Shimojyo M. of Neutron Scattering Research Group of Japan Atomic Energy Research Institute for their many advices in neutron

irradiation and to Dr. Yonezawa C. and Mr. Sasajima F. for their help in activation analysis of Au-foil. The present research was supported in part by a Grant in Aid for Scientific Research from the Japanese Ministry of Education, Science and Culture.

References

(1) "Proceedings of the 128th WE-Heraeus-Seminor on Ions and Atoms In Superfluid Helium" *Zeitschrift fur Physik*, 1995, B 98.

(2) Miyazaki, T.; Lee, K. P.; Fueki, K.; Takeuchi, A. *J. Phys. Chem.*, 1984, *88*, 4959.

(3)Miyazaki, T; Iwata, N.; Lee, K. P.; Fueki, K. *J. Phys. Chem.*, 1989, *93*, 3352.

(4) Miyazaki, T. *Radiat. Phys. Chem.*, 1991, *37*, 635.

(5) Miyazaki, T.; Kitamura, S.; Morikita, H.; Fueki, K. *J. Phys. Chem.* 1992, *96*, 10331.

(6) Kumada, T.; Komaguchi, K.; Aratono, Y.; Miyazaki, T. *Chem. Phys. Lett.*, 1996, *261*, 463.

(7) Takayanagi, T; Nakanura, K; Sato, S. *J. Chem. Phys.* 1989, *90*, 1641.

(8) Takayanagi, T; Masaki, N; Nakanura, K; Okamoto, K; Sato, S; Schatz, G. C. *J. Chem. Phys.* 1987, *86*, 6133.

(9) Takayanagi, T; Sato, S, *J. Chem. Phys.* 1990, *92*, 2862.

(10) Takayanagi, T; Masaki, N. *J. Chem. Phys.* 1991, *95*, 4154.

(11) Hancock, G. C.; Mead C. A.; Truhlar D. G.; Varandas A. J. C. *J. Chem. Phys.* 1989, *91*, 3492.

(12) Hayden, M. E.; Hardy. W. N.. *J. Low Temp. Phys.* 1995, *99*, 787.

(13) Miyazaki, T.; Fujitani,Y.; Shibata, M.; Fueki, K. ; Masaki, N. M.; Aratono, Y.; Saeki, M.; Tachikawa, E. *Bull. Chem. Soc. Jpn.* 1992, *65*, 735.

(14) Lee, J. K.; Musgrave, B.; Rowland, F. S. *J. Chem. Phys.* 1960, *32*, 1266.

(15) Chou, C. C.; Rowland, F. S. *J. Chem. Phys.* 1967, *46*, 812

(16)Liu, B. *J. Chem. Phys.* 1973, *58*, 1925. Siegbahn, P.; Liu, B. *J. Chem. Phys.* 1978, *68*, 2457. Truhlar, D.G.; Horowitz, C.J. *J. Chem. Phys.* 1978, *68*, 2466; 1979, *71*,1514(E).

(17)Takayanagi, T; Kobayashi, H; Tsunashima, S. *J. Chem. Soc., Faraday Trans.* 1996, *92*, 1311.

(18) Bowman, J. M. *J. Phys. Chem.*, 1991, *95*, 4960

(19) Bowman, J.M.; Wagner, A.F. *The Theory of Chemical Reaction Dynamics*. Clary, D.C. Ed.; Reidel: Dordrecht, 1986; pp. 47-76.

(20)Boothroyd, A. I.; Keogh, W. J.; Martin, P. G.; Peterson M. R. *J. Chem. Phys.*, 1991, *95*, 4343.

(21) Komaguchi K.; Kumada, T.; Aratono Y.; Miyazaki T. *Chem. Phys. Lett.* 1997, 493-497.

Table 1 Distribution of HT and DT under the various experimental conditions and experimental isotope effects

^{3}He:^{4}He	state	additives	HT (%)	DT (%)	isotope effects
0.282:0.718 [a]	s	H_2, 1 vol %	100	0	-------
(b)	s and n	D_2, 1 vol %	62.8±2.9	37.2±2.9	-------
0.282:0.718	s	H_2/D_2=1/9, 1 vol %	94.6±1.1	5.4±1.1	158
0.670:0.330	n	H_2/D_2=1/9, 1 vol %	94.2±0.8	5.8±0.8	146
0.282:0.718	s	HD, 1 vol %	95.2±0.1	4.8±0.1	19.8

(a) deuterated quartz tube
(b) ^{3}He : ^{4}He=0.670 : 0.330 and 0.282 : 0.718

Table 2 Isotope effects for T + $H_2(D_2)$ → HT(DT) + H(D) at various temperatures

Phase	Temp.	Isotope Effect	I.K.E.*	Remarks	Ref.
gas	room	2.7	192 keV[a]	scavenged	(14)
gas	room	1.55±0.06	192 keV[a]	unscavenged	(14)
gas	room	0.98±0.03	2.8 eV[b]	-------	(15)
solid	77 K	7	2.7 MeV[c]	-------	(13)
liquid	1.3 K	146, 158	192 keV[a]	present results	

*) I.K.E.: Initial Kinetic Energy.
Tritium atom was produced by the following processes.
a) ^{3}He(n, p)T, b) TBr —(photolysis)→T + Br, c) ^{6}Li(n, α)T

Table 3 Thermal rate constants *k(T)* calculated with the reduced dimensionality theory (in units of cm^3 molecule^{-1} s^{-1})

T / K	T+H_2	T + D_2	T + DH	T + HD
300	1.4(-16)	6.5(-18)	2.6(-17)	9.7(-17)
200	1.6(-18)	2.9(-20)	1.6(-19)	7.7(-19)
100	2.1(-22)	4.7(-26)	2.4(-24)	1.3(-23)
50	3.4(-24)	6.9(-30)	1.2(-26)	2.0(-26)
10	2.5(-25)	8.2(-32)	8.2(-28)	4.4(-28)
5	1.8(-25)	5.7(-32)	6.1(-28)	2.7(-28)
1.3	1.4(-25)	5.9(-32)	5.8(-28)	2.2(-28)

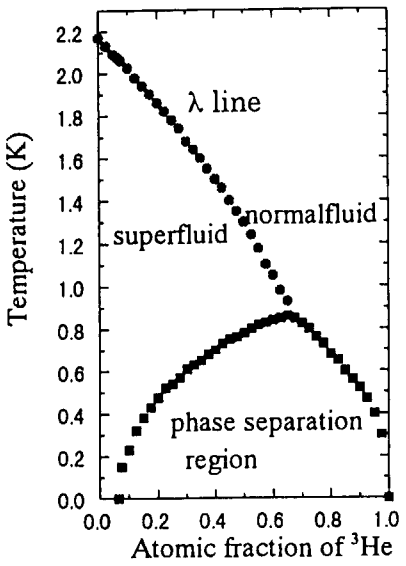

Figure 1 Phase diagram of ^{3}He - ^{4}He system under saturated vapor pressure.

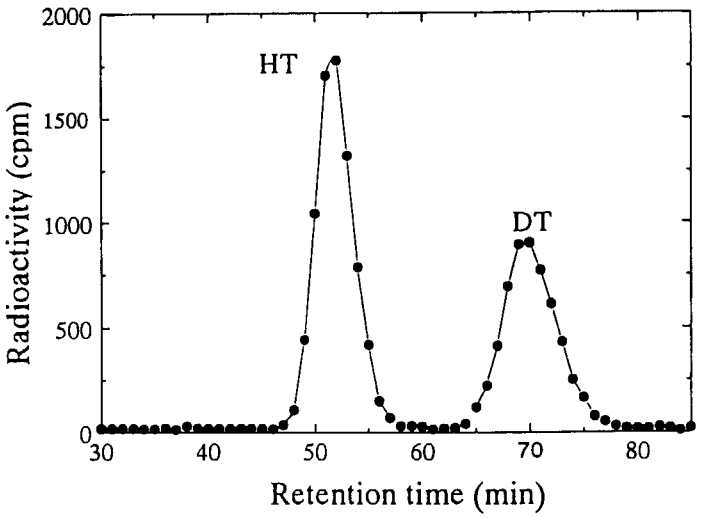

Figure 2 Typical radio-gaschromatogram of HT and DT.

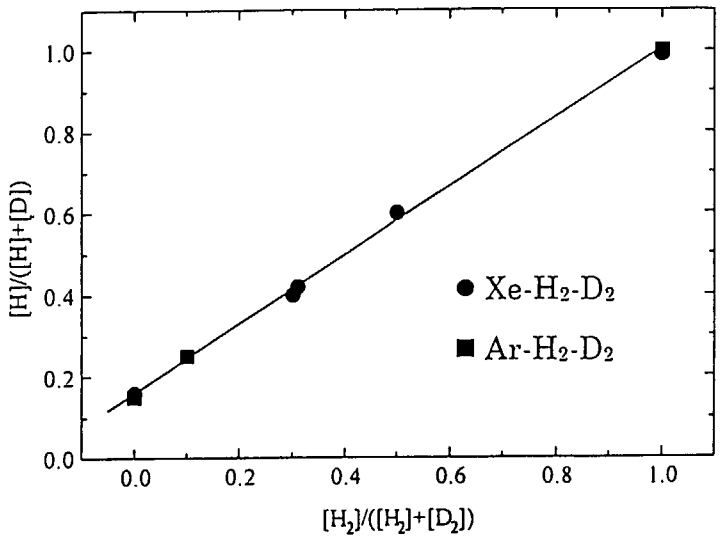

Figure 3 Fraction of H produced by γ- ray irradiated Xe-H_2-D_2(H_2+D_2=1 mol %) at 4.2K and x-ray irradiated Ar-H_2-D_2(H_2+D_2=1 mol %) at 4.5K.

● Xe-H_2-D_2(H_2+D_2=1 mol %) at 4.2K

■ Ar-H_2-D_2(H_2+D_2=1 mol %) at 4.5K

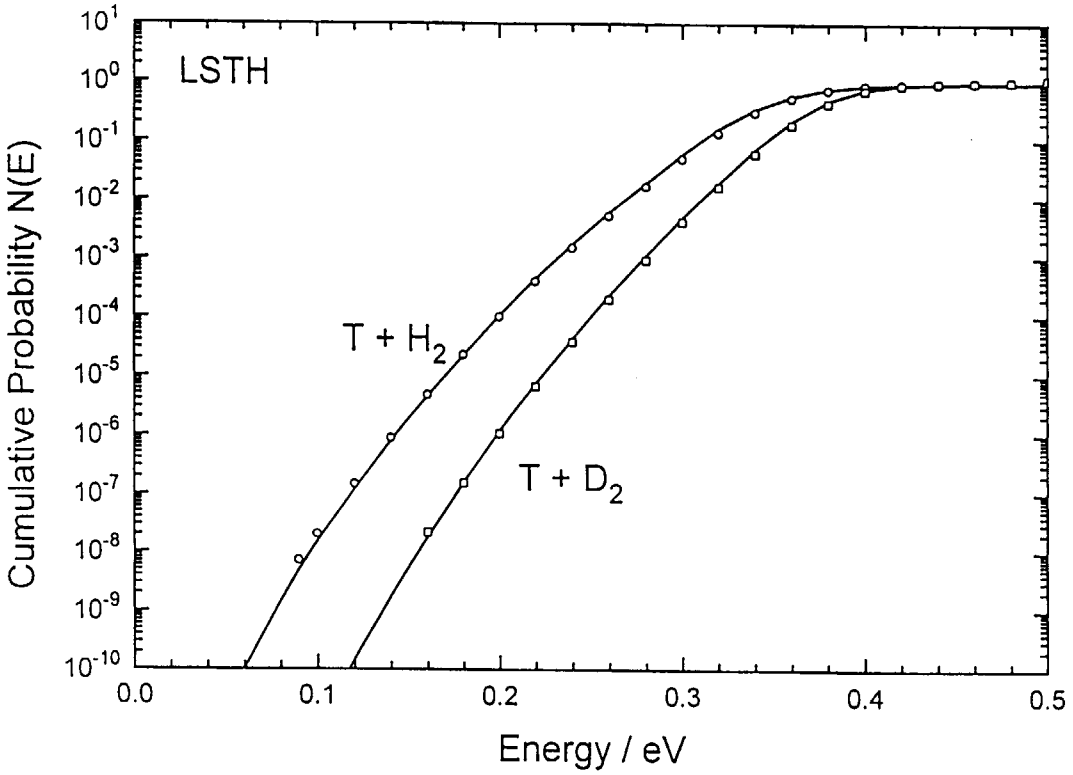

Figure 4 Cumulative reaction probabilities for T + H_2 and D_2 as a function of energy. The energy is measured from the ro-vibrational ground state of H_2 or D_2. Open circles and squares are the accurate three-dimensional quantum scattering results. Solid lines are the reduced-dimensionality results.

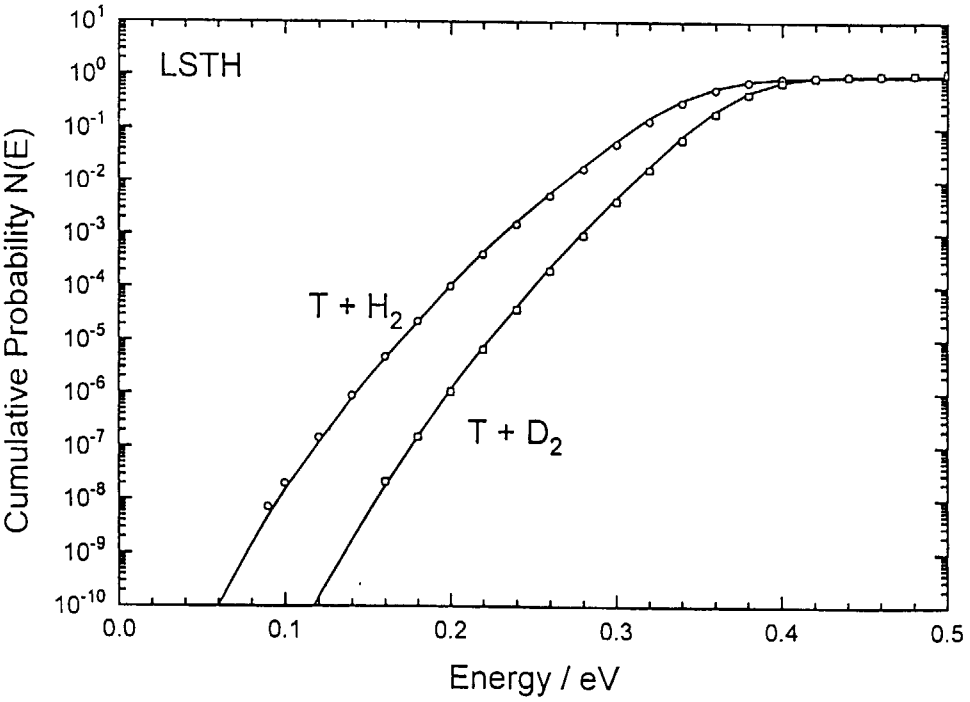

Figure 5 Arrhenius plot of thermal rate constants for T + H_2, D_2, and HD in the temperature range 10-300 K.

6. The second order recombination of atomic deuterium at low temperatures in a low magnetic field

T.Arai, M.Yamane, A.Fukuda and T.Mizusaki

Department of Physics, Graduate School of Science, Kyoto University, Kyoto 606-01, Japan

We measured the 2nd order recombination rates of atomic deuterium in a ^{4}He coated sample cell using the hyperfine resonance of β (F = 1/2, m_F = -1/2) - δ (F = 3/2, m_F = -1/2) transition in a low magnetic field (39 Gauss) at temperatures between 0.5 K and 1.2 K. We observed three decay channels, the solvation of D atoms into the liquid helium at high temperatures, the volume recombination at intermediate temperatures and the surface recombination at low temperatures. The volume recombination rate constant divided by helium vapor density was $k_{DD} = (3.3\pm 1.7)\times10^{-32}$ cm^6 sec^{-1}. At low temperatures we found the surface recombination cross length was $l_{DD} = (5.5\pm1.3)\times10^{-2}$ nm and the adsorption energy of D on ^{4}He surface was $\varepsilon_a = 3.97\pm0.1$ K. Both the volume and the surface recombination rates at the low field were much smaller than the values expected from the recombination rates measured at high fields by other groups, using the scaling of the $1/B^2$ dependence. This implies that at high fields the resonant recombination mechanism is dominant for both the volume and the surface recombination. We compared the results for deuterium with hydrogen.

1. Introduction

The simple chemical reactions between hydrogen (H) or deuterium (D) atoms, such as H + H → H_2, D + D → D_2 and D + H → HD, are interesting to investigate at low temperatures because those are the few chemical processes for which the reaction rate can be calculated from the first principle. We studied the reaction rate of D + D → D_2 at low temperatures and compared it with that of H + H → H_2 in order to investigate the isotope effect of the reactions.

Since H was first stabilized at low temperature by Silvera and Walraven[1], more works have been reported[2] on H than on D. For the purpose of reducing the recombination rate of the atoms into molecules (H + H → H_2), they used a superfluid-^{4}He-coated sample cell to minimize the adsorption of the atoms on the surface and polarized the electron spin in a strong magnetic field of B = 8.0 T. The research in this field has been focused on the achievement of Bose-Einstein Condensation (BEC) in the H gas. Extensive works have been reported on the recombination mechanisms of H during the stabilization of H at low temperatures. One of the 2nd order recombination mechanisms is the direct recombination[3] where two hydrogen atoms and a third particle (in this case, He atom) collide with each other and the hydrogen atoms form a molecule through the singlet interatomic potential. Comparison between the volume recombination rates of H in high and low magnetic fields clarified that the resonant recombination process exists at high fields[4,5]. The resonant recombination occurs when two hydrogen atoms form a metastable singlet molecular bound state (inverse predissociation), and the third particle collides to relax it to stable states. This mechanism at low temperatures is possible when the Zeeman energy of the two separate spin-polarized atoms is lower than the energy of the metastable molecule and thus a threshold exists in the magnetic field. Therefore, it is important to study the field dependence of the 2nd order recombination rate. In the case of H[4-6], it was confirmed that the volume recombination in high magnetic fields (B = 4 T) was dominated by the resonant recombination and the surface recombination

was dominated by the direct recombination for entire fields.

Soon after the stabilization of H at low temperatures, Silvera and Walraven[7] succeeded to stabilize D by a similar method as H. There existed a large contamination of H signal due to a long life time of H atoms and some fraction of the observed density of gas came from H. After the contribution from H was subtracted, the density of D was determined. It was found that the observed decay of D was much faster than H. Rapid decay was mainly due to the large adsorption energy of D on ^{4}He surface, and, as a result, the fast recombination to molecule occurred on the surface. The adsorption energy which they measured from the temperature dependence of surface recombination, ε_a = 2.6 K, was few times as large as that of H (ε_a = 1.0 K).

Since then, there has been fewer data reported for recombination of D. The contamination of H in a sample gas is inevitable since deuterium gas always contains about 0.1% impurity of hydrogen and D decays much faster than H, and it is necessary to find a way to distinguish D from the isotopic mixture of H. Magnetic resonance detection of D is a possible solution for this problem. Mayer and Seidel[8] tried to detect D atoms using ESR at 9 GHz in B = 0.3 T, but they could not observe D signal even though they succeeded to observe H signal in the same way for D. They suggested that the recombination rate of D was much faster than that of H atoms.

The first ESR experiment of D was reported by Shinkoda *et al.*[9], at 115 GHz in B = 4.07 T. They measured the rapid surface recombination rate and estimated the zero-field value of the surface recombination cross length $l_{DD}(0)$ = 560 nm, using the result of ref.(7) for the adsorption energy. At higher temperatures, the 2nd order volume recombination was measured and it agreed with the later theoretical calculation[10] of the resonant recombination mechanism through the intermediate metastable molecular state $D_2(21, 0)$, where (v, J) are the vibrational and rotational quantum numbers of the molecule. At lower temperatures, they could not measure the 2nd order recombination process because D atoms became doubly polarized and the decay of D atoms were controlled by the nuclear relaxation process.

Reynolds *et al.*[11,12] performed a hyperfine resonance experiment of D at T = 1 K. They measured the first order density decay due to the solvation of D atoms into the liquid ^{4}He and they found the solvation energy E_s = 13.6 K. This value agreed with the calculation by Saarela and Krotscheck[13].

Hayden *et al.*[14,15] used the 1420 MHz zero field hyperfine resonance signal of H impurity in the mixture of H and D and extracted informations about D at 1 K. The transverse relaxation time T_2 of H was limited by H-D spin exchange collision, and T_2^{-1} was proportional to the density of D, n_D. They measured n_D from T_2 of H signal. The measured volume recombination rate coefficient k_{DD} was 2.4×10^{-32} cm^6 sec^{-1} at T = 1 K.

In this work, we measured the temperature dependence of the density decay rate of a D gas in a ^{4}He-coated sealed sample cell by the hyperfine resonance in a nearly zero magnetic field at $0.5 < T < 1.2$ K. The decay of D was governed by three channels: solvation of D into liquid ^{4}He, volume recombination and surface recombination. To our knowledge, this work is the first measurement of the surface recombination rates near zero magnetic field. We compared the results with data measured in high magnetic fields. We found that the surface recombination cross length of D atoms at zero field, $l_{DD}(0)$, was about two orders of magnitude smaller than that was expected from high field measurements, and the volume recombination rates in a low field are much smaller than the values at high fields, using the $1/B^2$ dependence of the direct recombination rate constant. We compared the results of D with H and found that $l_{DD}(0)$ was very similar to that of H atoms $l_{HH}(0)$.

2. The rate equation

2.1 Rate equation

This experiment was designed to measure the temperature dependence of the rate constant of the recombination reaction of D atoms,

$$D + D + X \rightarrow D_2 + X . \quad (2.1)$$

Since our sample cell is coated with a superfluid ^{4}He film, this reaction occurs both in the volume and on the He-surface. The third body X is a ^{4}He atom in the vapor or on the surface. Another D atom could act as X, however, because its density n_D, typically less than 10^{12} atoms/cm^3 in our case, is much smaller than the density of ^{4}He atoms n_{He}(>10^{17} atoms/cm^3), then contributions of the three body collision of D atoms are negligible. Thus the recombination is the second order process about n_D. The rate equation of n_D is given by ,

$$\frac{dn_D}{dt} = -K^{eff} n_D^2 . \quad (2.2)$$

The effective 2nd order recombination rate constant K^{eff} is the sum of the contributions from the volume (K_v) and from the surface (K_s^{eff}). The volume recombination rate constant K_v is proportional to the He density, n_{He}, and is given by

$$K_v = k_{DD} n_{He} . \quad (2.3)$$

For the surface recombination, the rate equation can be expressed in terms of the volume density n_D with the help of the adsorption isotherm

$$\sigma_D = n_D \Lambda_{th} \exp\left(\frac{\varepsilon_a}{k_B T}\right) \quad (2.4)$$

, where σ_D is the surface density of D, $\Lambda_{th} = \sqrt{2\pi\hbar^2/mk_B T}$ is the thermal de Broglie length and ε_a is the adsorption energy. And the effective surface recombination rate constant is given by,

$$K_s^{eff} = l_{DD} \bar{v}_s \left(\frac{A}{V}\right) \Lambda_{th}^2 \exp\left(\frac{2\varepsilon_a}{k_B T}\right) \quad (2.5)$$

, where l_{DD} is the two dimensional analogue of the cross section which is called recombination cross length, $\bar{v}_s = \sqrt{\pi k_B T/2\mu}$ is the two dimensional mean speed of D-D pair with reduced mass μ (= m_D/2) and A/V is the ratio of the surface area to the volume of the sample cell.

Although we are interested in k_{DD} and l_{DD} which characterize the features of the volume and the surface recombination mechanisms, there exist another decay channel at higher temperatures: solvation of D into liquid ^{4}He[12]. Since the solvation rate is proportional to the flux of D atoms from the volume to the surface, it contributes to the rate equation as the first order term with the rate constant λ

$$\lambda = \frac{1}{4}\frac{A}{V}\bar{v}\alpha_{lv}\left(\frac{m}{m^*}\right)\exp\left(-\frac{E_S}{k_B T}\right) \quad (2.6)$$

, where m^* is the effective mass of the dissolved atom, α_{lv} is the probability that an atom will pass through the surface from the liquid to the vapor and E_S is the solvation energy.

Combining these decay channels, we write the rate equation for our system as

$$\frac{dn_D}{dt} = -\lambda n_D - K_2^{eff} n_D^2 . \quad (2.7)$$

2.2 Field dependence of the direct recombination rate constant

In order to compare our results of the recombination rate measurement with experiments of other groups in high magnetic fields, it would be necessary to consider the magnetic field dependence of the rate constant of the direct recombination mechanism, the theory of which was developed by Greben, Thomas and Berlinsky[3].

Since the interaction between D and He atoms is independent of the magnetic field, k_{DD} can be expressed as a sum of the products of the magnetic field dependent spin factor f_I and the magnetic field independent orbital factor F_I where I is the total nuclear spin,

$$k_{DD} = \sum_I f_I F_I . \quad (2.8)$$

Because of the requirement of the symmetrization of the molecular wave functions, the sum of the rotational quantum number J and I must be odd for D_2. That is why the orbital factor F_I has a subscript I. For I = 1, only even J's (para-D_2) are allowed. For even I's (I = 0 and 2), the same rotational molecular states (odd J, ortho-D_2) are allowed and then we may say that F_0 = F_2. Thus eq.(2.8) can be rewritten as

$$k_{DD} = f_{ortho} F_{ortho} + f_{para} F_{para} . \quad (2.9)$$

By multiplying n_{He} on both sides of eq.(2.9) and setting $K_{ortho} = n_{He}F_{ortho}$ and $K_{para} = n_{He}F_{para}$, we obtain

$$K^{v} = f_{ortho}K_{ortho} + f_{para}K_{para} . \qquad (2.10)$$

Note that K_{ortho} and K_{para} are independent of the magnetic field. For the surface recombination rate constant K^{s}, it should be expressed in the same form as eq.(2.10). Using the notations of Silvera and Walraven[2], f_{ortho} and f_{para} are given by,

$$\begin{aligned} f_{ortho} = \frac{1}{2}[&\eta_+^2\varepsilon_-^2\left(\hat{\alpha}\hat{\beta}+2\hat{\delta}\hat{\varepsilon}\right)+\varepsilon_+^2\eta_-^2\left(2\hat{\alpha}\hat{\beta}+\hat{\delta}\hat{\varepsilon}\right) \\ &+\eta_+^2\eta_-^2\left(\hat{\alpha}\hat{\delta}+2\hat{\beta}\hat{\varepsilon}\right)+\varepsilon_+^2\varepsilon_-^2\left(2\hat{\alpha}\hat{\delta}+\hat{\beta}\hat{\varepsilon}\right) \\ &+\varepsilon_+^2\left(\hat{\alpha}\hat{\gamma}+2\hat{\varepsilon}\hat{\zeta}\right)+\eta_+^2\left(2\hat{\alpha}\hat{\zeta}+\hat{\gamma}\hat{\varepsilon}\right) \\ &+\eta_-^2\left(\hat{\beta}\hat{\zeta}+2\hat{\gamma}\hat{\delta}\right)+\varepsilon_-^2\left(2\hat{\beta}\hat{\gamma}+\hat{\delta}\hat{\zeta}\right)+\left(\hat{\alpha}\hat{\varepsilon}+\hat{\beta}\hat{\delta}+\hat{\gamma}\hat{\zeta}\right)] \end{aligned}$$

$$\begin{aligned} f_{para} = \frac{1}{2}[&2\eta_+^2\varepsilon_+^2\left(\hat{\alpha}^2+\hat{\varepsilon}^2\right)+2\eta_-^2\varepsilon_-^2\left(\hat{\beta}^2+\hat{\delta}^2\right)+\eta_+^2\varepsilon_-^2\hat{\alpha}\hat{\beta} \\ &+\eta_+^2\eta_-^2\hat{\alpha}\hat{\delta}+\varepsilon_+^2\varepsilon_-^2\hat{\beta}\hat{\varepsilon}+\varepsilon_+^2\eta_-^2\hat{\delta}\hat{\varepsilon}+\varepsilon_+^2\hat{\alpha}\hat{\gamma}+\eta_-^2\hat{\beta}\hat{\zeta} \\ &+\eta_+^2\hat{\gamma}\hat{\varepsilon}+\varepsilon_-^2\hat{\delta}\hat{\zeta}+\hat{\gamma}\hat{\zeta}+\left(\eta_+^2-\varepsilon_+^2\right)^2\left(\hat{\alpha}\hat{\varepsilon}+\hat{\beta}\hat{\delta}\right)] \end{aligned}$$

(2.11)

At B=38.93 Gauss, which gives the minimum hyperfine frequency for β-δ transition and all the measurements of this work were performed at this magnetic field, $\varepsilon_+ = \left(1+\frac{1}{2}\left(1+\sqrt{3}\right)^2\right)^{-1/2}$, $\eta_+ = \left(1-\varepsilon_+^2\right)^{1/2}$, $\varepsilon_- = \eta_- = 1/\sqrt{2}$. And near zero fields, all the six hyperfine states are equally populated,

$$\hat{\alpha} = \hat{\beta} = \hat{\gamma} = \hat{\delta} = \hat{\varepsilon} = \hat{\zeta} = \frac{1}{6} . \qquad (2.12)$$

Then we have

$$\begin{aligned} K^{eff}(39\mathrm{G}) &\cong K^{eff}(0) \\ &= 1.667\times10^{-1}K_{ortho} + 8.796\times10^{-2}K_{para} \end{aligned}$$

(2.13)

The zero-field value of the rate constant $K^{eff}(0)$ is the same as $K^{eff}(38.93\mathrm{G})$.

In a very high magnetic field ($\mu^+B >> k_BT$), only the hyperfine states with electron spin 'down' are populated,

$$\eta_+ = \eta_- = 1,\ \varepsilon_+ = \varepsilon_- = \varepsilon_D \text{ with } \varepsilon_D = \frac{a_D}{\sqrt{2}\mu^+B} \qquad (2.14)$$

, where a_D is the hyperfine coupling constant of D,

$$\frac{3a_D}{2h} = 3273843525 \ \mathrm{MHz} .$$

If there is no nuclear spin polarization,

$$\hat{\alpha} = \hat{\beta} = \hat{\gamma} = \frac{1}{3},\ \hat{\delta} = \hat{\varepsilon} = \hat{\zeta} = 0 . \qquad (2.15)$$

In this case, we have

$$K^{eff}(B) = \frac{1}{3}\varepsilon_D^2\left(K_{ortho} + K_{para}\right) . \qquad (2.16)$$

Shinkoda *et al.*[9] determined K_{ortho} and K_{para} separately by using ESR at B = 4.07 T and obtained $K_{ortho} \approx K_{para}$ at all temperatures. Taking this result, from eqs.(2.13) and (2.16) we get

$$K^{eff}(0) = \frac{K^{eff}(B)}{1.309(a_D/\mu^+B)^2} \qquad (2.17)$$

and they showed $K^{eff}(B)$ by using eq.(2.16). We have to remember that the condition (2.15) is not always true in high magnetic fields, because γ is the doubly spin polarized state and it decays slower than α or β. The decay constant of the total density depends on each density of α, β and δ. In order to scale the rate constant of the high field data to the low field value in general, each density value of α, β and δ has to be specified.

3. Experimental setup and procedure

The low temperature part of the apparatus is shown in Fig.1. The sample cell (L) is immersed in superfluid ^{4}He and is cooled by the mixing chamber of the dilution refrigerator (B). To make the thermal contact between the sample cell and the mixing chamber, sintered silver (C) is placed at the bottom of the mixing chamber.

The 309 MHz resonator (K) is constructed around the sample cell holder and its resonance frequency can be adjusted by moving the tuning plate (F) connected to the bellows system (G). The resonator is coupled

with the external circuit through the coupling loop (M). The adjustable capacitor (N) is inserted in the signal line for the impedance matching to maintain the critical coupling with the receiver system. D atoms are created by the pulsed rf grow discharge ignited by the 200 MHz helical resonator (H). The discharge can be observed by a room temperature photo-diode through the optical fiber (I).

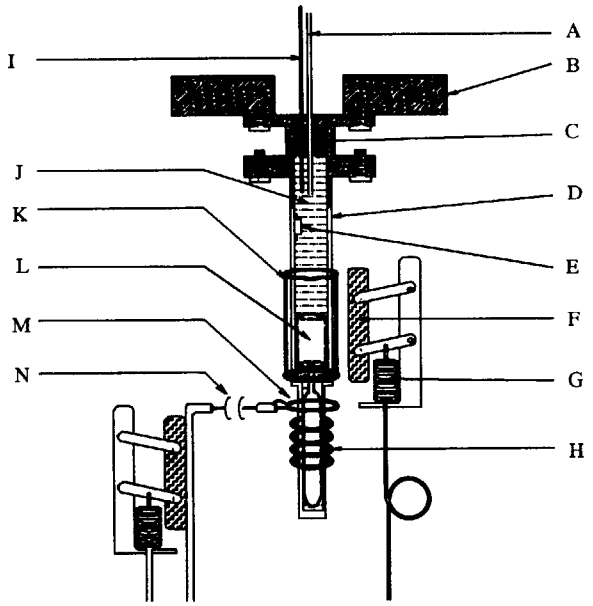

Fig.1 The low temperature part of the apparatus. A: He fill line, B: Mixing chamber of a dilution refrigerator, C: Sintered silver, D: Sample cell holder, E: Carbon thermometer, F: Tuning plate, G: Bellows, H: Discharge coil, I: Optical fiber, J: Liquid helium, K: Superconducting split ring resonator, L: Sealed quartz sample cell, M: Coupling loop, N: Adjustable capacitor for impedance matching.

To detect a very weak signal, a high quality factor (Q) resonator is required. A superconducting split-ring resonator[12,16], or a loop-gap cavity, is made from lead foil with a thickness of 0.1 mm. A 58 mm long and 18 mm diameter resonator is wound around the sample cell holder, and the inside of the gap of the split-ring resonator is bridged by another lead foil (22 mm width) separated by a thin layer of teflon. The outer turn acts as an inductor and the gap between the inner plate and the outer turn acts as a capacitor. Since the electric field is confined in this capacitor, the dielectric loss of the insulator must be small to keep high-Q. This is the reason why teflon is used. The intrinsic Q is 8.4×10^4 at low temperature when lead is superconducting. Outside of the resonator, a lead-plated half-pipe copper is placed near the gap. It is a tuning plate, which moves back and forth *in situ*.

The sample cell is made from quartz and it was sealed at room temperature with 1:1 mixture of ^{4}He and D_2 (99.6% isotopic purity), 3 bars in total. It consists of two volumes, the resonance volume (upper volume) and the dissociation volume (lower volume). These are connected through a 1mm diameter, 20mm long capillary. The D_2 molecules are dissociated in the dissociation volume by discharge, and the created D atoms distribute homogeneously in the sample cell. The resonance volume is a cylinder with $V_b = 2.38$ cm^3. V_b is much smaller than the resonator and thus is located in the homogeneous part of the rf field of the resonator. This would ensure the estimation of the absolute density calibration. Only the atoms in this volume contribute to the signal, while recombination occurs in the whole sample cell. The volume to the surface ratio of this sample cell is $A/V = 4.59$ cm^{-1}.

A superconducting magnet to create 39 Gauss bias field is attached to the outside of the vacuum can.

The temperature of the sample was monitored by the Matsushita carbon resistor thermometer immersed in liquid helium. This thermometer was calibrated against the calibrated Germanium thermometer placed on the mixing chamber. We used another carbon resistor on the mixing chamber for temperature control.

Before the magnetic resonance was performed, the resonator was connected to a network analyzer (HP 8753A) and the Q-value of the resonator was measured. During the cooling process, the Q-value suddenly changed at $T \sim 7$ K. This indicates the onset of the superconducting transition of the resonator lead foil. When the temperature was stabilized at working temperature, the resonator tuning and coupling were adjusted by pressurizing the bellows systems so that the tuned frequency f = 308.66092 MHz and the

receiver line was critically coupled. These pressures were independently regulated by controllers. Adjustable tuning range was about 3 MHz. At the critical coupling, the loaded quality factor Q_L = 4.2×10^4 was measured from the absorption line width.

To measure the atomic deuterium density decay, we measured free induction decay (FID) signals at different waiting time after discharge. Since the power radiated from the atoms depends on the cube of resonance frequency, the signal from D atoms (309 MHz) was much smaller than that from H atoms (1420 MHz)[17]. Because of the poor *S/N* ratio, signals were averaged for $N = 10^1 \sim 10^3$ times. Although the temperature was influenced by application of discharge pulses (typically 1 msec duration), the entire system was thermalized within 1 sec before we measured FID. To determine 90° condition, we adjusted the RF pulse duration to maximize the FID signal amplitude.

4. Signal analysis and results

The pulsed hyperfine longitudinal resonance between β (F = 1/2, m_F = -1/2) and δ (F = 3/2, m_F = -1/2) states of D at 38.93 Gauss was performed. The hyperfine energy diagram is shown in Fig.2.

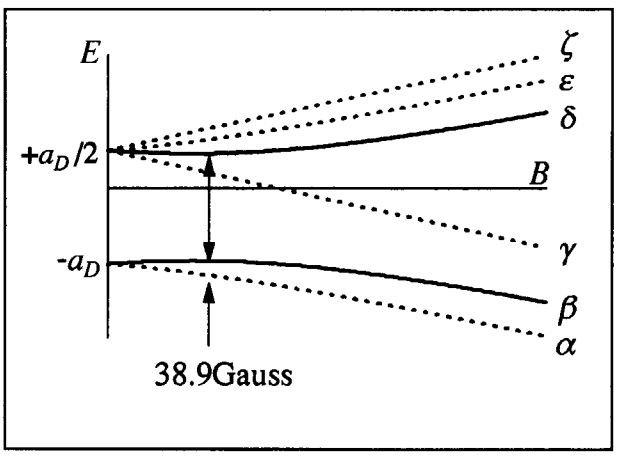

Fig.2 Energy diagram of the hyperfine states of an atomic deuterium as a function of the applied magnetic field.

In this work, the transition between β and δ states at 38.9Gauss, 308.66 MHz was used.

The resonance frequency of β-δ transition depends quadratically on the applied field around B_0 as follows,

$$f^{\beta\delta} = f_0^{\beta\delta} + c(B - B_0)^2 \qquad (4.1)$$

with $f_0^{\beta\delta}$ = 308.66092 MHz, c = 12.72859 kHz/Gauss^2 and B_0 = 38.93059 Gauss. It would be less sensitive to the field inhomogeneity near B_0. Since the energy splittings between the hyperfine levels are too small to polarize the electron spins, the results of the measured 2nd order recombination rate constants are regarded to be the zero-field values. We derived the density of the atoms n_D from the intensity of the resonance signal. We measured the field dependence of the resonance frequency for the calibration of the superconducting magnet and also determined B_0.

4.1 Absolute density calibration

In order to determine the second order recombination rate, the absolute calibration of n_D is necessary. Since the detected FID signal amplitude is proportional to n_D, it is required only to determine the amplification of the receiver and the filling factor η since the resonator was critically coupled to the receiver system and the loss of the coax in the receiver line is negligibly small. At critical coupling, the power transmitted to the receiver system P_{sig} is

$$P_{sig} = \frac{\omega\mu_0\eta Q_L V_b}{4} M_z^2 \qquad (4.2)$$

, where $\omega=2\pi f$ is the resonance angular frequency, η is the filling factor, V_b is the volume of the sample cell inside the resonator and M_z is the oscillating magnetization along the applied static magnetic field. In the case of 90° tipping pulse, M_z is expressed in the high temperature approximation,

$$M_z \approx \frac{1}{2}\hbar\gamma_e \frac{\hbar\omega}{6k_B T} n_D \qquad (4.3)$$

, where γ_e is the gyromagnetic ratio of an electron. P_{sig} is proportional to the square of A, so that

$$P_{sig} = pA^2 . \qquad (4.4)$$

The receiver amplification p was calibrated by a network analyzer. Only the parameter still unknown is η.

Since V_b is smaller than the resonator volume, the

oscillating magnetic field along the z-axis with an amplitude $2B_{1z}(\mathbf{r})$ is almost uniform in V_b. Under this condition, η is expressed as

$$\eta = \frac{\left[\int_{V_b} B_{1z}(\mathbf{r})dV\right]^2}{V_b \int_{\text{all space}} B_{1z}^2(\mathbf{r})dV}. \qquad (4.5)$$

We calculated the RF field profile of our superconducting resonator in the quasi-static approximation[12], and obtained $\eta = 0.05$. To confirm the result of this calculation, we checked it in several different ways such as the following. The 90° tipping pulse duration, raditaion damping effect of H which was measured by a similar configuration and spin-exchange relaxation measurements. We found similar values of η for all measurements within experimental error.

4.2 The second order recombination

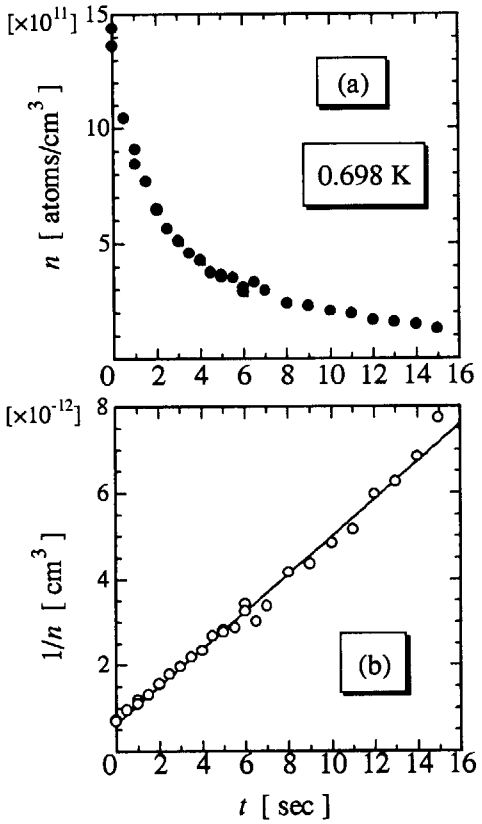

Fig.3 (a) The density decay after turing off the discharge, taken at T = 0.698K. (b) $1/n_D$ versus time. The solid line is the least square fit, the slope of which determines the second order recombination constant K^{eff}.

When the recombination is the 2nd order, the solution of eq. (2.2) is given by,

$$\frac{1}{n_D(t)} = K^{eff} t + \frac{1}{n_D(0)}. \qquad (4.6)$$

A typical decay data of n_D is shown in Fig.3(a). It was taken at $T = 0.698$ K. The circles in Fig.3(b) are the inverse of n_D of the same data. These fell on a straight line, that indicates the sample decay was dominated by the second order recombination and the effect of solvation was negligible at this temperature. The line in Fig.3(b) is the least square fit to eq.(4.6), and the slope of this line gives the second order recombination rate constant K^{eff}. As in this example, we found that the solvation was completely negligible below 1 K. The temperature dependence of K^{eff} is presented as $\sqrt{T}K^{eff}$ versus $1/T$ in Fig.4 for D and Fig.5 for H. Our data are shown by open circles and data by other groups are denoted by different symbols in the figures.

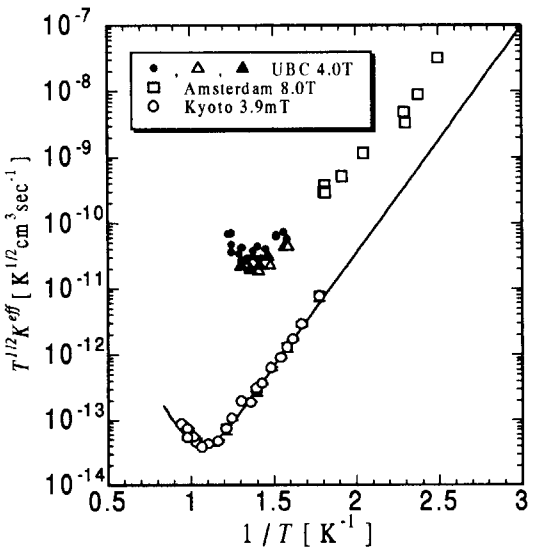

Fig.4 The temperature dependence of the second order recombination rate constant of atomic deuterium. The open circles are the measured values of this work and the solid line is the fit to them. The filled circles, open and filled triangles are taken from ref.(9). The squares are taken from ref.(7), assuming A/V=8.09 cm^{-1} and zero nuclear polarization. The high field data of other groups were scaled to the value of B = 39 Gauss and A/V=4.59 cm^{-1}.

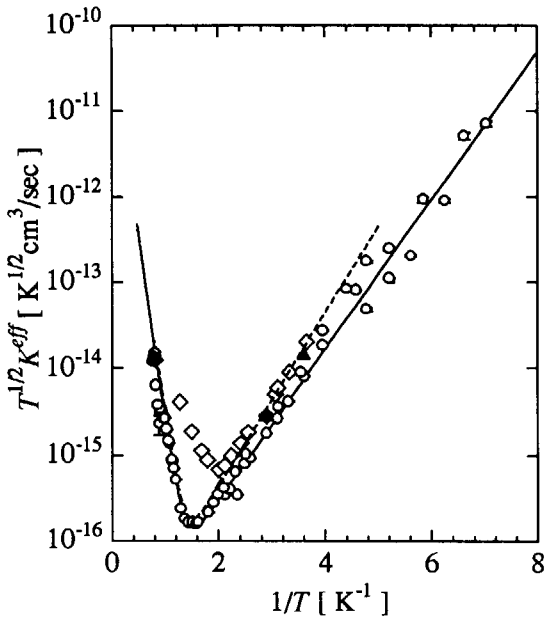

Fig.5 The temperature dependence of the second order recombination rate constant of atomic hydrogen. The open circles and the solid line are our zero-field results. The triangles are taken from ref.(19). The open squares are taken from ref.(4). These high field data were scaled to zero magnetic field and A/V=4.59 cm^{-1}. The broken line (ref.(20,22)) and the filled squares (ref.(21)) are the zero-field results of UBC group.

4.2.1 Surface recombination and adsorption energy for D

At lower temperatures below 0.91 K ($1/T > 1.1$ K^{-1}), the surface recombination was the dominant decay channel, and the rate constant K_s^{eff} was given by eq.(2.5). We assume that there is no temperature dependence in l_{DD} within this temperature regime. Then the prefactor of the exponential in eq.(2.5) is proportional to $\bar{v}\Lambda_{th}^2$ and thus to $1/\sqrt{T}$. By fitting the lower temperature part of Fig.4, we obtained the adsorption energy of D on ^{4}He,

$$\varepsilon_a / k_B = (3.97 \pm 0.1)\,\mathrm{K}, \qquad (4.7)$$

and the surface recombination cross length,

$$l_{DD} = (5.5 \pm 1.3) \times 10^{-2}\ \mathrm{nm}\ . \qquad (4.8)$$

4.2.2 Volume recombination

In Fig.4, there is a minimum at $1/T$ = 1.1 K^{-1} (T = 0.91 K). Above this temperature, the volume recombination is more important than the surface recombination. Below 1 K ($1/T$ > 1 K^{-1}), the $1/n_D$ versus t plot is still aligned on a straight line. This means the solvation of the atoms into the liquid is negligible. In the temperature regime between 1 K and 1.2K, both volume recombination and solvation are operative and data are fit to eq.(2.7) and determine both λ and K^{eff}. We obtained the value of λ which agrees with that of Reynolds *et. al.*[12]. Our temperature range, where the volume recombination was dominant against solvation process, was extended to higher temperatures than that of the Reynolds. This is because our density of D is much higher.

K_v thus determined was plotted against n_{He} and determined k_{DD} using eq.(2.3),

$$k_{DD} = (3.0 \pm 1.7) \times 10^{-32}\ \mathrm{cm^6\,sec^{-1}}\ . \qquad (4.9)$$

5. Discussions

In this work, we measured the volume and the surface second order recombination rates of atomic deuterium in a liquid ^{4}He-coated sample cell near zero magnetic field. The determined quantities are k_{DD} for the volume recombination given by eq.(2.3), l_{DD} for the surface recombination given by eq.(2.5) and the adsorption energy ε_a of D on ^{4}He surface. Table1 is the list of these quantities with the results of other works on H and D. The quantities measured in high magnetic fields by other groups were scaled by using eq.(2.17) for D and by a similar scaling equation for H. Among the works on H in high magnetic fields, the results of the state-selective measurements from which the nuclear polarization could be clarified were chosen for references. We reanalyzed the data of the Cornell group[19] for a comparison of the results of the zero field measurements of H. We derived K_{ortho} and K_{para} from the Fig.3 of ref.19 and their data were plotted as $K^{eff}(0) = (K_{para}+3K_{ortho})/16$.

	Hydrogen (H)	Deuterium (D)
Volume recombination k_{HH}, k_{DD} [cm^{6}sec^{-1}]	k_{HH} = (2.32±0.07)×10^{-3} (Kyoto[18], 0T) (2.0±0.3)×10^{-33} (UBC[20,22], 0T) (1.9±0.1)×10^{-33} (UBC[21], 0T) 1.8×10^{-33} (Theory[3])	k_{DD} = (3.0±1.7)×10^{-32} (Kyoto, 39G) (2.4±0.2)×10^{-32} (UBC[14], 0T)
Surface recombination l_{HH}, l_{DD} [nm]	l_{HH} = (2.5±0.4)×10^{-2} (Kyoto[18], 0T) (1.4±0.2)×10^{-2} (UBC[20,22], 0T) 4.3×10^{-2} (UBC[4], 4T)*1 2.0×10^{-2} (Cornell[19], 8.3T)*1	l_{DD} = (5.5±1.3)×10^{-2} (Kyoto, 39G) 560 (UBC[9], 4T)*1,*2
Adsorption energy on liquid ^{4}He surface ε_a/k_B [K]	ε_a/k_B = 1.00±0.02 (Kyoto[18]) 1.15±0.05 (UBC[20,22], 0T) 1.02 (UBC[4], 4T) 1.11 (Cornell[19], 8.3T)	ε_a/k_B = 3.97±0.1 (Kyoto, 39G) 2.6±0.4 (Amsterdam[3],8T)*3

*1 : These quantities were scaled to zero field value.

*2 : In order to determine these quantities, ε_a/k_B = 2.6 K was assumed.

*3 : Under the assumptions of zero nuclear polarization and $K_{ortho} = K_{para}$.

Our measured quantity of the volume recombination rate constant is k_{DD}=(3.0±1.7)×10^{-32} cm^{6}sec^{-1}. This agrees with the result of Hayden and Hardy[14], k_{DD} = (2.4±0.2)×10^{-32} cm^6 sec^{-1}. As mentioned, our density of D is about one order of magnitude larger than that of Hayden and Hardy and therefore the volume recombination is more important than the solvation process at the same temperature range and we believe that our value of k_{DD} is more accurate than theirs.

The case of zero field experiment on hydrogen volume recombination, k_{HH} was (2.32±0.07)×10^{-33} cm^6 sec^{-1} [18]. Morrow *et al.*[20,22] measured (2.0±0.3)×10^{-33} cm^6 sec^{-1}, Hayden and Hardy[21] measured more carefully and obtained (1.9±0.1)×10^{-33} cm^6 sec^{-1} at T = 1.23 K. The theoretical calculation of the direct recombination mechanism at 1 K by Greben *et al.*[3] was 1.8×10^{-33} cm^6 sec^{-1}. It agrees with the experimental measurements.

Compared with the H-H volume recombination rate k_{HH}, k_{DD} for D is one order of magnitude larger. The direct recombination might be the only possible mechanism in our experimental condition, and thus it is very desireable to calculate D-D volume recombination rate.

Both D-D and H-H volume recombination rates measured in high magnetic fields[4,9] were faster than those expected from the zero field measurements. The fast volume recombination in high magnetic fields were explained by the resonant recombination mechanism[5,10].

From the surface recombination measurement, we determined l_{DD} = (5.5±1.3)×10^{-2} nm and ε_a/k_B = 3.97±0.1 K. The adsorption energy is much larger compared with the theoretically calculated values: 1.11 K by Guyer and Miller[23], 1.39 K by Mantz and Edwards[24]. And it is also larger than the experimental result 2.6±0.4 K of Silvera and Walraven[3]. In our separate zero field experiment on H, the measured adsorption energy of H on ^{4}He[18] was 1.00±0.02 K and it agreed well with the commonly accepted quantity. This agreement indicated that the film in this work was saturated, the ^{4}He gas was sufficiently pure and the calibration of the thermometer was correct.

Our low field surface recombination rate was orders of magnitude slower than that was expected from high field data. The squares in Fig.4 are the results of Silvera and Walraven[7], measured in B = 8.0 T by the bolometric detection. Even though they did not measure K_{ortho} and K_{para} separately nor measured the population of the each individual hyperfine state, we

scaled their data with the assumption of zero nuclear polarization and $K_{ortho}=K_{para}$. We used A/V = 8.09cm^{-1}, where we neglected the surface area of the sintered silver in their sample cell. Filled and open triangles and filled circles are the data obtained by Shinkoda *et al.*[9] who detected α, β and γ - state atoms of D by ESR in B = 4.07 T and they determined the zero field value of l_{DD} to be 560 nm under an assumption of ε_a/k_B = 2.6 K. It is four orders of magnitude larger than our low field result.

In the case of H, the surface recombination rate constant, K_s^{eff}, measured in high magnetic fields scaled to zero field value agreed with zero field measurements. There is some difference in the recombination mechanisms between H and D. Our measured zero field value of l_{HH}[18] was $(2.5\pm0.4)\times10^{-2}$ nm and Morrow *et al.*[20,22] (broken line in Fig.5) reported $(2.0\pm0.3)\times10^{-2}$ nm.

What is the difference between the recombination mechanisms in high fields and in low fields in the case of D? Can it be explained by resonant recombination mechanism, as in the case of the volume recombination? Unfortunately, the calculation of Reynolds *et al.*[10] is only applicable to the volume recombination process. Papoular[25] suggested that D↓-D↓ adsorbed triplet dimer plays a role in the surface recombination process. However, this does not explain $K_{ortho} \approx K_{para}$ measured by Shinkoda *et al*[9].

Anyway, it is revealed that some other mechanism, which is different from the direct recombination, dominates the surface recombination process of D in high magnetic fields. We suppose it is the resonant recombination similar to that for the volume recombination process.

6. Summary

We measured the 2nd order recombination rate of atomic deuterium at low temperatures between 0.5K and 1.2 K in a superfluid-^{4}He-coated cell in a low magnetic field (39 Gauss). Compared the results with the high field data, we found that D atoms recombine much slower in a low magnetic field than in high magnetic fields both in the volume and on the surface. We suggest that the resonant recombination mechanism takes place not only in the volume but on the surface.

7. Acknowledgments

The authors would like to thank Dr.N.Masuhara, Dr.J.S.Korhonen and Dr.A.Matsubara for each taking part in the experiment and measurement of zero-field data of hydrogen in this work and for useful discussions.

References

(1). I.F.Silvera and J.T.M.Walraven, 'Stabilization of atomic hydrogen at low temperature', Phys. Rev. Lett. **44**, 164, (1980)

(2). For a general review, see I.F.Silvera and J.T.M.Walraven, 'Spin polarized atomic hydrogen', in *Progress in Low Temperature Physics X*, ed. by D.Brewer, p.139, (1986)

(3). J.M.Greben, A.W.Thomas and A.J.Berlinsky, 'Quantum theory of hydrogen recombination', Can. J. Phys. **59**, 945, (1981)

(4). M.W.Reynolds, I.Shinkoda, R.W.Cline and W.N.Hardy, 'Observation of predissociation of spin-polarized atomic hydrogen at low temperatures', Phys. Rev. **B34**, 4912, (1986)

(5). M.W.Reynolds and W.N.Hardy, 'Resonance recombination of spin-polarized atomic hydrogen at low temperatures', Can. J. Phys. **66**, 405, (1988)

(6). Issac F. Silvera, H.P.Godfried, E.R.Eliel, J.G.Brisson, J.D.Gillaspy, J.C.Mester and C.Mallardeau, 'Magnetic-field dependence of resonance recombination in spin-polarized atomic hydrogen', Phys. Rev. **B37**, 1520, (1988)

(7). I.F.Silvera and J.T.M.Walraven, 'Spin-polarized atomic deuterium: Stabilization, limitations on density and adsorption energy on helium', Phys. Rev. Lett. **45**, 1268, (1980)

(8). R.Mayer and G.Seidel, 'Electron-spin resonance of atomic hydrogen and deuterium at low temperatures', Phys. Rev. **B31**, 4199, (1985)

(9). I.Shinkoda, M.W.Reynolds, R.W.Cline and W.N.Hardy, 'Observation of doubly spin-polarized deuterium by electron-spin resonance', Phys. Rev.

Lett., **57**, 1243, (1986)
(10). M.W.Reynolds, M.E.Hayden and W.N.Hardy, 'Resonance recombination of spin-polarized deuterium', in *Spin Polarized Quantum Systems*, ed. by S.Stringari, World Scientific, Singapore, p.236, (1989)
(11). M.W.Reynolds, 'Resonant recombination of atomic hydrogen and deuterium at low temperatures', Ph.D. thesis, The University of British Columbia, (1989)
(12). M.W.Reynolds, M.E.Hayden and W.N.Hardy, 'Hyperfine Resonance of Atomic Deuterium at 1K', J. Low. Temp. Phys., **84**, 87, (1991)
(13). M.Saarela and E. Krotscheck, 'Hydrogen Isotope and ^{3}He Impurities in Liquid ^{4}He', J. Low Temp. Phys., **90**, 415, (1993)
(14). M.E.Hayden and W.N.Hardy, 'Atomic Hydrogen-Deuterium Mixtures at 1 Kelvin: Recombination Rates, Spin-Exchange Cross Sections, and Solvation Energies', J. Low Temp. Phys., **99**, 787, (1995)
(15). M.E.Hayden, 'Studies of Atomic Hydrogen Spin-Exchange Collisions at 1K and Below', Ph.D. thesis, The University of British Columbia (1991)
(16). W.N.Hardy and L.A.Whitehead, 'Split-ring resonator for use in magnetic resonance from 200-2000MHz', Rev. Sci. Instrum., **52**, 213, (1981)
(17). T.Arai, A.Matsubara, S.Hotta, J.S.Korhonen, N.Masuhara, T.Suzuki, A.Masaike, T.Mizusaki and A.Hirai, 'Diffusion measurement of Atomic Hydrogen in Helium Gas at Very Low Temperatures', Physica **B 194-196**, 901, (1994)
(18). Unpublished work at Kyoto University.
(19). B.Yurke, J.S.Denker, B.R.Johnson, N.Begelow, L.P.Levy, D.M.Lee and J.H.Freed, 'NMR-Induced Recombination of Spin-Polarized Hydrogen', Phys. Rev. Lett. **50**, 1137, (1983)
(20). M.R.Morrow, 'Magnetic Resonance on Atomic Hydrogen Confined by Liquid Helium Walls', Ph.D. thesis, The University of British Columbia (1983)
(21). M.E.Hayden and W.N.Hardy, 'Spin Exchange and Recombination in a Gas of Atomic Hydrogen at 1.2K', Phys. Rev. Lett. **76**, 2041, (1996)
(22). M.Morrow, R.Jochemsen, A.J.Berlinsky and W.N.Hardy, 'Zero-Field Hyperfine Resonance of Atomic Hydrogen for $0.18 \leq T \leq 1$K: The Binding Energy of H on Liquid ^{4}He', Phys. Rev. Lett. , **46**, 195, (1981); Erratum, Phys. Rev. Lett., **47**, 455, (1981), R.Jochemsen, M.Morrow, A.J.Berlinsky and W.N.Hardy, 'Magnetic resonance studies of atomic hydrogen at zero field and low temperature : Recombination and binding on liquid helium', Physica **109&110B**, 2108, (1982)
(23). R.A.Guyer and M.D.Miller, 'Interaction of Atomic Hydrogen with the Surface of Liquid ^{4}He', Phys. Rev. Lett. **42**, 1754, (1979)
(24). I.B.Mantz and D.O.Edwards, 'Binding of spin-polarized hydrogen to the free surface of liquid helium', Phys. Rev. **B20**, 4518, (1979)
(25). M.Papoular, 'On the dynamical stability of D↓', J. Low Temp. Phys., **50**, 253, (1983)

7. Quantum Nucleation in Supersaturated ^{3}He-^{4}He Liquid Mixtures.

K. Hatakeyama, E. Tanaka and T. Satoh

Department of Physics, Faculty of Science, Tohoku University, Sendai 980-77, Japan

A first order phase transition is the change of state from a metastable to a stable phase as the result of fluctuation in a homogeneous metastable medium. The fluctuation forms small quantities of a new stable phase, nuclei. There is a potential barrier due to the creation of an interface.

Usually, the fluctuation is a thermal fluctuation. However, in a temperature region extremely low compared with the barrier height, the thermal fluctuation is no longer effective. If we still have any first order phase transition in such a situation, the nucleation must be due to quantum tunneling. Quantum nucleation is a kind of macroscopic quantum tunneling phenomena, accompanying the decay of metastable system described with a macroscopic variable.

Below about 0.9K, a ^{3}He−^{4}He liquid mixture decomposes into the ^{3}He-dilute phase and the ^{3}He-concentrated phase. The dilute phase has a finite solubility of ^{3}He down to 0K. We measured the upper-limit of ^{3}He-concentration in a supersaturated dilute phase as a function of temperature. The difference from the equilibrium solubility is called the critical supersaturation.

In order to realize the supersaturated state, we developed the pressure-sweep method with a superleak, through which only the zero-entropy superfluid component of ^{4}He can flow. The measurments were done in the temperature range from 200mK down to 400μK.

The obsurved amount of critical supersaturation becomes independent of temperature below about 10mK, while it increases with temperature above about 10mK. The temperature-independent behavior suggests that we are

in the regime of quantum nucleation. The behavior of the increase with temperature suggests that the nucleation is due to quantum tunneling with dissipation. The effect of disipation is expected to increase with temperature. In order to obtain detailed information of the dissipation effect, we are preparing an experiment of sound transmission and reflection at the phase-separated interface of liquid ^{3}He−^{4}He mixtures.

References

[1] Critical Supersaturation of ^{3}He−^{4}He Liquid Mixtures,
T. Satoh, M. Morishita, M. Ogata and S. Katoh,
Phys. Rev. Lett. 69 (1992) 335-338

[2] Nucleation in Supersaturated ^{3}He−^{4}He Liquid Mixtures,
T. Satoh, M. Morishita, S. Katoh, K. Hatakeyama and M. Takashima,
Physica B 197 (1994) 397-405

[3] Sound Transmission Phenomena and Phase-separation Kinetics at the Superfluid-Normal Interface of Liquid ^{3}He−^{4}He Mixtures,
S. N. Burmistrov and T. Satoh,
Phys. Rev. B 52 (1995) 12867-12872

[4] Quantum Nucleation,
T. Satoh, and S. N. Burmistrov,
in Quantum Coherence and Decoherence (Edited by K. Fujikawa and Y. A. Ono) 93-98 (1996, Elsevir)

[5] Quantum Nucleation in a Supersaturated Liquid ^{3}He−^{4}He Mixture,
S. N. Burmistrov and T. Satoh,
Czechoslovak J. of Phys. 46 (S1) (1996) 195-196

8. Spectroscopy of atoms and molecules in liquid helium

Michio Takami
The Institute of Physical and Chemical Research (RIKEN)
Wako, Saitama 351-01, Japan

Superfluid helium provides a unique environment as a solvent; low temperature (~1 K), no apparent viscosity, extremely high thermal conductivity, low mobility of implanted particles, weak interaction, etc. Owing to recent technical development of dispersing metal atoms and molecules in the liquid,[1] substantial progress has been made in the past several years for the study of the physical and chemical properties of impurity particles in liquid helium.

Many neutral atoms are known to reside in bubble-like vacant cavities in liquid helium (bubble atom) formed by a strong short range repulsive force between the helium and impurity atoms.[2] Coupling of the bubble (a soft cage) with a trapped atom usually leads to large blueshifts and broadening of absorption lines while the emission lines are close to free atomic lines with relatively narrow widths. These spectral profiles have been interpreted by a so-called bubble model,[3] based on helium-impurity atom pair potentials and bubble energies for the shifts and also on the Anderson's line broadening theory for the profiles.[4] The bubble model reproduces some atomic line profiles reasonably well,[5] but recent observation shows that there are cases in which the model totally fails to reproduce the observed spectra.

One such example is the emission spectra of Be and Mg from their lowest $^1P_1$ excited states. While we made a systematic study of alkaline earth atoms,[6,7] the emission lines of Be and Mg were found to show redshift and broadening much larger than those observed in heavier alkaline earth atoms. Our preliminary calculation shows that these atoms form solid helium rings in the nodal planes of the $^1P_1$ state due to a strong attractive force from their ion cores exposed to the liquid.[8] Since this bonding occurs only in the excited states, the bound-free transitions produce much broader line widths. A second example is the anomalous spectra for group 1a and 1b atoms. It has been known for a while that the light alkali atoms (Li, Na, K) does not show any emission lines from their excited states.[9] Even for heavy alkali atoms, the D2 emission lines are very weak or even missing. For the former, Dupont-Roc[10] proposed an exciplex model which predicted that the emission lines of light alkali atoms are largely redshifted to the infrared region by bonding with several He atoms. For a heavier alkali atoms, on the other hand, the $^2P_{3/2}$ state can bond with at most two He atoms, allowing broad bound-free emission on the red side of the D1 lines with much smaller shift. We confirmed this model by observing such bound-free

emission from the $AgHe_2$ exciplex when the D2 line of Ag atom was excited in liquid helium.[11] We are currently extending this study to the dynamics of excited metal atoms in cold helium gas.[12-14]

The third example is a very narrow absorption line associated with an inner core electronic transition of Eu.[15] This atom has the Xe $4f^7(^8S_{7/2})6s^2\ ^8S_{7/2}$ ground state configuration. The transition lines of Eu in the visible region are divided into two groups, valence electron transitions where one of the 6s electron is excited and inner core electronic transitions where one of the 4f electrons is excited. The spectra of valence electron transitions show typical bubble spectra, indicating that the Eu atom is definitely trapped in a bubble. On the other hand, the inner core electronic transitions show very narrow absorption lines, with about 0.5 cm^{-1} line widths (HWHM) and very small (15-43 cm^{-1}) red shifts from the free atomic lines. The absorption spectra are accompanied with phonon bands extending over ~20 cm^{-1} but without clear roton/maxon peaks in contrast to the peaks observed in the spectrum of Glyoxal trapped in He clusters.[16] Temperature dependence of the band profiles shows drastic change from a clearly defined zero phonon peak with a phonon band at 1.6 K to a cusp-like profile at 3.1 K without clear zero phonon peak and phonon band. The small red shifts of the absorption lines are consistent with the fact that the interaction of surrounding liquid with Eu atom is mostly with the outermost $6s^2$ electrons, and the excitation of inner core electron only increases the polarizability of excited atom, causing small red shift of the absorption line. The drastic change of the line profiles may be attributed to the change of the bubble surface from well-defined liquid boundary at 1.6 K to diffuse surface or high density low temperature He gas environment at 3.1 K. However, origin of the absence of roton/maxon peaks is not well understood yet.

For molecular spectra in liquid helium, we reported the first complete emission and absorption bands for Cu_2 and Ca_2.[17] We are currently trying to measure electronic transitions of aromatic compounds and vibrational spectra of simple molecules in liquid helium. Unfortunately, we still don't have efinite evidence that we are dispersing isolated molecules in liquid helium. An attempt to confirm the spectra of monomer molecules in liquid helium is in progress.

This work was supported by a Grant for International Joint Research Projects for the New Energy and Industrial Technology Development Organization (NEDO), Japan, and Special Grant for Promotion of Research from The Institute of Physical and Chemical Research (RIKEN). I would like to thank my collaborators, Drs. J.H.M. Beijersbergen, Q. Hui, J.L. Persson, M.-P. Coquard, Z.J. Jakubek, Y. Kasai, and M. Yonekura for their contribution to the present work.

References

1. A. Fujisaki, K. Sano, T. Kinoshita, Y. Takahashi, and T. Yabuzaki, Phys. Rev. Lett. **71**, 1039 (1993).
2. A.P. Hickman and N.F. Lane, Phys. Rev. Lett. **26**, 1216 (1971).
3. H. Bauer, M. Beau, B. Friedel, C. Marchand, K. Miltner, and H.J. Reyner, Phys. Lett. A **146**, 134 (1990).
4. P. W. Anderson, Phys. Rev. **86**, 809 (1953).
5. S.I. Kanorsky, M. Arndt, R. Dziewior, A. Weis, and T.W. Hänsch, Phys. Rev. B **49**, 3645 (1994).
6. J.H.M. Beijersbergen, Q. Hui, and M. Takami, Phys. Lett. A **181**, 393 (1993).
7. Q. Hui, J.L. Persson, J.H.M. Beijersbergen, and M. Takami, Z. Phys. B **98**, 353 (1995).
8. Q. Hui and M. Takami, to be published.
9. Y. Takahashi, K. Sano, T. Kinoshita, and T. Yabuzaki, Phys. Rev. Lett. **71**, 1035 (1993). See also M. Takami, Comments At. Mol. Phys. **32**, 219 (1996) for a brief review of earlier work.
10. J. Dupont-Roc, Z. Phys. B **98**, 383 (1995).
11. J. L. Persson, Q. Hui, Z. J. Jakubek, M. Nakamura, and M. Takami, Phys. Rev. Lett. **76**, 1501 (1996).
12. Zygmunt J. Jakubek, Qin Hui, and Michio Takami, Phys. Rev. Lett. **79**, 629 (1997).
13. Z. J. Jakubek and M. Takami, Chem. Phys. Lett. **265**, 653 (1997).
14. T. Nakajima, N. Yonekura, Y. Matsuo, Q. Hui, amd M. Takami, to be published.
15. H. Hui and M. Takami, to be published.
16. M. Hartmann, F. Mielke, J. P. Toennies, and A. F. Vilesov, Phys. Rev. Lett. **76**, 4560 (1996).
17. J. L. Persson, Q. Hui, M. Nakamura, and M. Takami, Phys. Rev. A **52**, 2011 (1995).

9. Laser Spectroscopy of Neutral Atoms in Superfluid Helium

T. Yabuzaki, K. Ishikawa, A. Hatakeyama, T. Kinoshita*, S. Wada**, and Y. Takahashi
Department of Physics, Kyoto University, Kyoto 606-01, Japan

Several years ago the experimental difficulty in implantation of neutral atoms in liquid and solid helium could be overcome with laser sputtering techniques, which enabled us to study various kinds of atoms and molecules much easier than before [1,2]. Since then neutral foreign atoms and molecules in superfluid helium have attracted a great deal of attention because of their unique energy structures, dynamics and optical properties. In our early stage of our works, we studied alkaline earth atoms [1], but in recent years we have focus our attention to mainly onto alkali atoms (molecules [3-9]) and rare earth atoms [10]. The atoms in liquid and solid helium are interesting not only from atomic and molecular physics, but also from the point of view of their applications to fundamental physics, because the motion of atoms are slow enough to observe for a long period of time. In addition, as shown experimentally [4,7], optical pumping techniques can be applied to the atoms in liquid [4,7] and solid helium [11], which enables us to obtain nearly perfect polarization of electron and nuclear spins and to observe the magnetic resonance with high sensitivity by optical means. Since the spin relaxation time is expected to be very long, the works in this direction may be applied to the spin-related fundamental physics such as the search for the permanent electric dipole moment of atoms [12].

Among the works which we have done so far, we would like to focus here onto three kinds of our recent works. At first we mention the phenomena which cannot be explained essentially with a conventional spherical atomic bubble model. It is now known that neutral atoms form a bubble-like structure in surrounding helium. The atomic bubble model, where the atom is assumed to be in a spherical bubble, has so far explained the general features of observed optical spectra, for example the pressure dependence on the central wavelengths and widths of excitation and emission spectra[6,8]. The phenomena which cannot be explained with the spherical bubble model are (1) splitting of the D_2 excitation line and (2) the formation of alkali-helium exciplexes. This splitting of the D_2 excitation line was found to appear as the dynamic Jahn-Teller effect due to the quadrupole oscillation of bubble [6,8], although alkali atoms are in the ground S state. When the atoms are in the excited state; (2) they form alkali-helium exciplexes, i.e. excited molecules or clusters, which emit fluorescence in the infrared region 1-2 μm. The exciplex formation was found to be strongly dependent on the mass of alkali atom and the angular momentum in the excited state [13].

Secondly we would like to report on the spectroscopy of Tm atoms in liquid and solid helium [10]. The optical transitions in low-lying levels of Tm atoms those of electron in the inner core, to which two outer S electrons shield the surrounding helium. As the result optical spectra are much less affected with helium compared with alkali atoms. In fact we found that the line due to magnetic dipole transition was extremely narrow. We consider that Tm atoms in superfluid and solid helium can be used as a probe or a tracer, since the optical detection of these atoms do not perturb significantly the state of helium.

Finally we report on our quite recent experiment directed to realization of alkali-vapor cell at a liquid helium temperature [14]. We can expect that the lifetime of the vapor becomes long when the cell walls are coated with the liquid helium film. We discuss here the decay of the vapor density and the newly found phenomenon that the alkali atoms were reproduced with weak light from alkali dimers and clusters. This work is now underway in cooperation with Dr. A. Young and Prof. W. Happer in Princeton University.

* Present address: Laboratoire Kastler Brossel, ENS, Paris.
** Present address: Faculty of Integrated human Studies, Kyoto University, Kyoto.

1. T. Yabuzaki et al., *Atomic Physics 10*, ed. by Walther and Haensch (World Scientific,N.J. 1993) p.337.
2. A. Fujisaki *et al.*, Phys. Rev. Lett. **71**, 1039 (1993).
3. Y. Takahashi *et al.*, Phys. Rev. Lett. **71**, 1035 (1993).
4. T. Kinoshita *et al.*, Phys. Rev. B. **49**, 3648 (1994).
5. T. Yabuzaki *et al.*, Z. Phys. **98**, 367 (1995).
6. T. Kinoshita *et al.*, Z. Phys. **98**, 387 (1995).
7. Y. Takahashi *et al.*, Z. Phys. **98**, 391 (1995).
8. T. Kinoshita *et al.*, Phys. Rev. A **52**, 2707 (1995).
9. T. Kinoshita *et al.*, Phys. Rev. B **54**, 6600 (1996).
10. K. Ishikawa *et al.*, Phys. Rev. B **56**, 780 (1997).
11. A. Weis *et al.*, Z. Phys. **98**, 359 (1995).
12. The first proposal: M. Arndt *et al.*, Phys. Lett. **174**, 298 (1993).
13. T. Yabuzaki *et al.*, to be submitted.
14. A. Hatakeyama *et al.*, to be submitted.

10. Temperature Effect on Selective Tunneling Abstraction Reaction by H Atoms in Neopentane — Alkane Mixtures at 4 — 100K

Jun Kumagai,[1] Takayuki Kumada,[1] Naoki Kitagawa,[2] Norio Morishita,[3] and Tetsuo Miyazaki*,[1,2]

Advanced Science Research Center, Japan Atomic Energy Research Institute (Tokai), Tokai-mura, Naka-gun, Ibaraki 319-11, Japan, Department of Applied Chemistry, School of Engineering, Nagoya University, Furo-cho, Chikusa-ku, Nagoya 464-01, Japan, and Japan Atomic Energy Research Institute (Takasaki), 1233 Watanuki, Takasaki, Gunma, 370-12, Japan

*Correspondence should be addressed to T. Miyazaki (Nagoya University).

[1] Japan Atomic Energy Research Institute (Tokai)

[2] Nagoya University

[3] Japan Atomic Energy Research Institute (Takasaki)

Abstract

When H atoms are produced by the photolysis of HI or the radiolysis of neo-C_5H_{12} in the neo-C_5H_{12}－i-C_4H_{10}(2 mol%) mixtures above 40 K, the H atoms react selectively with the solute i-C_4H_{10}. The selective reaction is suppressed below 30 K. The reactions have been studied by electron spin resonance and electron spin echo measurements at 4 － 100 K. The drastic temperature effect on the reaction by H atoms suggests that the H atoms concerned are not hot atoms, but thermal atoms. The thermal H atoms react with the solute alkane by quantum tunneling at low temperature. Temperature effects on the ESR spectra and the spin－lattice relaxation times of the solvent neo-C_5H_{11} radicals and the solute t-C_4H_9 radicals indicate that local motions of the solute i-C_4H_{10} molecules take place above 40 K, while motions of the solvent neo-C_5H_{12} molecules are severely restricted even at 100 K. It is concluded that the local motions of the solute i-C_4H_{10} assist the tunneling abstraction reaction by H atoms, resulting in the selective reaction with the solute above 40 K.

Introduction

A nuclear tunneling effect on a chemical reaction has been one of the important problems in chemical kinetics especially at low temperature. Recent results on the tunneling reactions have been reviewed.[1] Tunneling reactions of H atoms with hydrogen molecules have been studied in detail in solid hydrogen at very low temperature.[2,3] A tunneling reaction of H atoms with ethane was studied in a rare-gas matrix at 50 K.[4]

When H atoms are produced by the photolysis of HI or the radiolysis of neopentane in the neopentane−alkane mixtures at 77 K, H atoms react by several hundreds times more selectively with the solute alkane than the solvent neopentane, resulting in the selective formation of solute alkyl radicals.[2,5] Though H atoms in the radiolysis of neopentane cannot be observed by ESR at 4 K, the detailed studies by Miyazaki et al. have concluded that H atoms produced by radiolysis react with the solute alkane by a hydrogen−atom−abstraction reaction at low temperature.[2] Though the selective reaction of H atoms in the radiolysis of neopentane−alkane mixtures takes place at 77 K, it is suppressed at 4 K.[6,7]

Recently, it has been observed that the rate constant for the tunneling reaction HD + D → H + D_2 in solid hydrogen increases significantly with increasing temperature above 5 K.[8] The result indicates that the tunneling reaction of hydrogen atoms in the solid phase is accelerated by the local motion of reactants. If the selective reaction of H atoms in the neopentane−alkane mixtures is a tunneling reaction, the selectivity in the tunneling reaction may be related to local motions of the solute alkane. Here, we have undertaken to elucidate the selective reaction of H atoms in relation to the local motion of the solute alkane by use of ESR and ESE(electron spin echo) measurements in the temperature range of 4 − 100 K.

Experimental Section

The purities of neopentane(neo-C_5H_{12}), isobutane(i-C_4H_{10}), and cyclopentane(c-C_5H_{10}) are more than 99.9, 99.7, and 99 mol%, respectively. An aqueous solution of HI was vaporized and passed through P_2O_5 to prepare

hydrogen iodide. Then, the hydrogen iodide was subjected to trap-to-trap sublimation on the vacuum line several times. The mixtures of neo-C_5H_{12} containing i-C_4H_{10} (or c-C_5H_{10}) at 2 mol% were sealed into a quartz tube. Helium gas at 260 mmHg was also sealed into the tube in order to cool the sample quickly at low temperature. In the experiment of the photolysis, HI at 0.5 mol% was added to the neopentane－isobutane mixtures.

The sample was irradiated by white X-rays (60 kV, 45 mA) or ultraviolet light at 254 nm. The temperatures were exactly controlled by a Model 9650 Cryogenic Temperature Indicator/Controller (Scientific Instruments Inc.) combined with a cryostat using liquid helium as a coolant within an error of $\pm$0.05 K.

After the irradiation the ESR spectra of radicals were measured by a JEOL JES-TE200 spectrometer at a microwave power level, at which microwave power-saturation of the signals did not occur. The yields of radicals were obtained by use of an HP 9000 Model 382 workstation with ESPRIT software connected to the spectrometer. The errors in the radical yields are about 20 %. The yields were obtained by average of the results in two or three runs. The electron spin echo (ESE) signals were measured with a JEOL JES-PX1050 pulse-ESR spectrometer at temperature range of 4 － 50 K. The spin-lattice and spin-spin relaxation times were obtained by the analysis of the ESE signals.

Results

Figure 1 shows the ESR spectra of the neo-C_5H_{12}－i-C_4H_{10}(2 mol%)－HI(0.5 mol%) mixtures after the irradiation of UV light for 5 min. Figure 1A was measured at 100 K after the irradiation at 100 K. The spectra consist of clear eight lines in ten lines of t-C_4H_9 radicals, in which CH_3 groups in the radical rotate freely. Figure 1B was measured at 30 K after the irradiation at 100 K. Though the spectra is due to t-C_4H_9 radicals, the free rotation of CH_3 groups in the radical is suppressed, resulting in the complex spectra which is probably caused by a tunneling rotation of the CH_3 groups. Figure 1C was measured at 100 K after the irradiation at 4 K. The spectra are due to neo-C_5H_{11} radicals, where the hyperfine splitting in the spectra is caused by γ-proton interaction in the radical. The rotations

around C-C bonds are partially restricted and one of CH_3 groups takes a preferred conformation against the p orbital containing the unpaired electron.[9,10] Figure 1D was measured at 70 K after the irradiation at 4 K. The absence of the hyperfine splitting by γ-protons indicates that even a slight motion in a neo-C_5H_{11} radical is completely suppressed below 70 K.

Figure 2 shows the effect of irradiation temperature on the yields of radicals produced by the UV-irradiation of the neo-C_5H_{12}−i-C_4H_{10}(2 mol%) −HI(0.5 mol%) mixtures. The yields were measured at 100 K after the irradiation at different temperatures. The yields (○) of the solute radicals (t-C_4H_9) increase gradually with increasing temperature above 40 K. The yields (□) of the solvent radicals (neo-C_5H_{11}), however, decrease complementally with increasing temperature above 40 K. Thus, the total yields (▲) of neo-C_5H_{11} and t-C_4H_9 radicals are approximately constant in the whole range of temperature.

Figure 3 shows the effect of irradiation temperature on the yields of radicals produced by the X-rays irradiation of the neo-C_5H_{12}−i-C_4H_{10}(2 mol%) mixtures. The yields of radicals were measured at 77 K after the irradiation at different temperatures. The yields (○) of t-C_4H_9 radicals increase gradually with increasing temperature above 40 K, whereas those (□) of neo-C_5H_{11} radicals decrease complementally with increasing temperature. Thus, total yields (▲) of t-C_4H_9 and neo-C_5H_{11} radicals are independent of the irradiation temperature. When the neo-C_5H_{12}−c-C_5H_{10}(2 mol%) mixtures are irradiated with X-rays and then measured at 77 K, the relative yields (◇) of cyclopentyl radicals are shown also in Figure 3. The yields increase gradually with increasing temperature above 40 K.

Figure 4 shows the temperature dependence of the spin-lattice (T_1^{-1}) and spin-spin (T_2^{-1}) relaxation rates for radicals produced by the UV-irradiation of the neo-C_5H_{12}−i-C_4H_{10}(2 mol%)−HI(0.5 mol%) mixtures. t-C_4H_9 and neo-C_5H_{11} radicals were produced by the irradiation at 4 and 100 K, respectively. The relaxation times (T_1 and T_2) were directly obtained by the electron-spin-echo method with the three pulse sequence. The temperature dependence of the line width of ESR spectra of t-C_4H_9 radicals was also shown in the Figure, since the line width gives a qualitative information on the spin-spin relaxation rates. The spin-lattice relaxation times of t-C_4H_9 radicals could not be measured above 30 K because of the very short relaxation time, while those of neo-C_5H_{11} radicals could be

measured up to 46 K.

Discussions

Selective Abstraction Reaction of H Atoms Figure 1A shows clearly that H atoms produced by the photolysis of HI react selectively with the solute isobutane in the neo-C_5H_{12}−i-C_4H_{10}(2 mol%)−HI(0.5 mol%) mixtures to form t-C_4H_9 radicals at 100 K.

$$HI \xrightarrow{h\nu} H + I \quad (1)$$

$$H + i\text{-}C_4H_{10} \longrightarrow H_2 + t\text{-}C_4H_9 \quad (2)$$

$$H + neo\text{-}C_5H_{12} \longrightarrow H_2 + neo\text{-}C_5H_{11} \quad (3)$$

63 % of H atoms produced in reaction (1) react with i-C_4H_{10} at 2 mol % (reaction (2)), while the rest of them react with the solvent neo-C_5H_{12} (reaction (3)) (cf. Figure 2). There is the possibility that HI and the solute i-C_4H_{10} form a complex and thus H atoms produced react promptly with i-C_4H_{10}. In order to check this possibility, H atoms are produced by the X-rays radiolysis of neo-C_5H_{12} in the neo-C_5H_{12}−i-C_4H_{10}(2 mol%) mixtures at 100 K in the absence of HI (cf. Figure 3).

$$neo\text{-}C_5H_{12} \sim\!\!\rightarrow neo\text{-}C_5H_{11} + H \quad (4)$$

H atoms produced by the radiolysis of neo-C_5H_{10} (reaction (4)) react selectively with the solute i-C_4H_{10} to produce t-C_4H_9 radicals significantly. Other mechanisms may be considered for the selective formation of t-C_4H_9 radicals in the radiolysis of the neo-C_5H_{12}−i-C_4H_{10} mixtures. The detailed studies, reported previously, concluded that the solute t-C_4H_9 radicals are neither formed by an energy transfer from irradiated neopentane to the solute, nor by a radical site migration of solvent neopentyl radicals to the solute. Therefore, the solute radicals are formed by a selective reaction of a H atoms with the solute alkane.[2]

The selective formation of t-C_4H_9 radicals by H atoms, produced by the photolysis of HI or the radiolysis of neo-C_5H_{12}, is suppressed gradually with decreasing temperature below 100 K, while the yields of neo-C_5H_{11} radicals increase with decreasing temperature (cf. Figures 2 and 3). The remarkable temperature effect on the reaction of H atoms indicates that the H atoms are not hot atoms, but probably thermal atoms. Since the barrier height for reaction (2) is 6.4 kcal mol^{-1},[11] the abstraction reaction by the H

atoms takes place at low temperature by a tunneling effect.[12] The mechanism of the selective tunneling abstraction by thermal H atoms at 77 K is also supported by the following previous results. The selective hydrogen atom abstraction by H atoms in the neopentane－alkane mixtures at 77 K occurs more effectively with the decrease in the initial energy of the H atoms.[13] H atoms trapped in the rare-gas matrix react with ethane at 50 K.[4]

The selective tunneling reaction of H atoms with the solute i-C_4H_{10} is suppressed below 30 K (cf. Figures 2 and 3). There is the possibility that the suppression of the selective reaction below 30 K may be due to the characteristic property of i-C_4H_{10}. Thus, the temperature effect on the selective reaction of H atoms with the solute has been studied in the X-rays radiolysis of the neopentane containing cyclopentane(2 mol %) as a solute. In Figure 3 the selective formation of cyclopentyl radicals decreases gradually with decreasing temperature below 100 K and finally suppressed at 30 K, at which the selective reaction of H atoms with the solute isobutane is also stopped. Therefore, the selective abstraction reaction by H atoms in the neopentane－alkane mixtures takes place above 40 K, and suppressed below 30 K.

Selective Reaction of H Atoms and Local Motion of Solute Molecules

The information on the local motions of the solute i-C_4H_{10} molecules and the solvent neo-C_5H_{12} molecules will be obtained approximately from the motions of the solute t-C_4H_9 radicals and the solvent neo-C_5H_{11} radicals. When CH_3 groups in a t-C_4H_9 radicals rotate freely, equally-separated ten lines of ESR spectra are expected. In Figure 1A the eight lines of them can be observed clearly. Since the eight lines were observed above 40 K, the CH_3 groups in a t-C_4H_9 radical rotate freely above this temperature. The drastic change of the spectra of t-C_4H_9 radicals below 30 K (cf. Figure 1B) indicates the suppression of the free rotation of the CH_3 groups. On the contrary to the free rotation around C-C bonds in the solute t-C_4H_9 radical above 40 K, the rotation around the $(CH_3)_3C$-CH_2 · bond in a neo-C_5H_{11} radical is completely restricted even at 100 K.[9] A CH_3 group in the neo-C_5H_{11} radical can take one preferable orientation and the CH_3 group rotates at 100 K, indicated by hyperfine structures of ESR spectra in Figure 1C.

Since the hyperfine structures disappear below 70 K (cf. Figure 1D) , even the slight local motion of the CH_3 group that takes the preferable orientation is suppressed below this temperature. Thus, the local motion of solvent neopentane molecules is severely restricted. The appearance of the local motion of the solute isobutane molecules at 40 K may be related to the onset of the selective reaction of H atoms above 40 K.

The difference in the local motions between the solvent neo-C_5H_{11} radicals and the solute t-C_4H_9 radicals are observed in the difference of their spin－lattice relaxation rates, measured directly from the ESE recovery method. The alkyl radical formed at 77 K by γ-rays irradiation of n-$C_{16}H_{34}$ had much faster spin－lattice relaxation rates when the radical was located next to the terminal methyl group than when it was located between methylene groups.[14] It was suggested that the higher mobility of the end of the alkane chain which causes a modulation of hyperfine interaction contributes to the rapid relaxation of the radicals located to the terminal methyl group.[14] Though the mechanism of the spin－lattice relaxation is complex, the relaxation time gives a qualitative information on the local motion of the radicals. In Figure 4 the spin-lattice relaxation rate (T_1^{-1}) of the solute t-C_4H_9 radicals above 30 K becomes quite fast and exceeds the limit of the measurement, whereas those of the solvent neo-C_5H_{11} radicals could be measured up to 46 K. The fast relaxation rate of the t-C_4H_9 radicals above 30 K suggests that the local motion of the solute radicals becomes significant above this temperature. The spin-spin relaxation rate (T_2^{-1}) of the solvent neo-C_5H_{11} radicals are approximately constant in the temperature range of 4 － 46 K, while the rates of the solute t-C_4H_9 radicals decrease gradually with increasing temperature in the same temperature range. The local motion of the solute radicals averages the local magnetic fields surrounding the radicals, resulting in the decrease of the spin-spin relaxation rate.

H atoms may become mobile above 40 K in the neopentane matrix and react selectively with the solute isobutane. Since the CH_3 groups in a solute i-C_4H_{10} molecule rotate in the neopentane matrix, the isobutane molecule can take an orientation favorable for the hydrogen abstraction reaction by H atoms than rigid neopentane molecules, resulting in the selective reaction with H atoms. The difference in the bond energy between a tertiary C-H bond of i-C_4H_{10} and a primary C-H bond of neo-C_5H_{12},

which corresponds to the difference in the barrier height for the reaction, may be also another factor in the selective abstraction reaction in the neo-C_5H_{10}－i-C_4H_{10} mixtures, as pointed out previously.[2]

When H atoms are produced in the neo-C_5H_{12}－C_2H_6 mixtures at 77 K, they react by 490 times more selectively with the solute C_2H_6 than the solvent neo-C_5H_{12}.[2] Since both neo-C_5H_{12} and C_2H_6 consist of primary C-H bonds, the difference in the barrier height for the abstraction reaction by H atoms is quite small. In fact, the barrier heights for the reactions (5) and (3) were measured as 9.4 and 9.6 kcal mol^{-1}, respectively.[11]

$$H + C_2H_6 \longrightarrow H_2 + C_2H_5 \quad (5)$$

$$H + \text{neo-}C_5H_{12} \longrightarrow H_2 + \text{neo-}C_5H_{11} \quad (3)$$

If the above reactions take place by a quantum tunneling at 77 K, the rate constants (k) for the reactions can be estimated by the model that the potential energy curve for the reaction is approximated to an Eckart barrier,[15] where the barrier height for the reverse reaction is taken as 12.7 kcal mol^{-1}.[11] The ratio (k_5/k_3) of the rate constants for the reactions (5) and (3) is less than 2.2, which is much smaller than the experimental value (490). Thus, the large experimental value of k_5/k_3 for the reactions (5) and (3) in the neo-C_5H_{12}－C_2H_6 mixtures cannot be explained by the small difference in the barrier height between reactions (5) and (3). C_2H_5 radicals, produced by γ-rays radiolysis of the neo-C_5H_{12}－C_2H_6(4.8 mol%) mixtures at 77 K, show well-resolved ESR spectra[16], which indicate a free rotation of a CH_3 group in the C_2H_5 radical. The local motion of the solute C_2H_6 molecules causes a selective tunneling abstraction by H atoms, resulting in the selective formation of C_2H_5 radicals.

It is concluded that the selective tunneling abstraction by H atoms in the neopentane－alkane mixtures above 40 K is caused by the local motions of the solute alkane in the rigid neopentane matrix. Tunneling reactions assisted by the local motion of the reactants in the solid phase have been observed in the following reactions; HD + D reaction in the solid hydrogen, a proton transfer reaction to a $C_6H_6^-$ anion in ethanol glass, and a H_2 molecule detachment from a 2,3-dimethylbutane cation in solid alkane.[17]

Acknowledgment. This work was supported in part by a grant-in-Aid for Scientific Research from the Japanese Ministry of Education, Science and Culture.

References

(1) Benderskii, V. A.; Makarov, D. E.; Wight, C. A. *Chemical Dynamics at Low Temperature*; John Wiley & Sons, INC.: New York, 1994.

(2) Miyazaki, T. *Radiat. Phys. Chem.* **1991**, 37, 635, and related papers cited therein.

(3) Miyazaki, T.; Kitamura, S.; Morikita, H.; Fueki, K. *J. Phys. Chem.* **1992**, 96, 10331.

(4) Muto, H.; Nunome, K.; Iwasaki, M. *J. Phys. Chem.* **1980**, 84, 3402.

(5) Wakayama, T.; Miyazaki, T.; Fueki, K.; Kuri, Z. *J. Phys. Chem.* **1973**, 77, 2365.

(6) Kinugawa, K.; Miyazaki, T.; Hase, H. *Radiat. Phys. Chem.* **1977**, 10, 341.

(7) Iwasaki, M.; Muto. H.; Toriyama, K. Fukaya, M.; Nunome, K. *J. Phys. Chem.* **1979**, 83, 1590.

(8) Kumada, T.; Komaguchi, K.; Aratono, Y.; Miyazaki, T. *Chem. Phys. Lett.,* **1996**, 261, 463.

(9) Lin, J.; Williams, F. *J. Phys. Chem.* **1968**, 72, 3707.

(10) Ingold, K. U.; Walton, J. C. *J. Am. Chem. Soc.* **1982**, 104, 616.

(11) Kerr, J. A.; Moss, S. J. (Eds.) *CRC Handbook of Bimolecular and Termolecular Gas Reactions*, 1981, CRC Press, Inc. Florida.

(12) Miyazaki, T.; Hirayama, T. *J. Phys. Chem.* **1975**, 79, 566.

(13) Miyazaki, T.; Guedes, S.; Fueki, K. *Bull. Chem. Soc. Jpn.*, **1980**, 53, 1813.

(14) Gillbro, T.; Lund, A. *Chem. Phys.* **1974**, 5, 283.

(15) Bell, R. P. *The Tunnel Effect in Chemistry*, 1981, Chapman and Hall, London.

(16) Miyazaki, T.; Wakayama T.; Fukaya M.; Saitake, Y.; Kuri, Z. *Bull. Chem. Soc. Jpn.* **1973**, 46, 1030.

(17) Miyazaki, T.; Kumada, T.; Komaguchi, K.; Aratono, Y. *Radiat. Phys. Chem.* **1997**, in press.

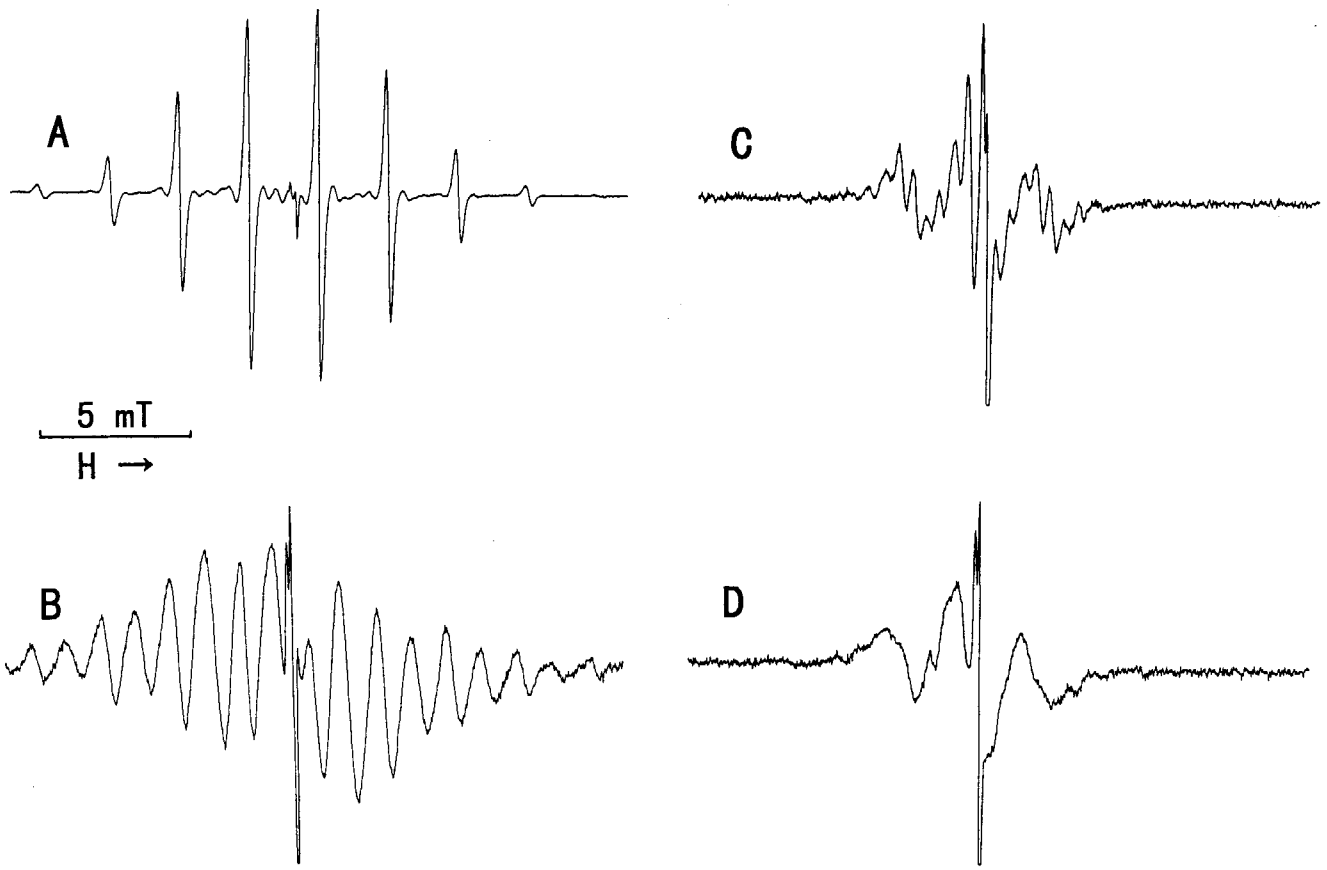

Figure 1. ESR spectra of neo-C_5H_{12} − i-C_4H_{10}(2 mol%) − HI(0.5 mol%) mixtures after UV-irradiation. Relative ESR gain setting of spectra A, B, C, and D are 1.0, 12.5, 10, and 12.5, respectively. (A) measured at 100 K after irradiation at 100 K; (B) measured at 30 K after irradiation at 100 K; (C) measured at 100 K after irradiation at 4 K; (D) measured at 70 K after irradiation at 4 K.

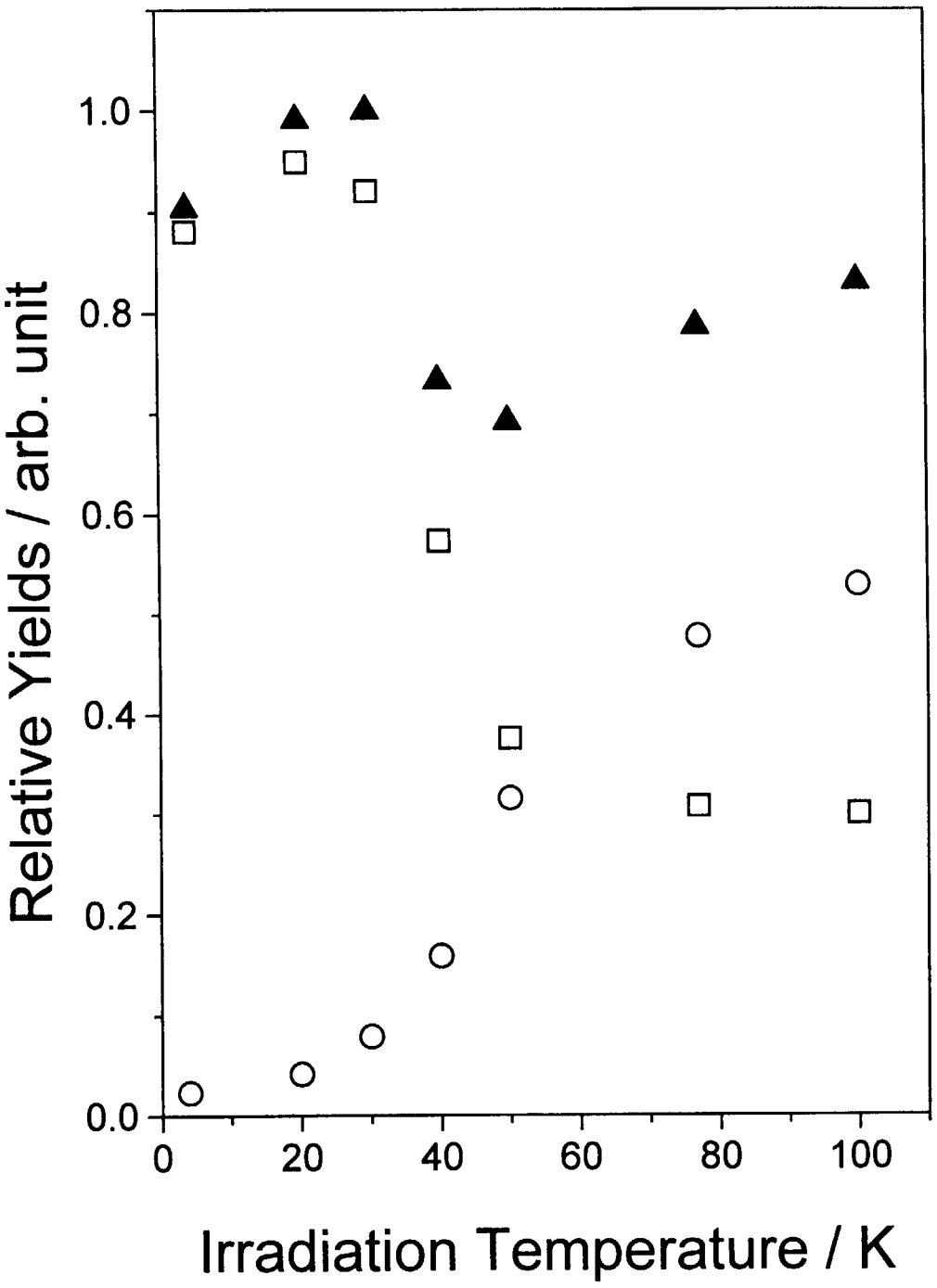

Figure 2. Effect of irradiation temperature on yields of radicals produced by UV-irradiation of neo-C_5H_{12}－i-C_4H_{10}(2 mol%)－HI(0.5 mol%) mixtures. (▲) sum of neo-C_5H_{11} and t-C_4H_9; (□) neo-C_5H_{11}; (○) t-C_4H_9.

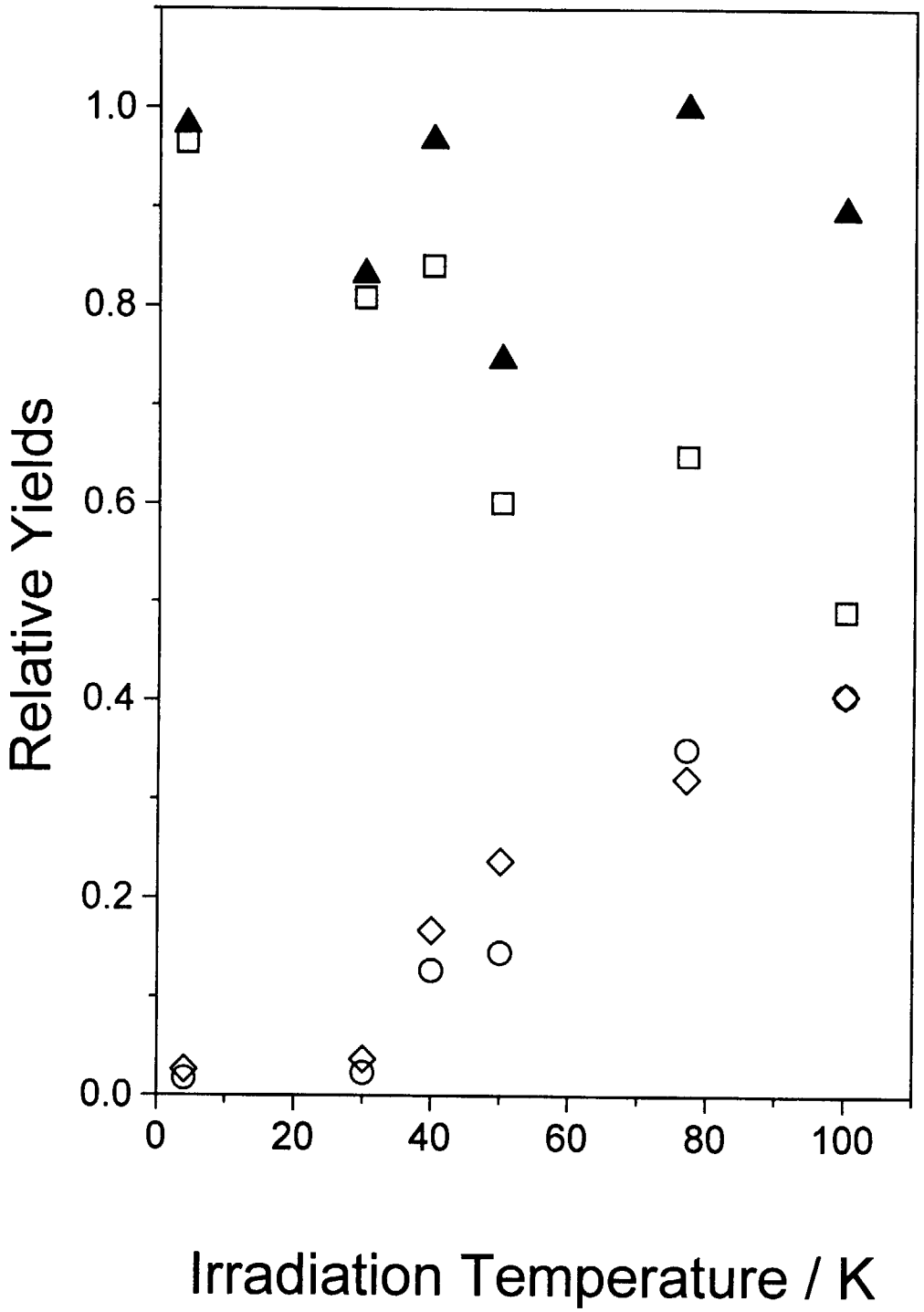

Figure 3. Effect of irradiation temperature on yields of radicals produced by X-rays irradiation of neopentane－alkane mixtures. (▲) sum of neo-C_5H_{11} and t-C_4H_9 in neo-C_5H_{12}－i-C_4H_{10}(2 mol%) mixtures; (□) neo-C_5H_{11} in neo-C_5H_{12}－i-C_4H_{10}(2 mol%) mixtures; (○) t-C_4H_9 in neo-C_5H_{12}－i-C_4H_{10}(2 mol%) mixtures; (◇) c-C_5H_9 in neo-C_5H_{12}－c-C_5H_{10}(2 mol%) mixtures. The relative yield of c-C_5H_9 at 100 K is normalized to the value of t-C_4H_9 at 100 K.

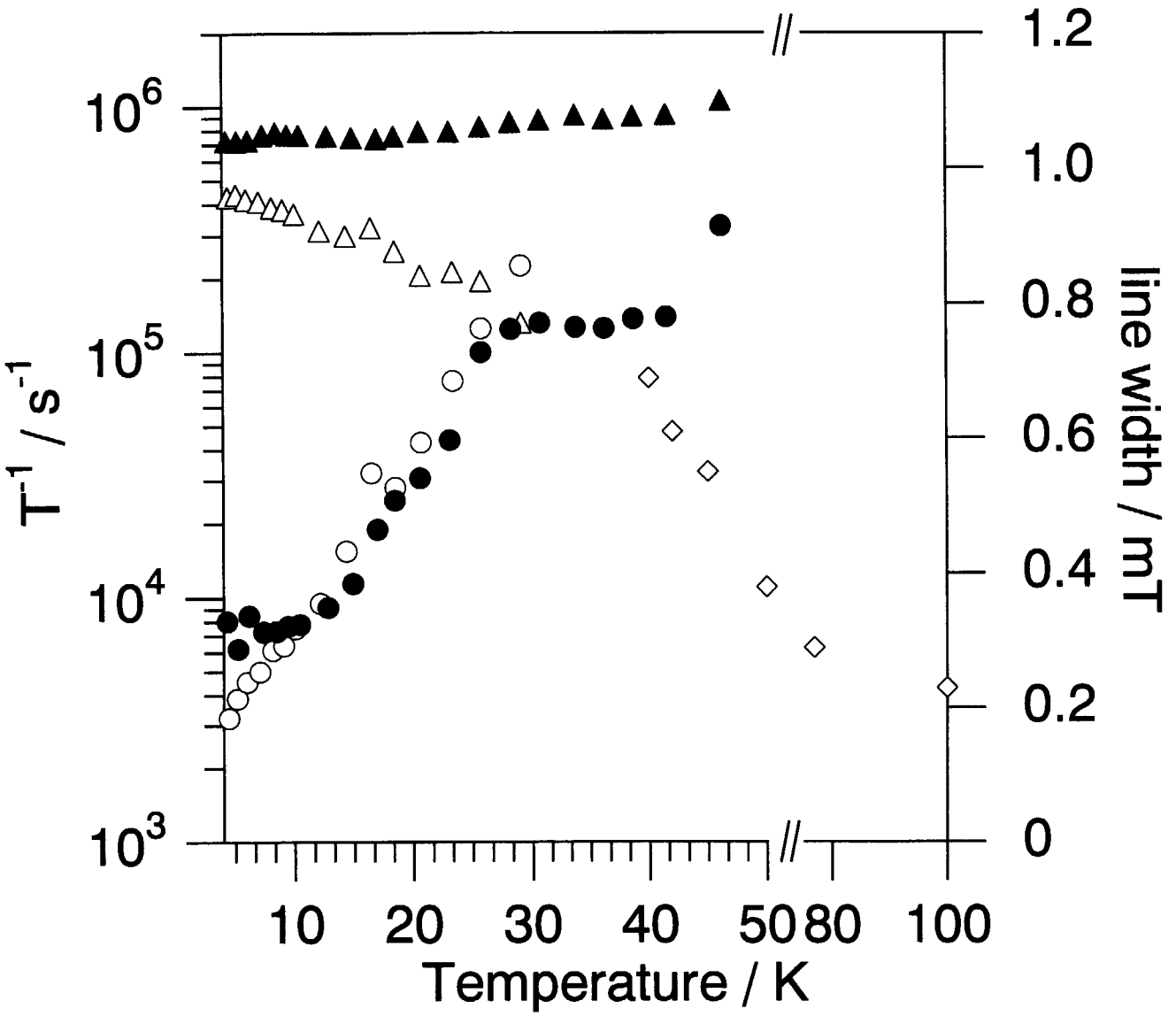

Figure 4. Temperature dependence of the spin–lattice (T_1^{-1}) and spin–spin (T_2^{-1}) relaxation rates of t-C_4H_9 and neo-C_5H_9 radicals produced by UV-irradiation of neo-C_5H_{12}—i-C_4H_{10}(2 mol%)—HI(0.5 mol%) mixtures. (●) T_1^{-1} of neo-C_5H_{11}; (○)T_1^{-1} of t-C_4H_9; (▲)T_2^{-1} of neo-C_5H_{11}; (△)T_2^{-1} of t-C_4H_9; (◇)ESR line width of t-C_4H_9.

11. Tunneling Effects on the Sigmatropic Hydrogen Shifts in the Photorearranged Intermediates of Phenyl Acetate and N-Acetylpyrrole Studied by Laser Photolysis

H. Shizuka and S. Tobita
Department of Chemistry, Gunma University, Kiryu, Gunma 376 Japan

The rate constants for the sigmatropic hydrogen shifts in the ground state of the photo-rearranged intermediates of phenyl acetate and *N*-acetylpyrrole produced by laser photolysis at 266nm are directly measured in several solvents. On the basis of the experimental results of temperature and isotope effects, it is shown that the intramolecular 1,3-hydrogen (or deuterium) shift of the photo-Fries rearranged intermediate of phenyl acetate and the 1,2-hydrogen (or deuterium) shift of the photorearranged intermediate of *N*-acetylpyrrole in methylcyclohexane proceed via tunnelling processes at two vibrational energy levels under experimental conditions. The theoretical considerations for the tunnelling mechanism are made by use of the tunnel effect theory proposed by Formosinho.

1. Introduction

Sigmatropic hydrogen shift is one of the most important and elementary processes in both chemistry and biochemistry. Until recently, a number of theoretical [1-5] and experimental [6-12] studies on the intramolecular hydrogen shifts both in the ground and excited states have been reported. Since hydrogen atom is the lightest atom, participation of not only thermally-activated processes but also quantum mechanical tunnelling processes in the intramolecular hydrogen shifts is of essential importance . In the present work, the rates of the intramolecular 1,3-hydrogen (or deuterium) shift of the photo-Fries rearranged intermediate of phenyl acetate (PAH) [13,14] and the 1,2-hydrogen (or deuterium) shift of the photorearranged intermediate of *N*-acetylpyrrole (NAH) [15] in methylcyclohexane (MCH) at various temperatures were directly measured by means of the 266nm laser photolysis method. The photochemical rearrangement reactions of PAH [16] and NAH [17] have been elucidated as shown in Scheme 1 and 2.

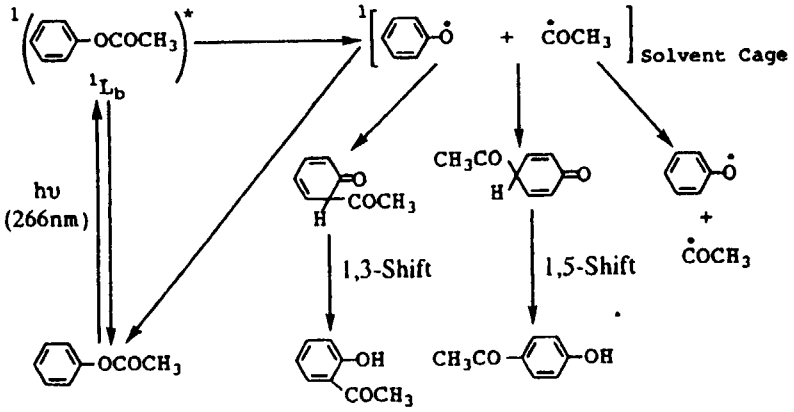

Scheme 1

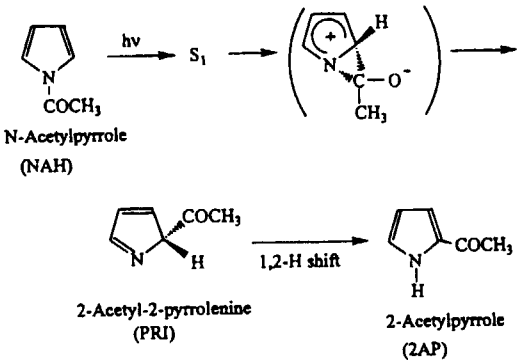

Scheme 2

On the basis of the experimental and theoretical results of temperature and isotope effects, it is shown that the intramolecular hydrogen shifts in the photorearranged intermediates of PAH (1,3-H shift) and NAH (1,2-H shift) in MCH proceed via quantum mechanical tunnelling at two vibrational energy levels under the present experimental conditions.

2. Experimental

Laser photolysis experiments were carried out by using the fourth harmonic (266nm) of a Nd^{3+}:YAG laser (Spectra-Physics GCR-130, pulse width 4-5ns) [13-15]. The monitoring system consisted of a 500-W xenon lamp (USHIO, UXL-500D), a monochromator (JOBIN YVON HR 320), and a photomultiplier (Hamamatsu, R928). The transient signals were recorded on a digitizing oscilloscope (Tektronix, TDS-540) and transferred to a personal computer (NEC PC-9801 BX3). Kinetic data analysis was made by use of nonlinear least-squares fitting programs.

To avoid the accumulation of photochemical products, fresh samples were used for each laser photolysis. The kinetic measurements were carried out by using a 1-cm or 1-mm quartz cell. The 1-mm cell was used in order to prevent the effect of diffusion on

the rise rate. It was confirmed that the effect of dissolved oxygen on the rates for the hydrogen and deuterium shifts was negligible. Therefore, the experiments were carried out under aerated conditions. For temperature and concentration effects experiments in nonpolar solvents, the samples were prepared in a drybox filled with nitrogen gas. Molecular orbital calculations were performed at a Hartree-Fock/3-21G level by using the GAUSSIAN 94 program .

3. Results and Discussion

Intramolecular Hydrogen Shifts in the Photo-Fries Rearranged Intermediate of Phenyl Acetate. Figure 1a shows the transient absorption spectra obtained by 266nm laser photolysis of PAH (5 x 10^{-3}M) in MCH.

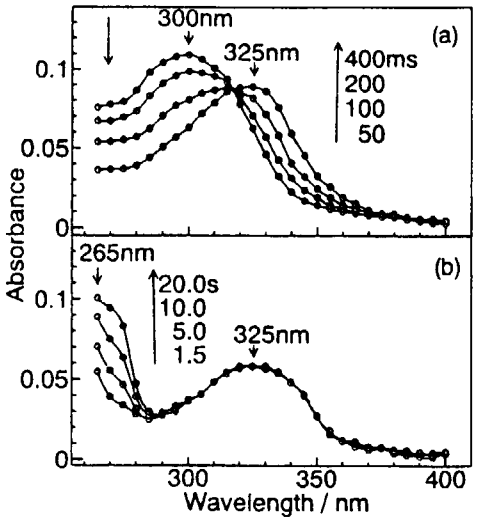

Figure 1

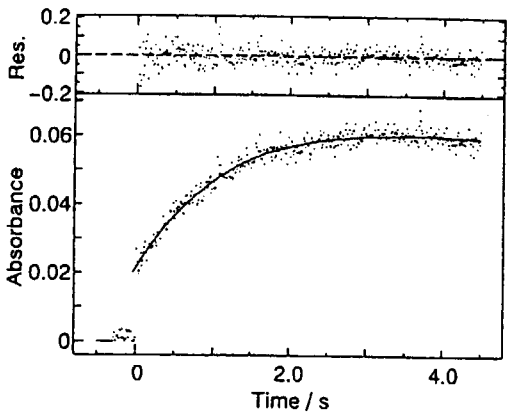

Figure 2

With a lapse in time an absorption peak at 325nm appears with a decrease of the peak around 300nm. The absorption peak around 325nm is ascribable to the absorption of ortho-final product, *o*-hydroxyacetophenone. The existence of an isosbestic point at 318nm demonstrates that the 300nm band corresponds to the absorption band of the ortho-rearranged intermediate. The formation rate of the ortho-final product which corresponds to the rate of the 1,3-hydrogen shift was determined by measuring the rise time at 325nm. Figure 2 shows a typical time trace of the ortho-final product monitored at 325nm in MCH at 293K. Since the absorption at 325nm is a superposition between those of ortho-rearranged intermediate and ortho product, the time trace can be analyzed by a composite function with rise and decay components as

$$A_{1,3}(t) = A \exp(-k_{1,3}t) + A'\{1 - \exp(-k'_{1,3}t)\} \quad (1)$$

where $A_{1,3}(t)$ is the observed absorbance at 325nm, A is the initial absorbance of the ortho-rearranged intermediate, A' is the final absorbance of ortho-final product, and $k_{1,3}$ and $k'_{1,3}$ are the decay and rise rate constants of ortho-rearranged intermediate and ortho-final product, respectively. By the least-square fitting of eq 1 to the rise curve in Figure 2, $k_{1,3}$ and $k'_{1,3}$ were determined to be 7.2 ($\pm$1.0) and 7.1($\pm$1.0)s^{-1} in MCH at 293K, respectively, showing $k_{1,3} \approx k'_{1,3}$. In Figure 2, the solid line displays the best fitted line calculated by eq 1.

The measurements of the temperature effect on the 1,3-sigmatropic hydrogen (or deuterium) shift by 266nm laser photolysis were carried out at a low concentration of PAH (2 x 10^{-3}M) in MCH to avoid the intermolecular interactions. Figure 3 shows the plots of $k_{1,3}^{H}$ (or $k_{1,3}^{D}$) as a function of T^{-1} in MCH.

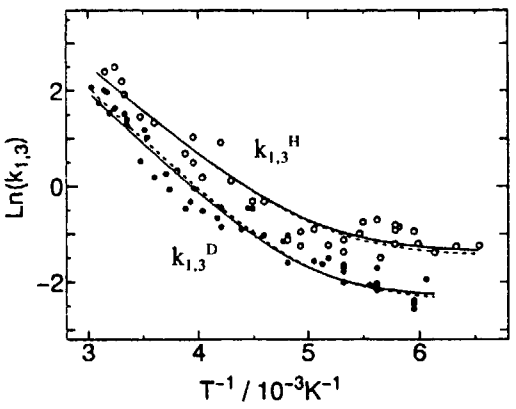

Figure 3

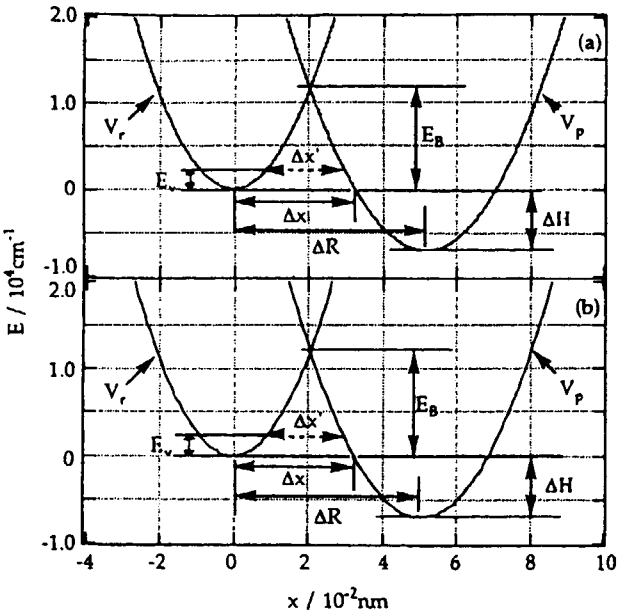

Figure 4

The values of $k_{1,3}^{H}$ are greater than those of $k_{1,3}^{D}$ at each temperature. The slopes of the plots becomes small in the low temperature range $\leqq$200K. The observed rate of $k_{1,3}$ can be expressed by eq 2, taking into account the Boltzmann distribution between two vibrational energy levels ($v = v_0$ and $v = v_1$) [18]

$$k_{1,3} = \frac{k_1 + k_2 \exp(-\Delta E / RT)}{1 + \exp(-\Delta E / RT)} \qquad (2)$$

where ΔE is the energy difference between the two levels, and k_1 and k_2 are their temperature-independent reaction rates. By the best fitting of eq 2 to the plots of $k_{1,3}^{H}$ vs

T^{-1} in Figure 3, the values of k_1^H, k_2^H and ΔE^H were determined to be $0.25s^{-1}$, $4.5 \times 10^3 s^{-1}$ and 3.9kcalmol^{-1} for the 1,3-hydrogen shift, respectively. Similar analysis was carried out for $k_{1,3}^D$ vs T^{-1}, and k_1^D, k_2^D and ΔE^D were determined as $9.9 \times 10^{-2} s^{-1}$, $5.5 \times 10^3 s^{-1}$, and 4.4 kcalmol^{-1}, respectively.

The theoretical treatment of the hydrogen atom transfer via tunnelling has been extensively studied by Formosinho [19-24]. The potential surfaces of the ortho-rearranged intermediate and ortho-final product for the 1,3-hydrogen shift were calculated on the basis of the Formosinho's theoretical treatment as shown in Figure 4. According to the tunnel effect theory [18, 22], the tunnelling rate constants of $k_{1,3}^H$ and $k_{1,3}^D$ can be calculated by use of the values E_B and Δx in Figure 4 as

$$k_{1,3} = \nu \exp\{-(2\pi/h)[2\mu(E_B - E_v)]^{1/2}\Delta x\} \qquad (3)$$

where ν is the average frequency for the tunnelling (the value was assumed as $10^{13} s^{-1}$) and the value of E_v is equal to ΔE. Here μ is the reduced mass estimated by eq 4

$$\mu^{1/2} = \mu_{CO}^{1/2} + \mu_{CH}^{1/2} \qquad (4)$$

where μ_{CO} and μ_{CH} are the reduced masses for CO and CH vibrations.

By using eq 3, the tunnelling rate constants, k_1, for 1,3-hydrogen and deuterium shifts at $E = 0$ ($\nu = \nu_0$) were calculated to be 2.3×10^{-1} and $9.2 \times 10^{-2} s^{-1}$, respectively. For the 1,3-hydrogen and deuterium shifts at $E = E_v$ ($\nu = \nu_1$), the values of k_2 were obtained as 4.5×10^3 and $6.1 \times 10^3 s^{-1}$, respectively. These results are summarized in Table 1 together with parameters used in the calculations.

Table 1

	1,3-H Shift		1,3-D Shift	
	$\nu = 0$	$\nu = \nu_1$	$\nu = 0$	$\nu = \nu_1$
$\mu/10^{-26}$ kg	2.21[b]	2.21[b]	2.29[b]	2.29[b]
$E_b/10^4$ cm^{-1}	1.20	1.20	1.20	1.20
$E_v/10^3$ cm^{-1}	0	1.36	0	1.55
$\Delta R/10^{-2}$ nm	5.20	5.20	5.08	5.08
$\Delta x/10^{-2}$ nm	3.28		3.26	
$\Delta x'/10^{-2}$ nm		2.40		2.30
k_1/s^{-1}	2.3×10^{-1}		9.2×10^{-2}	
k_2/s^{-1}		4.5×10^3		6.1×10^3

By use of these parameters the values of $k_{1,3}$ for the 1,3-sigmatropic hydrogen and deuterium shifts at various temperatures were calculated according to eqs 2 and 3. The calculated values of $k_{1,3}$ agree with the experimental ones as shown in Figure 3 as broken lines. It is concluded that the intramolecular 1,3-sigmatropic hydrogen (or deuterium)

shift proceeds via tunnelling processes at both E = 0 ($\nu = \nu_0$) and E = E_v (=3.9kcalmol^{-1} for the hydrogen shift and 4.4kcalmol^{-1} for the deuterium shift) ($\nu = \nu_1$) under the experimental conditions.

Intramolecular Hydrogen Shift in the Photorearranged Intermediate of *N*-Acetylpyrrole. The steady-state photolysis of NAH has been reported previously [25,26]. The rate for the 1,2-hydrogen shift of the photorearranged intermediate of NAH was directly measured by laser photolysis in MCH at 293K. Figure 5 shows the transient absorption spectra obtained by 266nm laser photolysis of NAH (2.82 x 10^{-4}M) in MCH at 293K.

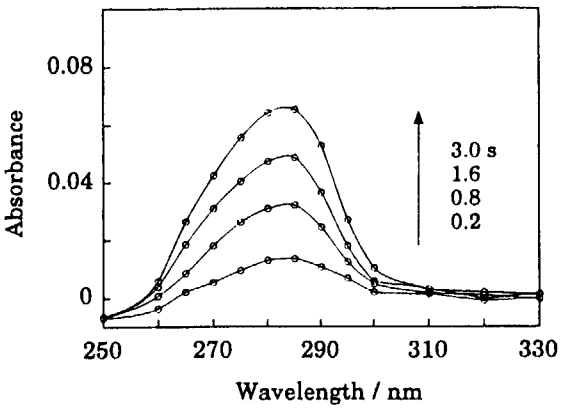

Figure 5

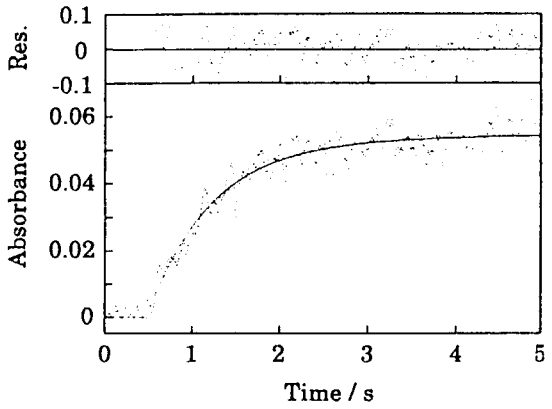

Figure 6

With a lapse in time, an absorption peak around 285nm appears. The absorption band around 285nm is ascribable to the absorption due to photoproduct (2-acetylpyrrole; 2AP) because the shape and the position of this transient spectra are in good agreement with those of 2AP [25]. The formation rate of 2AP corresponding to the rate of the 1,2-hydrogen shift can be determined by measuring the rise time at 290nm. Figure 6 shows a typical time trace monitored at 290nm in MCH at 293K. Since the spectral overlap between the photoproduct (2AP) and intermediate at 290nm is negligible, the time trace can be analyzed by the following equation

$$A_{1,2}(t) = A\{1 - \exp(-k_{1,2}t)\} \qquad (5)$$

where $A_{1,2}(t)$ is the observed time-dependent absorpbance at 290nm, A is the final absorbance, and $k_{1,2}$ is the rise rate of 2AP.

The measurements of the temperature effect on the 1,2-sigmatropic hydrogen (or deuterium) shift in the photorearranged intermediate produced by 266nm laser photolysis were carried out at a low concentration of NAH or *N*-acetylpyrrole-d_7 (NAD) (1.7 x

10^{-4}M) in dehydrated MCH to avoid the intermolecular reactions with the starting material (NAH or NAD) or a trace of water in MCH. Figure 7 shows the plots of the observed rates $k_{1,2}$ ($k_{1,2}^{H}$ or $k_{1,2}^{D}$) as a function of T^{-1} in dehydrated MCH.

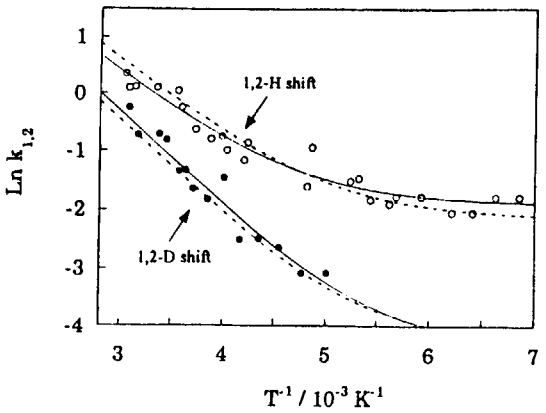

Figure 7

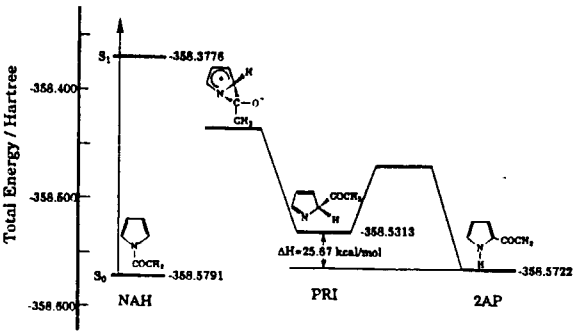

Figure 8

The Arrhenius plots give a straight line in the high-temperature range ≧ ca. 250K. However, the slope of the plots gradually becomes small in the low-temperature range ≦ ca. 250K. This fact suggests that 1,2-sigmatropic hydrogen and deuterium shifts proceed via quantum mechanical tunnelling in the electronically ground state.

The temperature dependence of the rate constants of 1,2-hydrogen ($k_{1,2}^{H}$) and 1,2-deuterium ($k_{1,2}^{D}$) shifts for NAH and NAD can be expressed by eq 2 as in the case of PAH and PAD by taking the Boltzmann distribution between two discrete vibrational energy levels into account. By the best fit of eq 2 to the plots of $\ln k_{1,2}$ vs T^{-1} in Figure 7, the values of k_1^{H}, k_2^{H}, and ΔE^{H} were determined to be $0.15s^{-1}$, $1.1 \times 10^{2}s^{-1}$, and 2.9kcalmol^{-1} for the 1,2-hydrogen shift of NAH, respectively. Similarly, the values of k_1^{D}, k_2^{D}, and ΔE^{D} were determined to be $1.3 \times 10^{-2}s^{-1}$, $1.0 \times 10^{2}s^{-1}$, and 3.3kcalmol^{-1} for the 1,2-deuterium shift of NAD, respectively. The best fitted values of $k_{1,2}$ are shown by solid lines in Figure 7.

To confirm the quantum mechanical tunnelling mechanism for the 1,2-sigmatropic hydrogen shift in the photorearranged intermediate of NAH, theoretical considerations were made in a similar manner as in the case of NAH. The energy diagram for the photorearrangement of NAH calculated by the ab initio MO method is shown in Figure 8. The enthalpy change (ΔH) for the 1,2-hydrogen shift was estimated to be -25.67kcalmol^{-1}, showing that the 1,2-hydrogen shift in this system is an exothermic reaction. By using Formosinho's theoretical treatment, potential energy curves for the 1,2-hydrogen and deuterium shifts were calculated as shown in Figure 9 (a) and 9(b) for NAH and NAD, respectively.

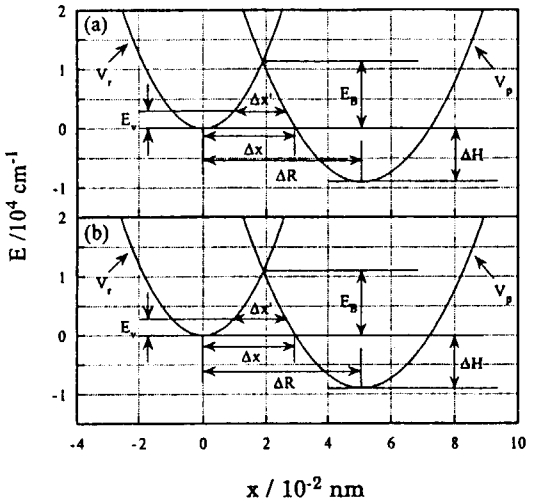

Figure 9

The parameters used to obtain the potential energy curves are summarized in Table 2.

Table 2

	1,2-hydrogen shift				1,2-deuterium shift			
	exptl		theoretical		exptl		theoretical	
	$v=0$	$v=v_1$	$v=0$	$v=v_1$	$v=0$	$v=v_1$	$v=0$	$v=v_1$
$f_r/10^7$ cm^{-1} nm^{-2}			6.30	6.30			6.02	6.02
$f_p/10^7$ cm^{-1} nm^{-2}			3.95	3.95			3.92	3.92
$\Delta R/10^{-2}$ nm			5.09	5.09			5.09	5.09
$\Delta x/10^{-2}$ nm			2.96				2.95	
$\Delta x'/10^{-2}$ nm				2.28				2.18
$E_B/10^4$ cm^{-1}			1.12	1.12			1.09	1.09
$E_v/10^3$ cm^{-1}	0	1.0	0	1.0	0	1.2	0	1.2
$\mu/10^{-26}$ kg			2.04[b]	2.04[b]			2.46[b]	2.46[b]
k_1/s^{-1}	0.15		0.12		1.3×10^{-2}		1.4×10^{-2}	
k_2/s^{-1}		1.1×10^2		1.4×10^2		1.0×10^2		0.9×10^2

By using the tunnelling parameters in Table 2 and eq 3, the tunnelling rate constants, k_1 and k_2 for the 1,2-hydrogen shift at v = 0 and v = v_1, were obtained as $0.12s^{-1}$ and $1.4 \times 10^2 s^{-1}$, respectively. For the 1,2-deuterium shift, k_1 and k_2 at v = 0 and v = v_1, were obtained as $1.4 \times 10^{-2} s^{-1}$ and $0.9 \times 10^2 s^{-1}$, respectively. By use of these tunnelling rate constants k_1 and k_2, the values of $k_{1,2}$ can be calculated by eq 2 at various temperatures. The calculated $k_{1,2}$ values for the 1,2-hydrogen and deuterium shifts are plotted in Figure 7. The agreements between the experimental and theoretical values for $k_{1,2}$ show that the 1,2-hydrogen and deuterium shifts in the photorearranged intermediate of PAH proceeds via tunnelling processes at two vibrational energy levels.

References

1) Evanseck, J. D.; Houk, K. N. *J. Phys. Chem.* **1990**, *94*, 5518.
2) Dorigo, A. E.; McCarrick, M. A.; Loncharich, R. J.; Houk, K. N. *J. Am. Chem. Soc.* **1990**, *112*, 7508.
3) Bernardi, F.; Olivucchi, M.; Robb, M. A.; Tonachini, G. *J. Am. Chem. Soc.* **1992**, *114*, 5805.
4) Sobolewski, A. L. *Chem. Phys. Lett.* **1993**, *211*, 293.
5) Tapia, O.; Andrés, J.; Safont, V. S. *J. Phys. Chem.* **1994**, *98*, 4821.
6) Duhaime, R. M.; Weedon , A. C. *Can. J. Chem.* **1987**, *65*, 1867.
7) Grellmann, K. H.; Weller, H.; Tauer, E. *Chem. Phys. Lett.* **1983**, *95*, 195.
8) Al-Soufi, W.; Grellmann, K. H.; Nickel, B. *J. Phys. Chem.* **1991**, *95*, 10503.
9) Al-Soufi, W.; Eychmüller, A.; Grellmann, K. H. *J. Phys. Chem.* **1991**, *95*, 10503.
10) Reid, P. J.; Wickham, S. D.; Mathies, R. A. *J. Phys. Chem.* **1992**, *96*, 5720.
11) Liu, M. T. H.; Bonneau, R. *J. Am. Chem. Soc.* **1992**, *114*, 3604.
12) Liu, M. T. H. *Acc. Chem. Res.* **1994**, *27*, 287.
13) Arai, T.; Tobita, S.; Shizuka, H. *J. Am. Chem. Soc.* **1995**, *117*, 3968.
14) Arai, T.; Tobita, S.; Shizuka, H. *Chem. Phys. Lett.* **1994**, *223*, 521.
15) Kimura, Y.; Yamamoto, M.; Tobita, S.; Shizuka, H. *J. Phys. Chem.* A **1997**, *101*, 459.
16) see references cited in ref. 13.
17) see references cited in ref. 15.
18) Bell, R. P. *The Tunnelling Effects in Chemistry*; Chapman and Hall: London 1980.
19) Formosinho, S. J. *J. Chem. Soc. Faraday Trans.* 2 **1976**, *72*, 1313.
20) Formosinho, S. J.; Arnaut, L. G. *Advances in Photochemistry*; John Wiley & Sons: New York, **1991**; Vol. 16, p67.
21) Formosinho, S. J. *Mol. Photochem.* **1976**, *7*, 41.
22) Formosinho, S. J. *J. Chem. Soc. Faraday Trans.* 2 **1974**, *70*, 605.
23) Formosinho, S. J.; da Silva, J. D. *Mol. Photochem.* **1974**, *6*, 409.
24) Varandas, A. J. C.; Formosinho, S. J. *J. Chem. Soc. Faraday Trans.* 2 **1986**, *82*, 953.
25) Shizuka, H.; Okutsu, E.; Mori, Y.; Tanaka, I. *Mol. Photochem.* **1969**, *1*, 135.
26) Shizuka, H.; Ono, S.; Morita, T.; Tanaka, I. *Mol. Photochem.* **1971**, *3*, 203.

12. Tunneling in the Mu + F_2 → MuF + F reaction :the role of van der Waals potential[1]

Toshiyuki Takayanagi and Yuzuru Kurosaki
Advanced Science Research Center, Japan Atomic Energy Research Institute,
Tokai-mura, Naka-gun, Ibaraki 319-11, Japan

1. Introduction

The H + F_2 reaction is an important example of prototypical atom-diatom chemical reaction with a large exothermicity. Since this reaction is the basis of an efficient chemical laser, extensive experimental studies have been reported mostly on the vibrational distribution of the product HF. In 1989, Gonzalez et al.[2] made an important contribution on tunneling for this reaction by measuring thermal rate constants for the Mu + F_2 → MuF + F reaction, where Mu is a light isotope of hydrogen atom. They found a significant curvature in the Arrhenius plot of the rate constants for Mu + F_2 in the temperature range between 100 and 450 K.[2] They have also compared their experimental rate constants to the theoretical ones[3] and found a serious disagreement. This is due to the inaccuracy of the semi-empirical potential energy surface employed in the theoretical calculations.[3] In this work, we carry out extensive ab initio calculations for the H + F_2 reaction and develop new potential energy surfaces for this reaction. We also present the theoretical rate constants calculated using the new potential surfaces.

2. Theory

Ab initio molecular orbital calculations were carried out at the coupled-cluster with single and double substitutions (CCSD) using the 6-311++G(3df,3pd) basis set. About 200 points of the potential energies were calculated within collinear geometries and the classical barrier height was calculated to be 3.7 kcal/mol. The bend angle dependence of the potential energy as well as the long-range van der Waals interaction in the asymptotic regions were also calculated at the same level of theory.

We then developed new potential energy surfaces using the ab initio computational results. We employed the London-Eyring-Polanyi-Sato (LEPS) functional form with the angle-dependent Sato parameters[4] in order to reproduce the angle-dependent potentials obtained from the ab initio calculations. The van der Waals potential was also added to the LEPS function in order to take the ab initio asymptotic behavior of the potential energy into account. The classical barrier height of 3.7 kcal/mol obtained at the CCSD/6-311++G(3df,3pd) level of theory was slightly lowered since this value is considered to be too large. Finally, we have developed two potential energy surfaces having slightly different classical barrier heights; Surface I and II. Both the potential surfaces approximately reproduce the ab initio results except barrier height; The classical barrier height for Surface I is 0.7 kcal/mol, while 1.0 kcal/mol for Surface II.

Thermal rate constants were theoretically calculated using the approximate quantum scattering method since accurate three-dimensional quantum scattering calculations are not feasible because of the large exothermicity of the H + F_2 reaction. We have employed the reduced-dimensionality method originally developed by Bowman.[5,6] In the reduced

dimensionality theory for atom-diatom chemical reactions, two stretch degrees of freedom are treated quantum mechanically, while the remaining bending motion is treated as an adiabatic bend during collision. Thus, the problem we have to solve reduces to a usual two-dimensional collinear quantum scattering problem. The two-dimensional Schrödinger equation was numerically solved using a standard R-matrix propagation on a natural collision coordinate system. Bending vibrational energies were calculated on all the two-dimensional grid points using a standard Harmonic basis set expansion method. The details of the computational procedure are described elsewhere.[7]

3. Results and Discussion

Figure 1 compares the rate constants calculated using Surface I to the experimental data of Gonzalez et al.[2] Essentially the same plot was obtained for Surface II, although the calculated rate constants were somewhat smaller than those for Surface I. Solid lines in this figure indicate the rate constants using the potential energy surface without the van der Waals potential, while dotted lines show those calculated using the potential surface including the van der Waals interaction. Figure 1 clearly demonstrates how the inclusion of the van der Waals potential affects the rate constants. It can be seen that for the Mu + F_2 reaction the inclusion of van der Waals potential significantly increases the rate constants especially at low temperatures for both surfaces. Also plotted in Figure 1 are the experimental[8,9] as well as theoretical rate constants for the H + F_2 reaction. The theoretical rate constants seem to be slightly larger than the experimental ones. However, note that the agreement between the two experimental results is not good.

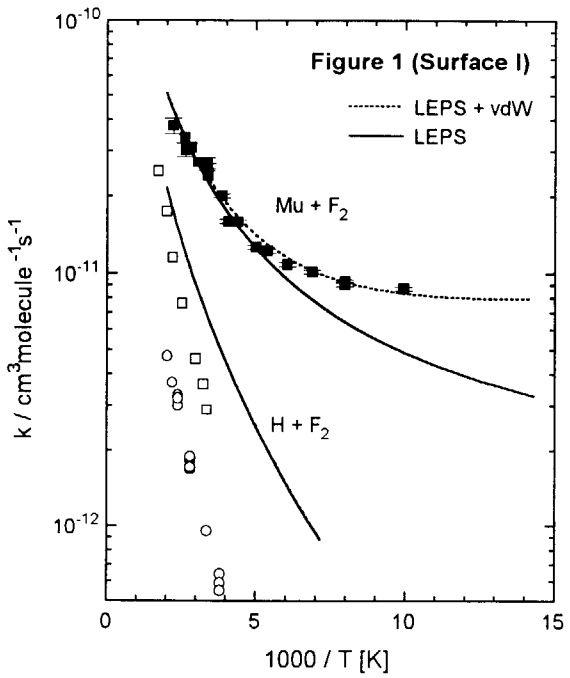

The effect of the van der Waals potential on the rate constants can qualitatively be understood in terms of the vibrationally adiabatic potential profile for the Mu + F_2 reaction plotted in Figure 2. Since the LEPS potential is purely repulsive in the asymptotic region, the tunneling barrier width increases with a decrease in the translational energy. On the other hand, if we include the van der Waals interaction in the potential surface, the tunneling barrier width

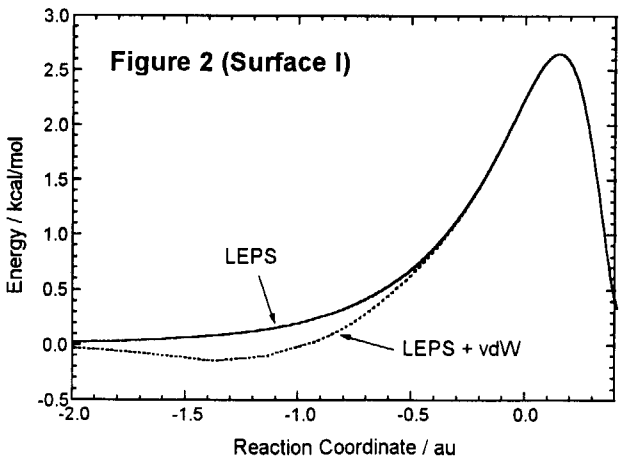

becomes a finite value with a decrease in the translational energy. This result implies that the barrier width is much more important than the barrier height at low temperatures where quantum tunneling is dominant. The present work also suggests that tunneling correction using an Eckart potential would not be a good approximation to predict a low temperature behavior of the rate constants for the Mu + F_2 reaction since the Eckart potential is repulsive and fails to account for the van der Waals mimima.

References

(1) This work is published in T. Takayanagi and Y. Kurosaki, *J. Phys. Chem.*, **101**, 7098 (1997).
(2) A.C. Gonzalez, I.D. Reid, D.M. Garner, M. Senba, D.G. Fleming, D.J. Arseneau, and J.R. Kempton, *J. Chem. Phys.*, **91**, 6164 (1989).
(3) B.C. Garrett, R. Steckler, and D.G. Truhlar, *Hyperfine Interact.*, **32**, 779 (1986).
(4) T. Takayanagi and S. Sato. *Chem. Phys. Lett.*, **144**, 191 (1988).
(5) J.M. Bowman, *J. Phys. Chem.*, **95**, 4960 (1991).
(6) J.M. Bowman and A.F. Wagner, In "Theory of Chemical Reaction Dynamics" edited by D.C. Clary, Reidel: Dordrecht, 1986.
(7) T. Takayanagi and S. Sato. *J. Chem. Phys.*, **92**, 2862 (1990).
(8) R.G. Albright, A.F. Dodonov, G.K. Lavrovsjaya, I.I. Morosov, and V.L. Tal'rose, *J. Chem. Phys.*, **50**, 3632 (1969)..
(9) R.H. Homann, H. Schweinfurth, and J. Warnatz, *Ber. Bunsenges, Phys. Chem.*, **81**, 724 (1977).

13. Reaction between Atoms and Small Molecules : Matrix Isolation ESR Studies and Modeling by Semiempirical SCF Calculations

Paul H. Kasai
IBM Research Division, Almaden Research Center
650 Harry Road, San Jose, CA 95120-6099

Reactions between paramagnetic atoms and small molecules may be examined by cocondensing the subject atoms and molecules in inert gas matrices at low temperature and examining the resulting matrices by electron spin resonance (ESR) spectroscopy. The electronic ground state and structure of the resulting species may be deduced cogently from the hyperfine structure(s) of the spectra. Thus it was shown some time ago that a hydrogen atom reacts with an acetylene molecule to form a vinyl radical in which "the original acetylenic hydrogen atoms" assume the trans positions.[1] A later work revealed that an aluminum atom reacts with acetylene also to form an adduct radical of the vinyl form; the disposition of the hydrogen atoms in the product radical, however, was of the cis form.[2] More recently it was shown that, when Li atoms and acetylene molecules were cocondensed in an argon matrix, a side-on complex is formed between a Li atom and an acetylene molecule bent cis-wise.

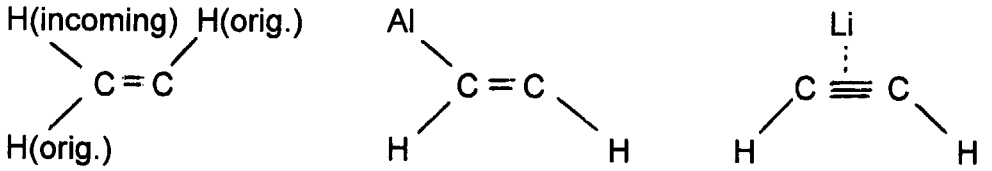

Little is known about the reaction passages leading to these product species.

The accuracy and reliability of semiempirical SCF calculations at the MNDO or AM1 level for predicting the ground state structures of molecules have been well demonstrated.[4]. Performing geometry optimization on reacting species by such computational methods following the steepest energy trough should provide an insight for the reaction passage viable at the electronic ground state. The reaction passages of the H/C_2H_2, Al/C_2H_2, and Li/C_2H_2 systems were examined

accordingly. The calculations revealed the importance of the dative interaction of the bonding π orbital electrons in determining the earlier course of reaction. The approaching atom thus acquires a net negative charge in the earlier stage of reaction in every case. The expected Al→ C_2H_2 and Li→ C_2H_2 electron transfer occurs at a later stage. The calculations yielded the final structure in agreement with the observed result in each case. Figure 1 presents schematically the pertinent features of the reaction passages and products given by the AM1 method for the three reaction systems. The reaction passages and the product structures can be rationalized in terms of the atomic and molecular orbital levels of the reacting species (Figure 2).

Another recent matrix-isolation ESR study revealed that an aluminum atom, on encounter with HCl, forms the insertion product H-Al-Cl.[5] The production of free hydrogen atoms was also observed. Examination of the Al/HCl system by the MNDO method showed that the Al atom moves toward HCl driven by the energy stabilizing interaction between the singly occupied Al 3p orbital and the vacant HCl antibonding σ orbital. The Cl atom monopolizes the incoming charge, and dispels the hydrogen atom. When the approach commences on the hydrogen side of the antibonding σ orbital, the insertion product H-Al-Cl is formed. When the approach begins on the Cl side, the displacement reaction Al• + Cl-H → Al-Cl + H• occurs. The insertion reaction dominates reflecting the expanse of the hydrogen 1s orbital in the HCl antibonding σ orbital.

Most recently we examined, by the AM1 method, the reaction between a Li atom and a HCN molecule **prior to experiments**. The calculation predicted the formation of a side-on complex in a manner completely analogous to the formation of the Li:C_2H_2 side-on complex; but also the formation of a linear end-on complex when the Li atom approaches HCN from the nitrogen end. The end-on complex is a meta-stable state; it is ~10 Kcal/mol. less stable than the side-on complex.

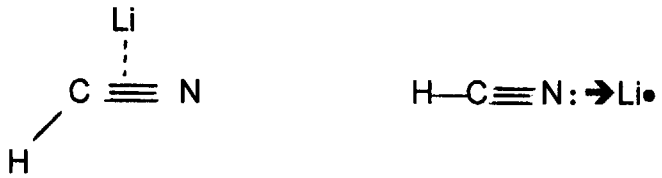

We subsequently performed a matrix isolation ESR study of the Li/HCN/Ar and Li/CH_3CN/Ar systems. Basically the identical results were obtained for both systems. Figure 3a shows the spectrum of the Li/CD_3CN/Ar system observed as prepared. The signals labeled A are due to isolated Li atoms. The quartet pattern labeled B is assigned to the end-on complex predicted by the theory. The triplet feature conspicuously recognized in each component is attributed to the nitrogen nucleus. The broad, central signal C has a profile (indicated above the signal) consistent with the pattern expected for the side-on complex predicted by the theory (the pattern due to the nitrogen hyperfine coupling tensor of an extreme uniaxial asymmetry, $A_{\parallel} >> A_{\perp} \cong 0$). The pattern was unambiguously resolved when the experiment was repeated using ^6Li isotope.[6] Intriguingly when the matrix was irradiated with near IR light (λ=850±50 nm), the quartet due to the end-on complex disappeared completely with concurrent increase of the signal due to the side-on complex. See Figure 3b. The signals due to the isolated Li atoms remained unaffected. When the matrix was subsequently irradiated with red light (λ=700±50 nm), the signals due to isolated Li atoms disappeared completely and strong signals due to methyl radicals, CD_3, appeared. The signal C due to the side-on complex remained unaffected. The 2s→2p transition of Li atoms occurs at 680 nm. It must be that an electron capture by isolated CH_3CN leads to the dissociative process, $CH_3CN + e^- \rightarrow CH_3\bullet + CN^-$.

The several examples of matrix isolation ESR studies and modeling by semiempirical SCF molecular orbital calculations presented above clearly demonstrate the efficacy and power of such calculations in elucidating the reaction passage and mechanism. A "Slide-Show" of reactions discussed in this report can be viewed on: http://www.almaden.ibm.com/st/people/kasai.

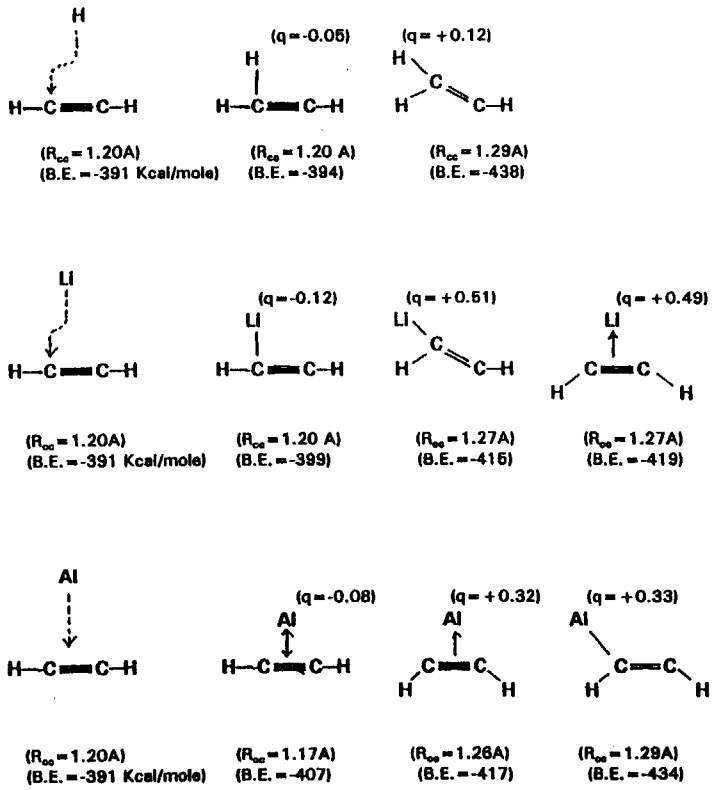

Figure 1

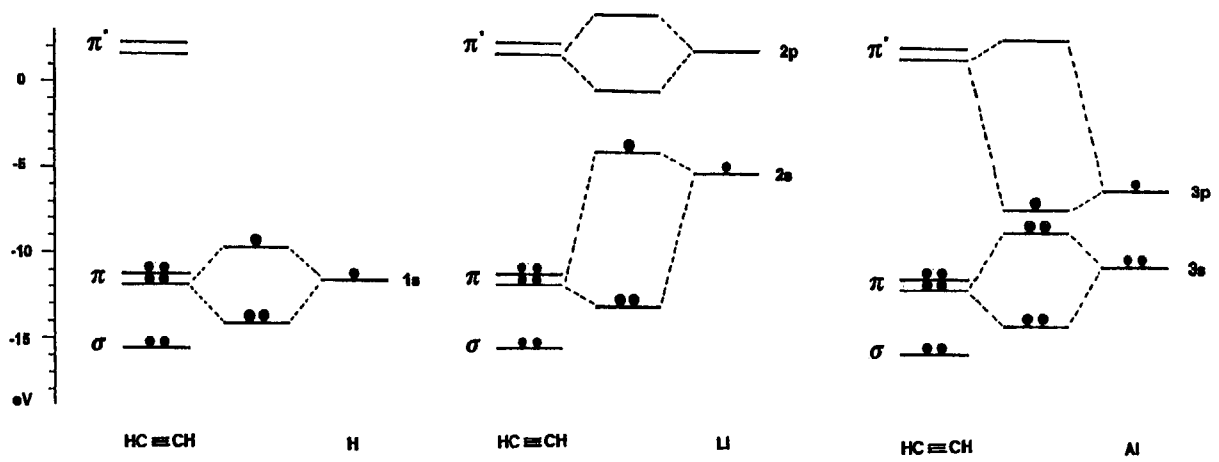

Figure 2

Figure 3

References:

[1] E. L Cochran, F.J. Adrian, V. A. Bowers *J. Chem. Phys.* 40, 213 (1964).

[2] P. H. Kasai *J. Am. Chem. Soc.* 104, 1165 (1982).

[3] P. H. Kasai, *J. Am. Chem.* Soc. 114, 3299 (1992).

[4] See, for example, J. J. P. Stewart *J. Computer-Aided Mol. Design 4*, 1 (1990).

[5] R. Köppe, P. H. Kasai *J. Am. Chem. Soc.* 118, 135 (1996).

[6] P. H. Kasai (to be published).

14. Structure and Dynamics of Radical Cations of Selectively Deuteriated Cyclohexanes — An ESR and Ab Initio Study —

Masaru Shiotani and Peng Wang
Faculty of Engineering, Hiroshima University Higashi-Hiroshima 739, Japan

An ESR spectroscopic study was carried out to elucidate static and dynamic Jahn-Teller structures of the radical cations of selectively deuteriated cyclohexanes in c-C_6F_{12} matrix formed by ionizing radiation at low temperature. Based on the ESR spectra combined with an *ab-initio* and density functional theory the geometrical structure of the radical cations was concluded to be distorted into a C_{2h} symmetry from the original D_{3d} symmetry. The experimental temperature dependent ESR spectra were analyzed in terms of dynamical averaging among the C_{2h} structures with slightly different zero-point vibration energies due to the substituted deuterium mass effects.

Introduction

Structure on alkane radical cations has attracted many attentions, since in the neutral form they usually have a degenerate or nearly degenerate highest occupied molecular orbital (HOMO).[1,2] Ionization is followed by a geometrical distortion, well known as the Jahn-Teller effect, which demonstrates the instability of degenerate electronic state. The radical cation of cyclohexane is of particular interest because of its high molecular symmetry and a fundamental molecule. A number of ESR and theoretical studies have been reported for the cyclohexane and related radical cations,[3-11] however, details of their static and dynamic structures have not yet completely understood.

Iwasaki and Toriyama[3] have proposed a ^2A_g electronic state in C_{2h} symmetry for the cyclohexane radical cation based on the ESR data extrapolated from the temperature-dependent ^{1}H hyperfine (hf) splitting and *semi-empirical* INDO MO calculations. On the other hand, Lunell *et al.*[4] have suggested an electronic ground state of $^2A''$ in lower C_s symmetry from the results of *ab-initio* calculations. We have reported a series of ESR studies on structure distortion and dynamics in the radical cations of selectively alkyl-substituted cyclohexanes and related molecules. The radical cations were found to be classified into ^2A_g-like (in elongated C_{2h} structure), ^2B_g-like (in compressed C_{2h} structure), and $^2A''$-like (in C_s structure) with structural resemblance to the cyclohexane cation.[5-16]

Use of selectively ^{2}D-labelled compounds is essential for an unequivocal assignment of

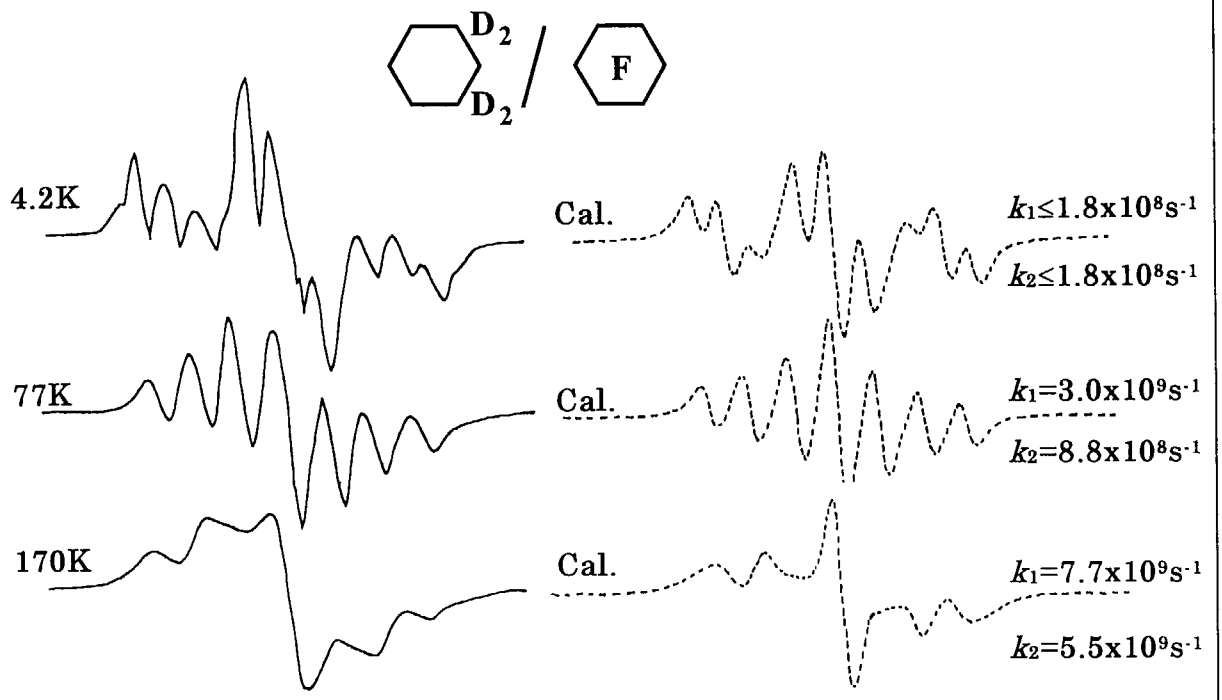

Figure 1. Temperature dependent ESR spectra of *c*C6-1,1,3,3-d_4^+ in cC_6F_{12} matrix. The simulated spectra are shown with the dotted lines together with the exchange rates employed in the calculations.

ESR spectra of organic radicals because of the difference in magnetic properties between proton and deuteron (spin labeling effects). [5] In addition, the mass difference between these hydrogen isotopes can affect the ESR spectrum significantly. In the present report, a detailed ESR study was carried out in order to obtain more conclusive information about static and dynamic Jahn-Teller effects on selectively deuteriated cyclohexane radical cations in a halocarbon matrix at low temperature. Combined with theoretical calculations employing an advanced *ab initio* and density functional theory (DFT) [15] the radical cations were concluded to take a ^2A_g electronic ground state in the C_{2h} symmetry in which the two C-C bonds are

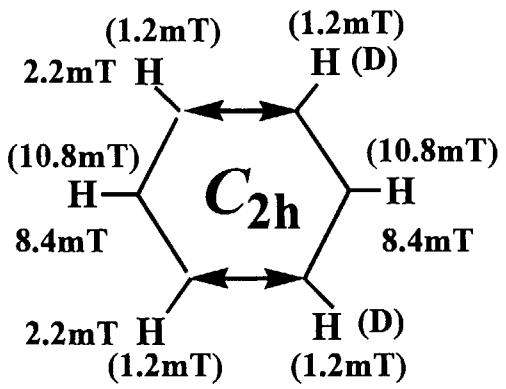

Figure 2. Assigument of the experimental ^{1}H hf splittings of *c*C6-1,1,3,3-d_4^+ in cC_6F_{12} at 4.2K. The values in parentheses are the theoretical hf splittings calculated for the equatorial hydrogens in a C_{2h} structure. The arrow (↔) stands for the elongated C-C bonds.

elongated and the other four C-C bonds are compressed. The temperature dependent ESR spectra were successfully analyzed in terms of dynamical averaging processes among three C_{2h} distorted forms with different zero-point vibration energies due to the substituted deuterium mass effects.

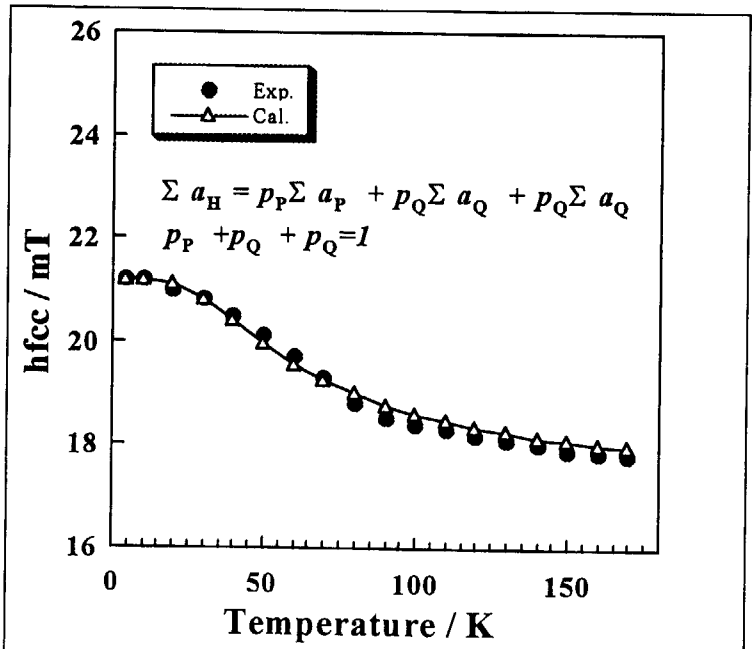

Figure 3. The experimental total ^{1}H hf splittings, Σa, are plotted against temperature for cC6-1,1,3,3-d_4^+ together with the calculated ones.

Experimental

The following five different deuteriated cyclohexane were used in the present ESR study: cyclohexane (cC6), cC6-1,1-d_2, cC6-1,1,3,3-d_4, cC6-1,1,4,4-d_4 and cC6-1,1,2,2,3,3-d_6. The radical cations were generated in halocarbon matrices such as cC_6F_{12}, CF_3-cC_6F_{11} by ionizing radiation at 77 K. The temperature dependent ESR spectra were observed on Brucker ESP-300 spectrometer from 4.2 K to 200 K.

Results and Discussion

The temperature dependent ESR spectra of cC6-1,1,3,3-d_4^+ are shown in Figure 1. The 4 K spectrum consists of essentially a triple triplet with isotropic ^{1}H hf splittings of a_1=8.4 mT and a_2=2.2 mT and axial symmetric g-factor, $g_{//}$=2.0109 and $g_\perp$=2.0046. Assuming a C_{2h} distorted structure with the both C3-C4 and C6-C1 bonds elongated, the larger (a_1) and smaller (a_2) triplets were attributable to two equatorial hydrogens at the C2 and C5 positions and two equatorial hydrogens at the C4 and C6 positions, respectively (Figure 2). The *ab initio* MO calculations of cC6$^+$ (Gaussian 94 at MP2/6-31G** level) resulted in the C_{2h} structure whose total energy was lower by 1.2 kcal/mol than the C_s structure (next stable structure). The ^{1}H-hf splittings were calculated for the two pairs of equatorial hydrogens at C2, C5 and C4, C6 in the C_{2h} structure. They are 10.4mT and 1.2mT, respectively, which are in a rather good agreement with the experimental values of a_1=8.4 mT and a_2=2.2 mT (Figure 2).

The ESR spectra of cC6-1,1,3,3-d_4^+ depend strongly on temperature. With increasing temperature from 4.2K the original triple triplet changes into a septet with an averaged hf splitting

of 6.2 mT (2H) and 3.1 mT (2H) at 77 K, and an apparent quintet at 170 K as shown in Figure 1. The total ^{1}H-hf splitting, Σa, was found to decrease with increasing temperature from 21.2 mT (4.2 K) to 17.8 mT (170 K) (Figure 3). The experimental results can be explained as follows:

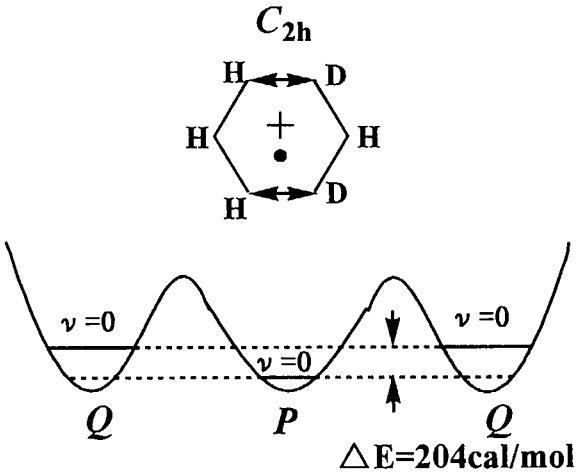

Figure 4. Potential energy curves with the ZPEs calculated for three C_{2h} geometrical structures (P and two Q) of *c*C6-1,1,3,3-d_4^+.

1) Depending on the sites which the deuterium atoms occupy, three C_{2h} distorted forms, P, Q and Q', are possible for *c*C6-1,1,3,3-d_4^+ (Figures 4 and 5). The theoretical calculations (DFT/6-31G** level) resulted in *P*-form whose zero-point vibrational energy (ZPE) was lower by 204 cal/mol than that of Q form. The Q and Q' forms are in a mirror image with the same ZPE.
2) The probabilities of finding the different form (p_P, p_Q, $p_{Q'}$) were assumed to be followed by Boltzmann distribution. Using the calculated ZPE values the probabilities were evaluated: for example, p_P: p_Q: $p_{Q'}$= 0.998: 0.001: 0.001 at 4.2 K and 0.478: 0.261: 0.261 at 170 K.
3) When the three forms are interchanged with the rates fast enough compared with the ESR time scale, a mean total ^{1}H-hf splitting, $<\Sigma a>$, is obtained:

$$<\Sigma a> = p_P\Sigma a_P + p_Q\Sigma a_Q + p_{Q'}\Sigma a_{Q'}$$

Using the calculated values of p_P, p_Q ($p_{Q'}$) and the experimental ones, Σa_P=21.2 mT and Σa_Q (=$\Sigma a_{Q'}$) = 15.0 mT, the temperature dependency of $<\Sigma a>$ was evaluated and compared with the experimental values in Figure 3. A good relationship has been seen between the experimental and theoretical total ^{1}H-hf splittings.
4) Then, the three C_{2h} forms were assumed to interchange with the rates of k_1 and k_2 (Figure 5) whose values were assumed to be inversely proportional to the lifetime at each form (which is determined by the Boltzmann distribution). The temperature dependent ESR spectra were simulated using the rate constants as adjustable parameters. [17] The calculated spectra are shown with the dotted lines in Figure 1.

The temperature dependent ESR line shapes were reproduced quite well employing the interchange (or jump) model among three C_{2h} forms with different ZPEs. Fig. 6 shows the Arrhenius plot of the exchange rates, k_2. The plot shows a non-linear relation in the temperature range between 40 K and 180 K. The ESR spectra observed below 40 K were simulated by

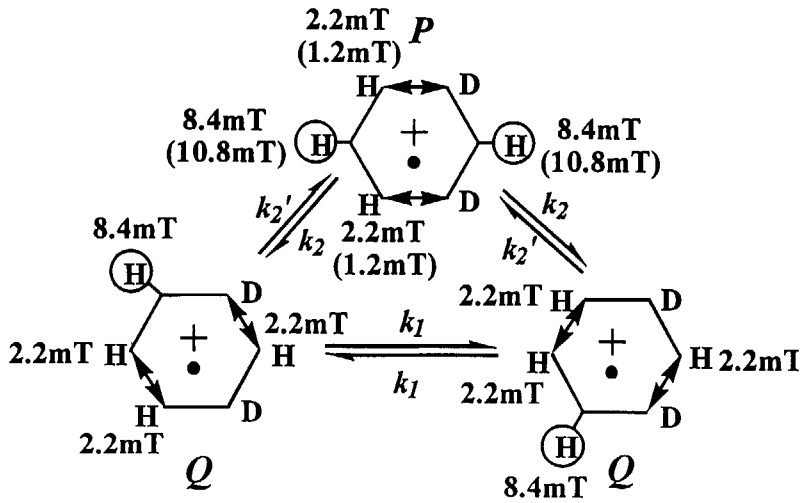

Figure 5. Schematics showing three sites exchange (or jump) among one C_{2h} (P) and two C_{2h} (Q) structures of cC6-1,1,3,3-d4+ with different ZPEs.

assuming the rigid limit line shape. This indicates that the rates (below 40K) fall to too low to be detected by the present ESR experiment, *i.e.*, less than *ca.* 1 x 10^8 sec^{-1}. With decreasing temperature below 40 K, p_p value approaches one so that *P* form dominates the conformations. In this case no interchange is possible between P and Q (and Q') forms because of no population in the latter forms. This can be the reason why we have observed the rigid limit ESR spectra in the low temperature range.

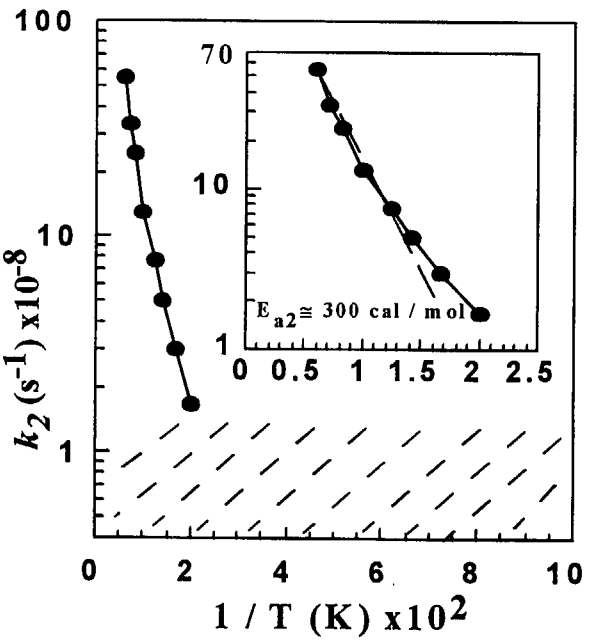

Figure 6. Arrhorius plots of the rates, k_2, evaluated by the simulations of the temperature dependent ESR spectra observed for *c*C6-1,1,3,3-d_4^+ in cC_6F_{12} matrix.

The temperature dependent ESR spectra were also observed for the other deuterated cyclohexane radical cations of *c*C6-1,1-d_2, *c*C6-1,1,4,4-d_4 and *c*C6-1,1,2,2,3,3-d_6. They were successfully analyzed using a similar method. Here we wish to just note a short summary on the results of *c*C6-1,1,4,4-d_4^+. The calculations

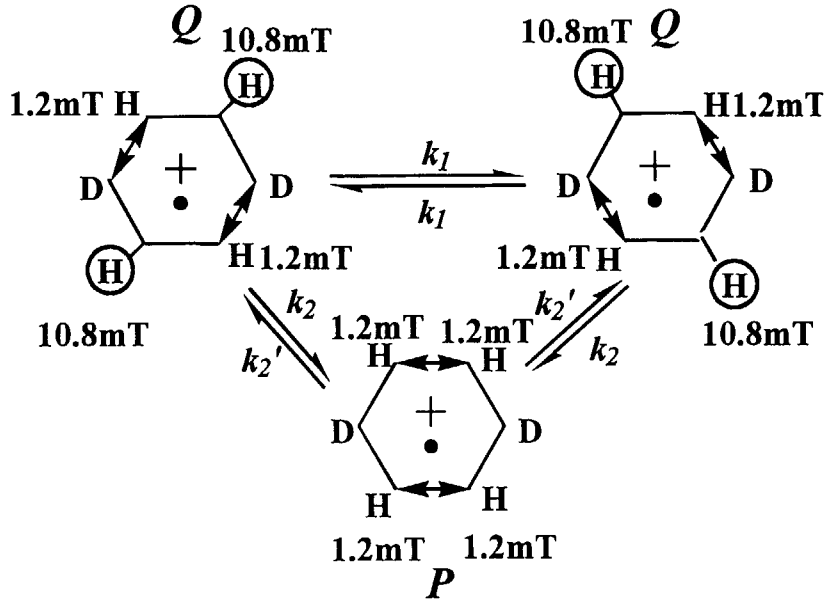

Figure 7. Schemetics showing three sites exchange among one C_{2h} (P) and two C_{2h} (Q) structures of cC6-1,1,4,4-d_4^+ with different ZPEs.

resulted in the cation with two equivalents *Q* forms, which have ZPE, lower by 408 cal/mol than *P* form (Fig. 7). The rates, k_1, evaluated from the simulations of the temperature dependent lineshapes were found to be almost temperature-independent below 40 K as shown in Fig. 8. This observation strongly suggests that the interchange between the two Q forms take place due to quantum mechanical tunneling.

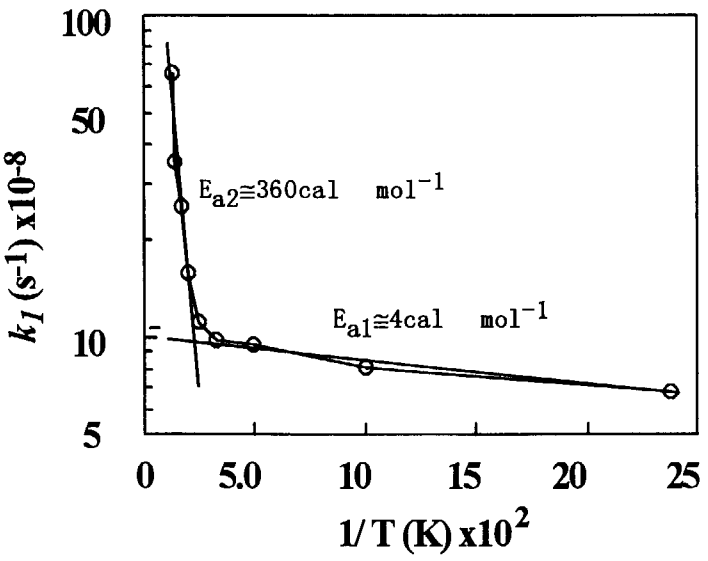

Figure 8. Arrhorius plots of the rate constants, k_1, evaluated by the simulation of the temperature dependent ESR spectra observed for *c*C6-1,1,4,4-d_4^+ in CF_3-*c*C_6F_{12} matrix.

References

[1] Shiotani, M. *Magn. Reson. Rev.* **1987**, *12*, 333.

[2] Lund, A.; Shiotani,M. *Radical Ionic. Systems*, Kluwer Academic Publishers, **1991**.
[3] Iwasaki, M.;Toriyama, K.. *Faraday Discuss. Chem. Soc.*, **1984**, *78*, 19.
[4] Lunell, S.; Huang, M.B.; Claesson, O.; Lund, A. *J. Chem. Phys.*, **1985**, 82, 5121.
[5] Lindgren, M. & Shiotani, M.; Shiotani, M. & Lund, A. *"Radical Ionic System"*, 115-175 (1991), kluwer.
[6] Shiotani, M.; Ohta, N.; Ichikawa, T. *Chem. Phys. Lett.* **1988**,*149*, 185.
[7] Lindgren, M.; Shiotani, M.; Ohta, N.; Ichikawa, T.; Sjöqvist, L. *Chem. Phys, Lett.* **1989**, *161*, 127.
[8] Shiotani, M.; Lindgren,M.; Ichikawa, T. *J. Am. Chem. Soc.*, **1990**, *112*, 967.
[9] Shiotani, M.; Lindgren, M.; Ohta, N.; Ichikawa, T. *J. Chem. Soc. PERKIN TRANS. 2*, **1991**, 711.
[10] Lindgren, M.; Matsumoto, M.; Shiotani, M. *J. Chem. Soc. PERKIN TRANS. 2* **1992**, 1397.
[11] Shiotani, M.; Matsumoto, M.; Lindgren, M. *J. Chem. Soc. PERKIN TRANS. 2*, **1993**, 1995.
[12] Shiotani, M.; Komaguchi, K.; Ohshita, J.; Ishikawa, M.; Sjoqvist, L. *Chem. Phys. Lett.* **1992**, *188*, 93.
[13] Komaguchi, K.; Shiotani, M.; Ishikawa, M.; Sasaki, K. *Chem. Phys. Lett.* **1992**, *200*, 580.
[14] Lindgren, M.; Komaguchi, K.; Shiotani, M.; Sasaki, K. *J. Phys. Chem.* **1994**, *98*, 8331.
[15] Fangstrom, T.; Lunell, S.; Engels, B.; Eriksson, L.; Shiotani, M.; Komaguchi, K. *J. Chem. Phys.* **1997**, *107*, 297.
[16] Komaguchi, K.; Shiotani, M. *J. Phys. Chem.* **1997**, *101*, 6983.
[17] Heinzer, J., *Mol. Phys.* **1971**, *22*, 167.

Author Index

This is a blank page.

国際単位系 (SI) と換算表

表 1　SI 基本単位および補助単位

量	名称	記号
長さ	メートル	m
質量	キログラム	kg
時間	秒	s
電流	アンペア	A
熱力学温度	ケルビン	K
物質量	モル	mol
光度	カンデラ	cd
平面角	ラジアン	rad
立体角	ステラジアン	sr

表 2　SI と併用される単位

名称	記号
分，時，日	min，h，d
度，分，秒	°，′，″
リットル	l，L
トン	t
電子ボルト	eV
原子質量単位	u

1 eV = 1.60218 × 10^{-19} J

1 u = 1.66054 × 10^{-27} kg

表 5　SI 接頭語

倍数	接頭語	記号
10^{18}	エクサ	E
10^{15}	ペタ	P
10^{12}	テラ	T
10^{9}	ギガ	G
10^{6}	メガ	M
10^{3}	キロ	k
10^{2}	ヘクト	h
10^{1}	デカ	da
10^{-1}	デシ	d
10^{-2}	センチ	c
10^{-3}	ミリ	m
10^{-6}	マイクロ	μ
10^{-9}	ナノ	n
10^{-12}	ピコ	p
10^{-15}	フェムト	f
10^{-18}	アト	a

表 3　固有の名称をもつ SI 組立単位

量	名称	記号	他の SI 単位による表現
周波数	ヘルツ	Hz	s^{-1}
力	ニュートン	N	m·kg/s^2
圧力，応力	パスカル	Pa	N/m^2
エネルギー，仕事，熱量	ジュール	J	N·m
工率，放射束	ワット	W	J/s
電気量，電荷	クーロン	C	A·s
電位，電圧，起電力	ボルト	V	W/A
静電容量	ファラド	F	C/V
電気抵抗	オーム	Ω	V/A
コンダクタンス	ジーメンス	S	A/V
磁束	ウェーバ	Wb	V·s
磁束密度	テスラ	T	Wb/m^2
インダクタンス	ヘンリー	H	Wb/A
セルシウス温度	セルシウス度	℃	
光束	ルーメン	lm	cd·sr
照度	ルクス	lx	lm/m^2
放射能	ベクレル	Bq	s^{-1}
吸収線量	グレイ	Gy	J/kg
線量当量	シーベルト	Sv	J/kg

表 4　SI と共に暫定的に維持される単位

名称	記号
オングストローム	Å
バーン	b
バール	bar
ガル	Gal
キュリー	Ci
レントゲン	R
ラド	rad
レム	rem

1 Å = 0.1 nm = 10^{-10} m

1 b = 100 fm^2 = 10^{-28} m^2

1 bar = 0.1 MPa = 10^5 Pa

1 Gal = 1 cm/s^2 = 10^{-2} m/s^2

1 Ci = 3.7 × 10^{10} Bq

1 R = 2.58 × 10^{-4} C/kg

1 rad = 1 cGy = 10^{-2} Gy

1 rem = 1 cSv = 10^{-2} Sv

（注）

1. 表 1 − 5 は「国際単位系」第 5 版，国際度量衡局 1985 年刊行による。ただし，1 eV および 1 u の値は CODATA の 1986 年推奨値によった。
2. 表 4 には海里，ノット，アール，ヘクタールも含まれているが日常の単位なのでここでは省略した。
3. bar は，JIS では流体の圧力を表わす場合に限り表 2 のカテゴリーに分類されている。
4. EC 閣僚理事会指令では bar，barn および「血圧の単位」mmHg を表 2 のカテゴリーに入れている。

換　算　表

力

N(=10^5 dyn)	kgf	lbf
1	0.101972	0.224809
9.80665	1	2.20462
4.44822	0.453592	1

粘度　1 Pa·s(N·s/m^2) = 10 P(ポアズ)(g/(cm·s))

動粘度　1 m^2/s = 10^4 St(ストークス)(cm^2/s)

圧力

MPa(=10 bar)	kgf/cm^2	atm	mmHg(Torr)	lbf/in^2(psi)
1	10.1972	9.86923	7.50062 × 10^3	145.038
0.0980665	1	0.967841	735.559	14.2233
0.101325	1.03323	1	760	14.6959
1.33322 × 10^{-4}	1.35951 × 10^{-3}	1.31579 × 10^{-3}	1	1.93368 × 10^{-2}
6.89476 × 10^{-3}	7.03070 × 10^{-2}	6.80460 × 10^{-2}	51.7149	1

エネルギー・仕事・熱量

J(=10^7 erg)	kgf·m	kW·h	cal(計量法)	Btu	ft·lbf	eV
1	0.101972	2.77778 × 10^{-7}	0.238889	9.47813 × 10^{-4}	0.737562	6.24150 × 10^{18}
9.80665	1	2.72407 × 10^{-6}	2.34270	9.29487 × 10^{-3}	7.23301	6.12082 × 10^{19}
3.6 × 10^6	3.67098 × 10^5	1	8.59999 × 10^5	3412.13	2.65522 × 10^6	2.24694 × 10^{25}
4.18605	0.426858	1.16279 × 10^{-6}	1	3.96759 × 10^{-3}	3.08747	2.61272 × 10^{19}
1055.06	107.586	2.93072 × 10^{-4}	252.042	1	778.172	6.58515 × 10^{21}
1.35582	0.138255	3.76616 × 10^{-7}	0.323890	1.28506 × 10^{-3}	1	8.46233 × 10^{18}
1.60218 × 10^{-19}	1.63377 × 10^{-20}	4.45050 × 10^{-26}	3.82743 × 10^{-20}	1.51857 × 10^{-22}	1.18171 × 10^{-19}	1

1 cal = 4.18605 J（計量法）

= 4.184 J　（熱化学）

= 4.1855 J　（15 °C）

= 4.1868 J（国際蒸気表）

仕事率　1 PS（仏馬力）

= 75 kgf·m/s

= 735.499 W

放射能

Bq	Ci
1	2.70270 × 10^{-11}
3.7 × 10^{10}	1

吸収線量

Gy	rad
1	100
0.01	1

照射線量

C/kg	R
1	3876
2.58 × 10^{-4}	1

線量当量

Sv	rem
1	100
0.01	1

（86 年 12 月 26 日現在）